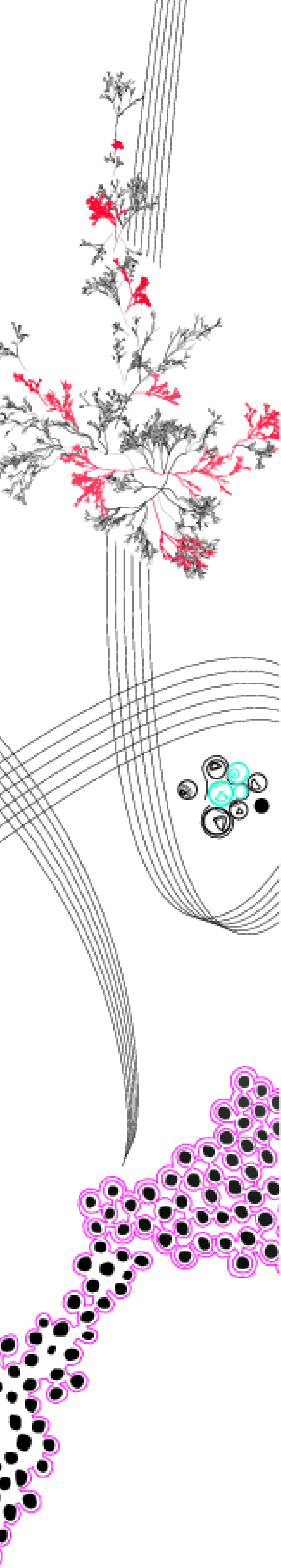

Bachelor Thesis

The Boundary Layer over a Flat Plate

July 4, 2014

M.P.J. Sanders

Faculty of Engineering Technology
Engineering Fluid Dynamics

Examination committee:
Prof.dr.ir. H.W.M. Hoeijmakers (Mentor/Chairman)
Dr. H.K. Hemmes (External Member)
Ir. R. Kommer (Mentor)

UNIVERSITY OF TWENTE.

I Abstract

The properties of the boundary-layer over a flat plate have been investigated analytically, experimentally and numerically employing XFOIL. With the theory from Blasius and von Kármán, the boundary-layer properties over an infinitesimally thin flat plate have been investigated analytically. A finite thickness plate, designed to behave aerodynamically as a flat plate, with a Hermite polynomial leading edge and a trailing edge corresponding to the last 70% of a NACA 4-series airfoil section, has been analyzed with XFOIL and has been investigated mounted at zero angle of attack in the Silent Wind Tunnel of the University of Twente.

Initial measurements have been performed to obtain the drag force and velocity profile. The drag force was measured with load cells and the velocity profile was determined with a Pitot tube and a single-wire Hot Wire probe (55P11) at various Reynolds numbers. The measurements indicate a delayed transition from laminar to turbulent flow at a Reynolds number around $\mathrm{Re}_{crit}=3{\cdot}10^6$ instead of the expected $\mathrm{Re}_{crit}=5{\cdot}10^5$. Leading-edge turbulence strips were also applied in order to investigate the drag force and the transitional boundary layer.

The found delayed transition is unfavourable for further research on the influence of the surface roughness on transition because of the maximum velocity achievable in the Silent Wind Tunnel. Since the turbulence level of the Silent Wind Tunnel is relatively low (approximately 0.25%), other possibilities have been investigated on the cause of the delayed transition. Results of numerical simulations using XFOIL indicated that a small change in the streamwise pressure gradient can delay transition substantially. Therefore, additional measurements have been performed on the streamwise pressure gradient in the Silent Wind Tunnel. These results indicate an existing streamwise pressure gradient in the test section of the Silent Wind Tunnel which is amplified when the plate is installed in the wind tunnel and may have been the cause of the delayed transition.

II Nomenclature

English Symbols

c	m	Length of the plate
c_d	-	The drag coefficient
c_f	-	Local skin friction coefficient
c_p	-	The pressure coefficient
C_f	-	Total skin friction coefficient
D	N	The total drag force
F	N	Force
g	m/s^2	Gravitational acceleration
m	kg	Mass
M	kg m/s	Momentum
N	-	The amplification factor
p	N/m	Pressure
p_∞	N/m	Free stream pressure
Re_c	-	Reynolds number of the entire plate
Re_x	-	Local Reynolds number
S	m^2	Surface area
t_i	N/m	Stress vector
Tu	%	Turbulence level
u	m/s	Velocity in the x-direction
u_j	m/s	Velocity vector
U_∞	m/s	Free stream velocity in the x-direction
v	m/s	Velocity in the y-direction
V	m^3	Volume
V_∞	m/s	Free stream velocity in the y-direction

Greek Symbols

δ	m	Boundary layer thickness
δ^*	m	Displacement thickness
η	-	Dimensionless parameter
θ	m	Momentum Thickness
μ	kg/ms	Viscosity
ν	m^2/s	Kinematic viscosity
ρ	kg/m^3	Density
ρ_∞	kg/m^3	Density in the free stream
σ_{ij}	N/m	Stress tensor
τ	N/m	Shear stress

Contents

1 Introduction

In 1908, H. Blasius, a student of Prandtl, published a paper about 'The Boundary Layers in Fluids with Small Friction'. The paper discusses among other things, the two dimensional flow over a flat plate. The boundary-layer equations that Blasius derived were much simpler than the Navier-Stokes equations. Blasius found that these boundary layer equations in certain cases can be reduced to a single ordinary differential equation for a similarity solution, which we now call the Blasius equation. This same method will be used in this report to derive the boundary layer equations over an infinitesimally thin flat plate. In 1921, von Kármán, a former student of Prandtl, developed another form of the boundary-layer equations which will also be shown in this report. We will start with the derivation of the continuity equation and Navier-Stokes equation to eventually be able to obtain Blasius' equation.

With the theory from Blasius and von Kármán we will analyse the properties of the boundary layer above an infinitesimally thin flat plate in two dimensional, steady and incompressible flow. Moreover, the drag force exerted on the plate will be measured as well as the velocity profile for different Reynolds numbers. Analytical results will be compared to data obtained from measurements. The measurements will be performed in the Silent Wind Tunnel of the University of Twente. Numerical simulations with XFOIL have also been used to simulate the flow over the designed plate to compare the validity of the derived theory and to investigate if the designed plate behaves aerodynamically as a flat plate with infinitesimally thickness.

The obtained results will give further insight in the basic principles of the flow over streamlined bodies. If we can successfully describe the flow over a simple geometry such as the flat plate, it becomes easier to describe the flow over more complicated geometries using the approximations made for the basic case of the flow over a flat plate.

2 Assumptions

Before we derive all the mathematical models, The assumptions that are made to analyse the incompressible, steady flow over an infinitesimally thin flat plate are listed.

1. 2-dimensional flow, $\frac{\partial}{\partial z} = 0$, i = 1,2
2. Steady flow, $\frac{\partial}{\partial t}$=0
3. Incompressible flow, ρ=constant
4. Neglect effects due to gravity $\vec{g} = \vec{0}$, and other body forces
5. Fourier's law for heat conduction $q_i = -k\frac{\partial T}{\partial x_i}$
6. The physical properties μ, c_p, k are constant
7. There are no heat sources
8. Newtonian fluid
9. The tension vector $\vec{t}$ by medium A on B: $t_i = \sigma_{ij}n_j$
10. The stress tensor: $\sigma_{ij} = -p\delta_{ij} + \tau_{ij}$
11. For a Newtonian fluid the viscous stress tensor is $\tau_{ij} = \mu\left(\frac{\partial u_i}{\partial x_j} + \frac{\partial u_j}{\partial x_i}\right) + \lambda\delta_{ij}\frac{\partial u_k}{\partial x_k}$
12. Stokes: $2\mu + 3\lambda = 0$

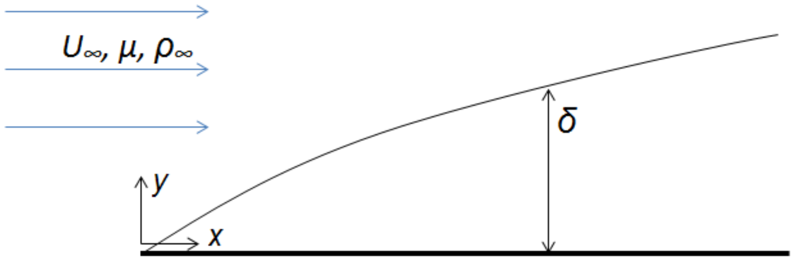

Figure 2.1: The two dimensional flat plate analysis

3 Continuity Equation

The mass m of a fluid with density ρ within a volume V is [1]:

$$m(t) = \iiint_{V(t)} \rho(\vec{x}, t) dV \tag{3.1}$$

Mass conservation tells us that the mass of a permeable control volume moving in space changes with time, due to the flux through the boundary of the control volume.

$$\frac{d}{dt} \iiint_{V(t)} \rho(\vec{x}, t) dV + \iint_{\partial V} \rho(\vec{u} - \vec{u}_{\partial V}) \cdot \vec{n} dS = 0 \tag{3.2}$$

Using the (Leibniz)-Reynolds transport theorem we can also rewrite the integral in Equation 3.2, to

$$\iiint_{V(t)} \frac{\partial \rho}{\partial t} dV + \iint_{\partial V(t)} \rho(\vec{u} - \vec{u}_{\partial V}) \cdot \vec{n} dS + \iint_{\partial V(t)} \rho(\vec{u}_{\partial V} \cdot \vec{n}) dS = 0 \tag{3.3}$$

Where $\vec{u}_{\partial V}$ is the velocity of the bounding surface. For a permeable boundary surface, the equation can be reduced to

$$\iiint_{V(t)} \frac{\partial \rho}{\partial t} dV + \iint_{\partial V(t)} \rho \vec{u} \cdot \vec{n} dS = 0 \tag{3.4}$$

Moreover, using the Einstein summation convention and writing ∂V as $S(t)$

$$\iiint_{V(t)} \frac{\partial \rho}{\partial t} dV + \iint_{S(t)} \rho u_j n_j dS = 0 \tag{3.5}$$

Where S(t) is denoted as the surface area of the control volume with volume V(t). If we want to apply this formulation to a local analysis on the flat plate, we need to convert the integral formulation to a differential formulation. We do this by using Gauss' theorem to rewrite the surface integral to a volume integral.

$$\iint_{S(t)} \rho u_j n_j dS = \iiint_{V(t)} \frac{\partial \rho u_j}{\partial x_j} dV \tag{3.6}$$

Substituting in Equation 3.5 we obtain

$$\iiint_{V(t)} \frac{\partial \rho}{\partial t} dV + \iiint_{V(t)} \frac{\partial \rho u_j}{\partial x_j} dV = 0 \tag{3.7}$$

$$\iiint_{V(t)} \left(\frac{\partial \rho}{\partial t} + \frac{\partial \rho u_j}{\partial x_j} \right) = 0 \tag{3.8}$$

This equation will hold for any control volume, implying

$$\frac{\partial \rho}{\partial t} + \frac{\partial \rho u_j}{\partial x_j} = 0 \qquad \text{For } \forall \ \vec{x} \in \text{V} \tag{3.9}$$

Because we assumed that we have steady flow, the time derivative of the density will be zero. Moreover, we have limited ourselves to a 2D flow situation and therefore we can rewrite Equation 3.9 to

$$\frac{\partial(\rho u)}{\partial x} + \frac{\partial(\rho v)}{\partial y} = 0 \tag{3.10}$$

Since the flow is incompressible (ρ is constant and not equal to zero) we can also rewrite to

$$\boxed{\frac{\partial u}{\partial x} + \frac{\partial v}{\partial y} = 0} \tag{3.11}$$

$$\text{or} \quad \boxed{\frac{\partial u_k}{\partial x_k} = 0, \qquad k = 1, 2} \tag{3.12}$$

4 Navier-Stokes Equation

Newton's second law states that the rate of change of momentum of an arbitrary control volume of fluid is equal to the forces acting on it [1]. We can define the momentum inside the control volume (Equation 4.1) and momentum conservation (Equation 4.2,4.3) as

$$\mathbf{M}(t) = \iiint_{V(t)} \rho(\mathbf{x}, t)\mathbf{u}(\mathbf{x}, t) dV \tag{4.1}$$

$$\frac{d\mathbf{M}}{dt} = \frac{d}{dt} \iiint_{V(t)} \rho \mathbf{u} dV \tag{4.2}$$

$$\frac{d\mathbf{M}}{dt} = \mathbf{F} \tag{4.3}$$

The forces acting on the blob of fluid now need to be identified. The surrounding fluid acting on the boundary of the control volume, where $\mathbf{t}$ is the stress vector, is defined as

$$\mathbf{F}_s = \iint_{S(t)} \mathbf{t}_s dS \tag{4.4}$$

We can identify a second force caused by gravity which acts on all points of the entire volume of the blob.

$$\mathbf{F}_V = \iiint_{V(t)} \rho \mathbf{g} dV \tag{4.5}$$

We can now formulate the momentum conservation equation for an impermeable control volume moving with the flow as

$$\frac{d}{dt} \iiint_{V(t)} \rho \mathbf{u} dV = \iint_{S(t)} \mathbf{t}_s dS + \iiint_{V(t)} \rho \mathbf{g} dV \tag{4.6}$$

Using the (Leibniz-)Reynolds transport theorem and Einstein summation convection we can rewrite this into the integral form

$$\iiint_{V(t)} \frac{\partial}{\partial t}(\rho u_i) dV + \iint_{S(t)} \rho u_i u_j n_j dS = \iint_{S(t)} t_i dS + \iiint_{V(t)} \rho g_i dV \tag{4.7}$$

$$i = 1, 2, 3$$

To obtain the differential form we can again use Gauss' divergence theorem to convert the surface integrals to volume integrals.

$$\iint_{S(t)} t_i dS = \iint_{S(t)} \sigma_{ij} n_j dS = \iiint_{V(t)} \frac{\partial \sigma_{ij}}{\partial x_j} dV \tag{4.8}$$

$$\iint_{S(t)} \rho u_i u_j n_j dS = \iiint_{V(t)} \frac{\partial}{\partial x_j}(\rho u_i u_j) dV \tag{4.9}$$

With these equations, the integral formulation can be rewritten

$$\iiint_{V(t)} \left(\frac{\partial}{\partial t}(\rho u_i) + \frac{\partial}{\partial x_j}(\rho u_i u_j) - \frac{\partial \sigma_{ij}}{\partial x_j} - \rho g_i \right) dV = 0 \tag{4.10}$$

Because we can choose any arbitrary control volume, the formulation can be written to differential form.

$$\frac{\partial}{\partial t}(\rho u_i) + \frac{\partial}{\partial x_j}(\rho u_i u_j) - \frac{\partial \sigma_{ij}}{\partial x_j} - \rho g_i = 0 \qquad \text{For } \forall\ \vec{x} \in \text{V} \tag{4.11}$$

With the assumptions we initially made; neglect gravity and assume steady flow, we can rewrite the equation

$$\frac{\partial}{\partial x_j}(\rho u_i u_j) - \frac{\partial \sigma_{ij}}{\partial x_j} = 0 \tag{4.12}$$

The stress tensor σ_{ij} (for a Newtonian fluid) is defined as

$$\sigma_{ij} = -p\delta_{ij} + \tau_{ij} \tag{4.13}$$

and

$$\tau_{ij} = \mu\left(\frac{\partial u_i}{\partial x_j} + \frac{\partial u_j}{\partial x_i}\right) - \frac{2}{3}\mu\delta_{ij}\frac{\partial u_k}{\partial x_k} \tag{4.14}$$

$$\delta_{ij} = \quad 0 \text{ if } i \neq j, \quad 1 \text{ if } i = j$$

$$\frac{\partial u_k}{\partial x_k} = 0 \text{ (Continuity equation for incompressible flow)}$$

Equation 4.12 then becomes

$$\frac{\partial}{\partial x_j}(\rho u_i u_j) = \frac{\partial}{\partial x_j}\left(\mu\left(\frac{\partial u_i}{\partial x_j} + \frac{\partial u_j}{\partial x_i}\right) - p\delta_{ij}\right) \tag{4.15}$$

We can also rewrite the left hand side of the equation using the chain rule of differentiation and the continuity equation ($\frac{\partial \rho u_j}{\partial x_j}$=0).

$$\frac{\partial}{\partial x_j}(\rho u_i u_j) = u_i\frac{\partial \rho u_j}{\partial x_j} + (\rho u_j)\frac{\partial u_i}{\partial x_j} \tag{4.16}$$

$$\frac{\partial}{\partial x_j}(\rho u_i u_j) = (\rho u_j)\frac{\partial u_i}{\partial x_j} \tag{4.17}$$

We can then observe that Equation 4.15 becomes

$$\boxed{(\rho u_j)\frac{\partial u_i}{\partial x_j} = \frac{\partial}{\partial x_j}\left(\mu\left(\frac{\partial u_i}{\partial x_j} + \frac{\partial u_j}{\partial x_i}\right) - p\delta_{ij}\right) \qquad \text{(Reduced Navier-Stokes)}} \tag{4.18}$$

From the Reduced Navier Stokes equation we would like to set up the x-momentum and y-momentum equation.

In the x-direction, (i=1)

$$\boxed{\rho\left(u\frac{\partial u}{\partial x} + v\frac{\partial u}{\partial y}\right) = -\frac{\partial p}{\partial x} + \mu\left(\frac{\partial^2 u}{\partial x^2} + \frac{\partial^2 u}{\partial y^2}\right)} \tag{4.19}$$

In the y-direction, (i=2)

$$\boxed{\rho\left(u\frac{\partial v}{\partial x} + v\frac{\partial v}{\partial y}\right) = -\frac{\partial p}{\partial y} + \mu\left(\frac{\partial^2 v}{\partial x^2} + \frac{\partial^2 v}{\partial y^2}\right)} \tag{4.20}$$

5 The Velocity Boundary Layer Equations for Steady Laminar Flow

We would like to introduce another assumption namely that for a flow along a surface, the boundary layer thickness $\delta << c$, also named the boundary layer assumption. It is the basic assumption that the boundary-layer thickness is much smaller than the length of the plate (c).

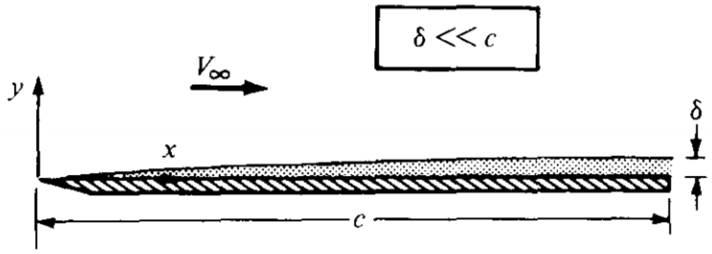

Figure 5.1: The boundary layer is very thin compared to the length of the plate (c) [5].

With this assumption we can further reduce the Navier-Stokes equation for the flat plate situation.

Equation 4.19 and 4.20 are given in dimensional variables. Let us rewrite these equations in terms of dimensionless variables, where U_∞ and V_∞ are the components of the free stream velocity:

$$p = p_\infty p', \quad u = U_\infty u', \quad v = V_\infty v', \quad x = cx', \quad y = \delta y'$$

5.1 Continuity equation

Let us first rewrite the continuity equation in terms of dimensionless variables.

$$\frac{\partial u}{\partial x} + \frac{\partial v}{\partial y} = 0 \tag{5.1}$$

$$\frac{\partial U_\infty u'}{\partial x' c} + \frac{\partial V_\infty v'}{\partial y' \delta} = 0 \tag{5.2}$$

$$\frac{\partial u'}{\partial x'} + \frac{V_\infty}{U_\infty}\frac{c}{\delta}\frac{\partial v'}{\partial y'} = 0 \tag{5.3}$$

The derivatives are of the order of magnitude equal to 1. Therefore in order for the equation to hold

$$\frac{V_\infty}{U_\infty}\frac{c}{\delta} = 1 \tag{5.4}$$

$$\boxed{V_\infty = U_\infty \frac{\delta}{c}} \tag{5.5}$$

5.2 X-momentum

Let us now rewrite the x-component of the momentum equation in terms of dimensionless variables and using the relation derived between V_∞ and U_∞.

$$u\frac{\partial u}{\partial x} + v\frac{\partial u}{\partial y} = -\frac{1}{\rho}\frac{\partial p}{\partial x} + \frac{\mu}{\rho}\left(\frac{\partial^2 u}{\partial x^2} + \frac{\partial^2 u}{\partial y^2}\right) \tag{5.6}$$

$$\frac{U_\infty^2}{c}\left(u'\frac{\partial u'}{\partial x'} + v'\frac{\partial u'}{\partial y'}\right) = -\frac{p_\infty}{\rho c}\frac{\partial p'}{\partial x'} + \frac{\mu U_\infty}{\rho \delta^2}\left(\left(\frac{\delta^2}{c^2}\right)\frac{\partial^2 u'}{\partial x'^2} + \frac{\partial^2 u'}{\partial y'^2}\right) \tag{5.7}$$

$$u'\frac{\partial u'}{\partial x'} + v'\frac{\partial u'}{\partial y'} = -\frac{p_\infty}{\rho U_\infty^2}\frac{\partial p'}{\partial x'} + \frac{\mu}{\rho U_\infty c}\frac{c^2}{\delta^2}\left(\left(\frac{\delta^2}{c^2}\right)\frac{\partial^2 u'}{\partial x'^2} + \frac{\partial^2 u'}{\partial y'^2}\right) \tag{5.8}$$

In order for the dimensions to be of comparable order of magnitude

$$\boxed{p_\infty = \rho U_\infty^2} \tag{5.9}$$

$$\boxed{\frac{\delta}{c} = \frac{1}{\mathrm{Re}_c^{\frac{1}{2}}} \qquad << 1, \qquad \mathrm{Re}_c >>> 1} \tag{5.10}$$

Furthermore we can observe that the second derivative of u' with respect to x is multiplied with $\frac{\delta^2}{c^2}$. This means that the term is negligibly small compared to the second derivative of u' with respect to y'. Therefore, after we rewrite the equation in terms of dimensional variables:

$$\boxed{u\frac{\partial u}{\partial x} + v\frac{\partial u}{\partial y} = -\frac{1}{\rho}\frac{\partial p}{\partial x} + \frac{\mu}{\rho}\left(\frac{\partial^2 u}{\partial y^2}\right)} \tag{5.11}$$

5.3 Y-momentum

The y-momentum was given as:

$$u\frac{\partial v}{\partial x} + v\frac{\partial v}{\partial y} = -\frac{1}{\rho}\frac{\partial p}{\partial y} + \frac{\mu}{\rho}\left(\frac{\partial^2 v}{\partial x^2} + \frac{\partial^2 v}{\partial y^2}\right) \tag{5.12}$$

In terms of dimensionless variables

$$U_\infty u'\frac{\partial V_\infty v'}{\partial c x'} + V_\infty v'\frac{\partial V_\infty v'}{\partial \delta y'} = -\frac{1}{\rho}\frac{\partial p' p_\infty}{\partial y' \delta} + \frac{\mu}{\rho}\left(\frac{\partial^2 V_\infty v'}{\partial c^2 x'^2} + \frac{\partial^2 V_\infty v'}{\partial \delta^2 y'^2}\right) \tag{5.13}$$

$$\frac{\delta^2}{c^2}\left(u'\frac{\partial v'}{\partial x'} + v'\frac{\partial v'}{\partial y'}\right) = -\frac{p_\infty}{\rho U_\infty^2}\frac{\partial p'}{\partial y'} + \frac{\mu}{\rho U_\infty c}\left(\left(\frac{\delta^2}{c^2}\right)\frac{\partial^2 v'}{\partial x'^2} + \frac{\partial^2 v'}{\partial y'^2}\right) \tag{5.14}$$

If we analyse the equation, we induce that the left hand side and the expression on the right are negligibly small because of the $\frac{\delta^2}{c^2}$ scaling. When rewriting the equation back in terms of dimensional variables, the y-momentum reduces to

$$\boxed{\frac{\partial p}{\partial y} = 0} \tag{5.15}$$

5.4 Summary

To summarize, we have obtained three equations:

$$\boxed{\frac{\partial u}{\partial x} + \frac{\partial v}{\partial y} = 0 \qquad \text{Continuity}} \tag{5.16}$$

$$\boxed{u\frac{\partial u}{\partial x} + v\frac{\partial u}{\partial y} = -\frac{1}{\rho}\frac{\partial p}{\partial x} + \frac{\mu}{\rho}\left(\frac{\partial^2 u}{\partial y^2}\right) \qquad \text{x-momentum}} \tag{5.17}$$

$$\boxed{\frac{\partial p}{\partial y} = 0 \qquad \text{y-momentum}} \tag{5.18}$$

The boundary conditions that are to be applied to this set of equations are:

$$\text{At the wall:} \qquad u(x,0) = 0, \quad v(x,0) = 0 \qquad \text{(no slip condition)} \tag{5.19}$$

$$\text{At the boundary layer edge:} \qquad u(x,\infty) = U_\infty \tag{5.20}$$

When we use the last boundary equation $u(x,\infty) = U_\infty$ (the free steam velocity is constant and the velocity becomes uniform at $y = \delta$) in the x-momentum equation, we obtain

$$\frac{\partial^k u(x,\infty)}{\partial x^k} = 0 \qquad \text{For } k \geq 1 \tag{5.21}$$

The x-momentum reduces to

$$\boxed{U_\infty \frac{dU_\infty}{dx} = -\frac{1}{\rho}\frac{\partial p}{\partial x} \qquad \text{(Euler's equation)}} \tag{5.22}$$

The y-momentum equation states that the pressure does not change in the y-direction i.e. normal to the plate. This implies that the pressure at the outer edge of the boundary layer is equal throughout the boundary layer $p(x, y) = p_e(x, y)$ for y $\in$ [0,$\delta(\infty)$]. However, because we have incompressible flow over an infinitesimally thin flat plate, the pressure will not change with x and we can leave out the pressure derivative with respect to x in the x-momentum equation. We can also reason that the free stream velocity U_∞ is constant and we can leave the pressure derivative out.

We can derive another boundary condition at the wall. Applying Equation 5.17 at the wall we can obtain

$$\boxed{\left(\frac{\partial^2 u}{\partial y^2}\right)_{y=0} = \frac{1}{\mu}\frac{\partial p_\infty}{\partial x}} \tag{5.23}$$

6 The Solution of the Velocity Boundary Layer Equations for Steady, Laminar Flow

6.1 The Blasius equation

If we can solve the continuity-and momentum equation for u an v, we will be able to determine the drag friction coefficient and boundary layer thickness of which the definition will be given later. To obtain these results, the boundary layer partial differential equations need to be reduced to a single ordinary differential equation.

Let us first introduce the stream function in order to satisfy the continuity equation.

$$u(x,y) = \frac{\partial \Psi}{\partial y} \tag{6.1}$$

$$v(x,y) = -\frac{\partial \Psi}{\partial x} \tag{6.2}$$

We can easily observe that the stream solution will indeed satisfy the continuity equation. Substituting u and v expressed in terms of the stream function into the x-momentum equation, one finds

$$\frac{\partial \Psi}{\partial y}\frac{\partial^2 \Psi}{\partial x \partial y} - \frac{\partial \Psi}{\partial x}\frac{\partial^2 \Psi}{\partial y^2} = \frac{\mu}{\rho}\frac{\partial^3 \Psi}{\partial y^3} \tag{6.3}$$

The question here would be how the stream function is to be determined in order to satisfy the momentum equation. Blasius reasoned that because there is no length scale in this flat plate problem (we assume an infinitely long plate), the nondimensional velocity profile e.g. $\frac{u}{U_\infty}$, should remain unchanged when plotted against the nondimensional coordinate normal to the wall $\frac{y}{\delta}$. These assumptions would suggest that there is a similarity solution because the flow looks similar in any direction at any time. This similarity would suggest that

$$\frac{u}{U_\infty} = function(\eta)$$

where η is a dimensionless parameter related to $\frac{y}{g(x)}$ and where g(x) is related to the boundary layer thickness $\delta(x)$. This suggests that g(x) is some function of the coordinate x along the plate and some constant B i.e.

$$\eta(x,y) = Bx^q y \tag{6.4}$$

For similarity, the stream function then also is a function of some variable x, a constant A and $f(\eta)$

$$\Psi(x,y) = Ax^p f(\eta) \tag{6.5}$$

We now need to find the unknown parameters. This can be achieved by using the boundary conditions and substituting the derivatives of the stream function in Equation 6.3 [2].

$$\frac{\partial \Psi}{\partial x} = Apx^{p-1}f(\eta) + ABqyx^{p+q-1}f'(\eta) \tag{6.6}$$

$$\frac{\partial \Psi}{\partial y} = ABx^{p+q}f'(\eta) \tag{6.7}$$

$$\frac{\partial^2 \Psi}{\partial x \partial y} = AB(p+q)x^{p+q-1}f'(\eta) + AB^2qyx^{p+2q-1}f''(\eta) \tag{6.8}$$

$$\frac{\partial^2 \Psi}{\partial y^2} = AB^2x^{p+2q}f''(\eta) \tag{6.9}$$

$$\frac{\partial^3 \Psi}{\partial y^3} = AB^3x^{p+3q}f'''(\eta) \tag{6.10}$$

Substituting all the obtained expressions into Equation 6.3 and rewriting results in

$$\boxed{(p+q)f'^2 - pff'' = \frac{\mu}{\rho}\frac{B}{A}x^{-p+q+1}f'''} \tag{6.11}$$

If we analyse this equation we can already find a relation between p and q. Because of similarity reasons, the equation should be independent of x and thus

$$-p + q + 1 = 0 \tag{6.12}$$

With the boundary conditions we are able to solve the set of equations.

$$u(x, 0) = 0 \tag{6.13}$$

$$\frac{\partial \Psi}{\partial y}(x, 0) = 0 \tag{6.14}$$

$$ABx^{p+q} f'(0) = 0 \tag{6.15}$$

A non-trivial solution would imply

$$f'(0) = 0 \tag{6.16}$$

The second boundary condition

$$v(x, 0) = 0 \tag{6.17}$$

$$-\frac{\partial \Psi}{\partial x}(x, 0) = 0 \tag{6.18}$$

$$-Apx^{p-1} f(0) - ABqyx^{p+q-1} f'(0) = 0 \tag{6.19}$$

Because we already found that $f'(0) = 0$, the non-trivial solution here would be

$$f(0) = 0 \tag{6.20}$$

And the final boundary condition

$$u(x, \infty) = U_\infty \tag{6.21}$$

$$\frac{\partial \Psi}{\partial y}(x, \infty) = U_\infty \tag{6.22}$$

$$ABx^{p+q} f'(\infty) = U_\infty \tag{6.23}$$

For this equation to be satisfied we need to set

$$ABf'(\infty) = U_\infty \tag{6.24}$$

$$p + q = 0 \tag{6.25}$$

With equation 6.12 and 6.25 we can solve for p and q.

$$p = \frac{1}{2} \tag{6.26}$$

$$q = -\frac{1}{2} \tag{6.27}$$

But also using Equation 6.24

$$f'(\infty) = 1 \tag{6.28}$$

$$\text{and} \quad AB = U_\infty \tag{6.29}$$

With these expressions and Equation 6.11 we can derive

$$\frac{\mu}{\rho}\frac{B}{A} = 1 \qquad \text{(Dimensionless)} \tag{6.30}$$

From Equations 6.29 and 6.30 then follows

$$B = \sqrt{\frac{U_\infty \rho}{\mu}} \tag{6.31}$$

$$A = \sqrt{\frac{U_\infty \mu}{\rho}} \tag{6.32}$$

We gave now obtained all the unknown parameters and can substitute them in the momentum equation to obtain the third order ordinary differential equation (with its boundary conditions).

$$\boxed{\begin{aligned} 2f''' + ff' &= 0 \\ f(0) &= 0 \\ f'(0) &= 0 \\ f'(\infty) &= 1 \end{aligned}} \qquad \begin{aligned}(6.33)\\(6.34)\\(6.35)\\(6.36)\end{aligned}$$

With the expressions for the stream function and η:

$$\boxed{\Psi(x,y) = f(\eta)\sqrt{U_\infty \frac{\mu}{\rho} x}, \qquad \eta(x,y) = y\sqrt{\frac{U_\infty \rho}{\mu x}}} \tag{6.37}$$

6.2 The Runge-Kutta Method for the Blasius Equation

The obtained third-order, nonlinear, ordinary differential equation cannot be solved analytically and has to be solved numerically. A technique that can be used is the Runge-Kutta method. The method integrates in small steps along the y-direction, starting from the wall. However, because we only have two of the boundary conditions at y=0 (the boundary condition for $f''(0)$ is missing), we have to assume a value for this boundary condition and check if at large η, the condition $f'(\infty) = 1$ is satisfied. This process is repeated until the solution is congruent. This method is also called the 'shooting-method' and Matlab will provide the help needed to find the solution.

Using the shooting-method we find

$$f''(0) = 0.3320 \tag{6.38}$$

This value is of specific interest because with it we can determine the skin friction coefficients.

To obtain the x-component of the velocity profile we need to use the derivative of Ψ with respect to y

$$u(x,y) = \frac{\partial \Psi}{\partial y} \tag{6.39}$$

$$u(x,y) = U_\infty f'(\eta) \tag{6.40}$$

The results from Matlab are shown below.

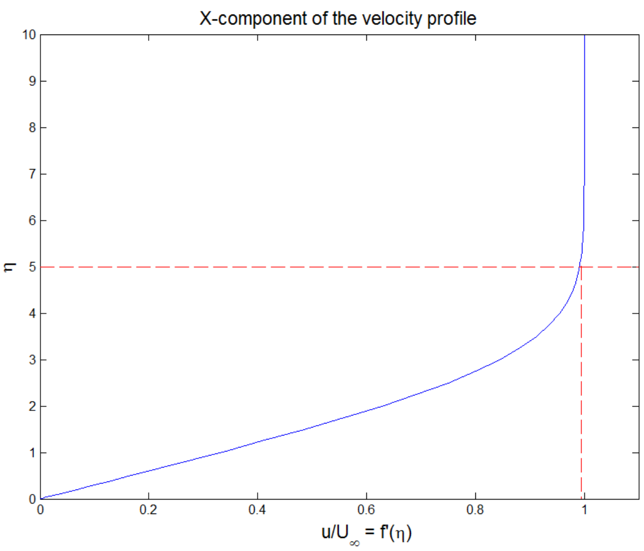

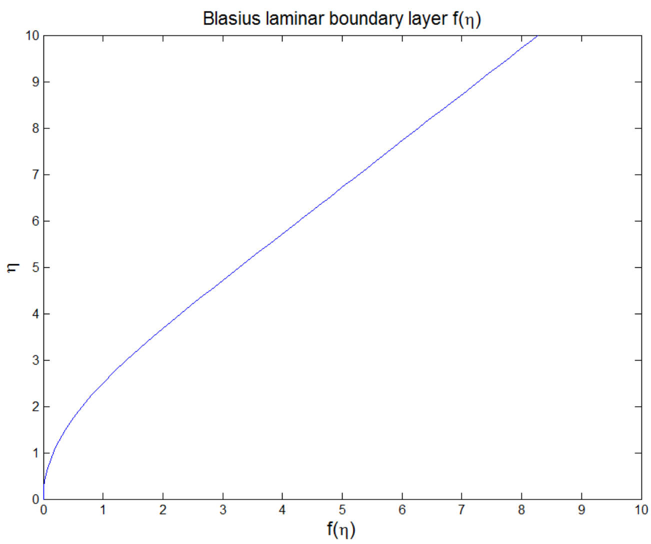

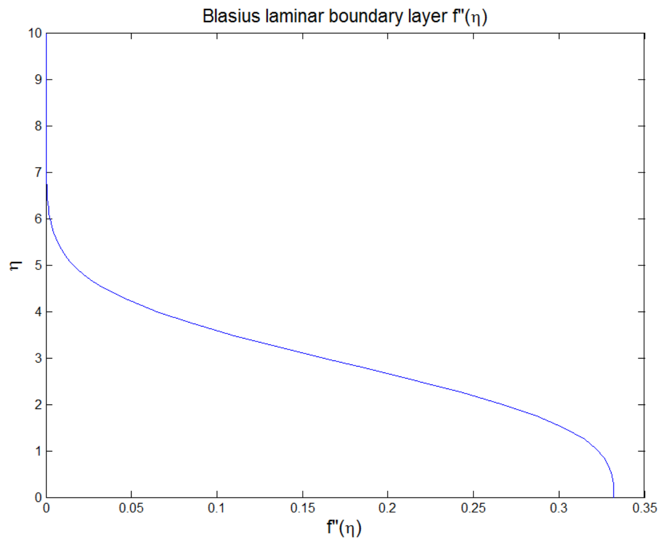

Figure 6.1: The Blasius laminar boundary layer solution

If we want to obtain the y-component of the velocity, we need to derive Ψ with respect to x.

$$v(x, y) = -\frac{\partial \Psi}{\partial x} \tag{6.41}$$

After rewriting, we obtain the dimensionless expression that we need.

$$\frac{v(x, y)}{U_\infty} \mathrm{Re}_x^{1/2} = -\frac{1}{2}(f(\eta) - \eta f'(\eta)) \tag{6.42}$$

The velocity profile of the y-component is shown below.

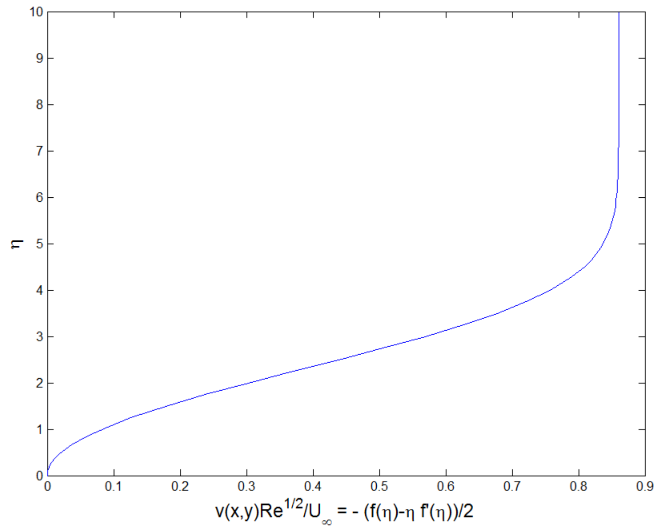

Figure 6.2: The vertical component of the velocity

6.3 The Skin Friction Coefficient

With the results obtained by solving the Blasius equation we can now find further results such as the skin friction coefficients. The local skin friction coefficient is defined as

$$c_f \equiv \frac{\tau_w}{\frac{1}{2}\rho U_\infty^2} \tag{6.43}$$

And the wall shear stress τ_w is defined as

$$\tau_w \equiv \mu \left(\frac{\partial u}{\partial y}\right)_{y=0} \tag{6.44}$$

We can use Equation 6.40 to find

$$u(x, y) = U_\infty f'(\eta) \tag{6.45}$$

$$\frac{\partial u}{\partial y} = U_\infty \frac{df'(\eta)}{dy} \tag{6.46}$$

$$\frac{\partial u}{\partial y} = U_\infty \sqrt{\frac{U_\infty \rho}{\mu x}} f''(\eta) \tag{6.47}$$

So that

$$\tau_w = U_\infty \sqrt{\frac{U_\infty \rho \mu}{x}} f''(0) \tag{6.48}$$

Substituting the obtained expression back into the local skin friction equation:

$$c_f = \frac{\sqrt{\frac{U_\infty \rho \mu}{x}}}{\frac{1}{2}\rho U_\infty^2} f''(0) \tag{6.49}$$

$$c_f = 2\sqrt{\frac{\mu}{U_\infty \rho x}} f''(0) \tag{6.50}$$

$$c_f = \frac{2f''(0)}{\mathrm{Re}_x^{1/2}} \tag{6.51}$$

Where Re_x is the local Reynolds number. With the obtained approximation for f"(0) we find an expression for the local skin friction coefficient.

$$\boxed{c_f(x) = \frac{0.664}{\mathrm{Re}_x^{1/2}} = \frac{0.664}{\mathrm{Re}_c^{1/2}} \left(\frac{x}{c}\right)^{-1/2}} \tag{6.52}$$

The skin friction coefficient as function of the coordinate along the wall for a laminar air flow is plotted in Figure 6.3.

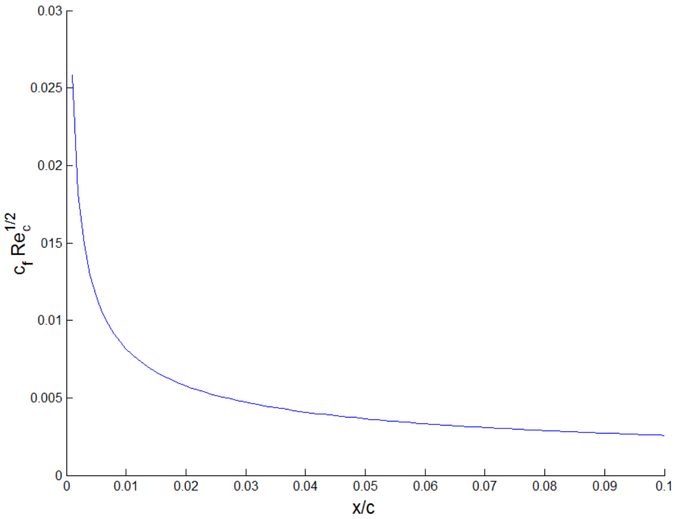

Figure 6.3: The local skin friction coefficient for laminar flow

From this expression we observe that the local skin friction coefficient is proportional to $\mathrm{Re}_c^{-1/2}$ and $\left(\frac{x}{c}\right)^{-1/2}$. The latter means that as the distance x increases from the leading edge, the local skin friction coefficient decreases. We can now derive the total skin friction coefficient on the top of the flat plate by integrating the local skin friction coefficient from x=0 to x=c.

$$C_f = \frac{1}{c}\int_0^c c_f dx \tag{6.53}$$

$$\boxed{C_f = \frac{1.328}{\mathrm{Re}_c^{1/2}}} \tag{6.54}$$

Re_c is the Reynolds number of the entire plate, meaning that the total skin friction coefficient decreases as the Reynolds number increases.

6.4 The Boundary Layer Thickness

We are now able to derive the expression for the approximated boundary layer thickness using the definition of η.

$$\eta = y\sqrt{\frac{U_\infty \rho}{\mu x}} \tag{6.55}$$

Because the approximation is congruent, a point needs to be defined at which we choose that the boundary layer ends. We will define this as:

$$u/U_\infty = 0.99 \tag{6.56}$$

The calculation that was made with Matlab shows that $\eta = 4.92$ for $u/U_\infty = 0.99$ (this can also be observed in the first graph of Figure 6.1).

$$\eta = \delta\sqrt{\frac{U_\infty \rho}{\mu x}} = 4.92 \tag{6.57}$$

$$\boxed{\delta(x) = \frac{4.92x}{\mathrm{Re}_x^{1/2}}} \tag{6.58}$$

$$\boxed{\frac{\delta}{c} = \frac{4.92\left(\frac{x}{c}\right)^{1/2}}{\mathrm{Re}_c^{1/2}}} \tag{6.59}$$

The velocity boundary layer thickness is shown graphically below.

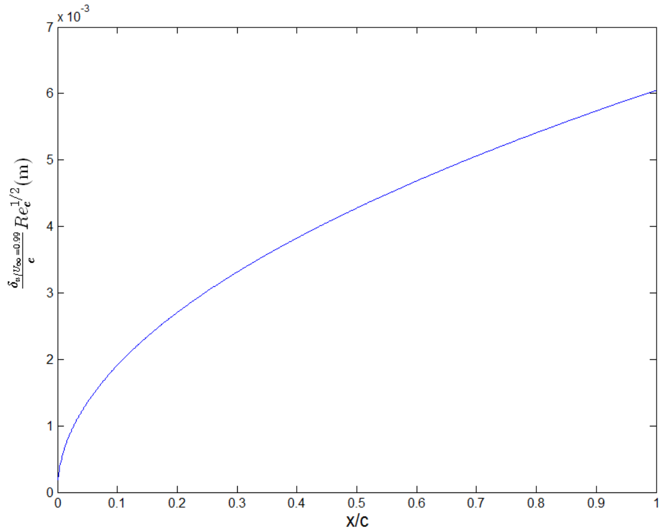

Figure 6.4: The boundary layer thickness

6.5 The Displacement Thickness

A very useful and frequently used boundary layer property is the displacement thickness. Consider the flow over a flat plate as shown in Figure 6.5 ($u_e = U_\infty$, $\rho_e = \rho_\infty$).

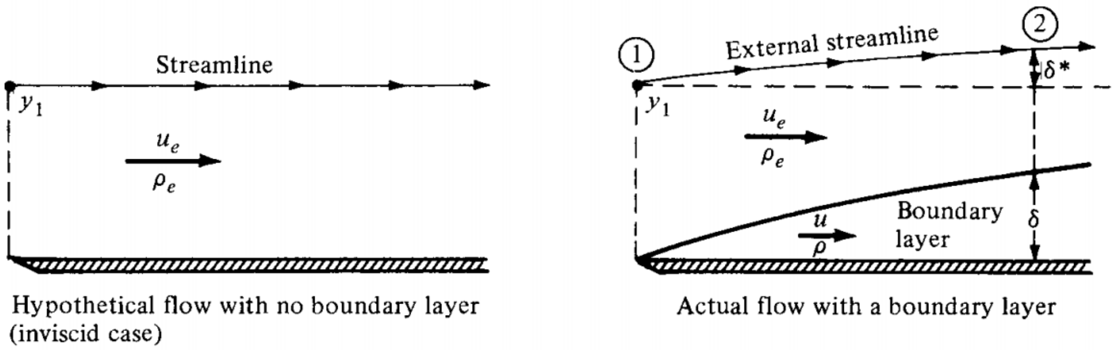

Figure 6.5: The Displacement Thickness [5]

On the left a hypothetical flow is shown and on the right the actual flow with a boundary layer is shown. In the case of hypothetical flow and at point 1 in the actual flow, the mass flow rate between the surface of the plate and the streamline through $(0, y_1)$, is defined as

$$\dot{m} = \int_0^{y1} \rho_\infty U_\infty dy \tag{6.60}$$

With an additional boundary layer, the mass flow at point 2 in the stream becomes

$$\dot{m} = \int_0^{y1} \rho u dy + \rho_\infty U_\infty \delta^* \tag{6.61}$$

The mass flow rate at both points has to be equal

$$\int_0^{y1} \rho_\infty U_\infty dy = \int_0^{y1} \rho u dy + \rho_\infty U_\infty \delta^* \tag{6.62}$$

Rewriting yields

$$\boxed{\delta^* = \int_0^{y1} \left(1 - \frac{\rho u}{\rho_\infty U_\infty}\right) dy} \tag{6.63}$$

For incompressible flow, the equation becomes

$$\delta^* = \int_0^{y1} \left(1 - \frac{u}{U_\infty}\right) dy \tag{6.64}$$

We also know that $\frac{u}{U_\infty} = f'(\eta)$ and then

$$\delta^* = \sqrt{\frac{\mu x}{\rho U_\infty}} \int_0^{\eta 1} \left(1 - f'(\eta)\right) d\eta \tag{6.65}$$

$$\delta^* = \sqrt{\frac{\mu x}{\rho U_\infty}} [\eta_1 - f(\eta_1)] \tag{6.66}$$

If we then consider points of η_1 anywhere above the boundary-layer we observe with Matlab that $\eta_1 - f(\eta_1)$ is constant at a value of approximately 1.72. Therefore the approximated value of the displacement thickness can be expressed as

$$\boxed{\delta^*(x) = \frac{1.72x}{\mathrm{Re}_x^{1/2}}} \tag{6.67}$$

$$\boxed{\frac{\delta^*}{c} = \frac{1.72\left(\frac{x}{c}\right)^{1/2}}{\mathrm{Re}_c^{1/2}}} \tag{6.68}$$

Equation 6.68 indicates that the displacement thickness is proportional to the square root of x. Moreover, when we compare this result with the result in Equation 6.59 we find that for the flat-plate boundary layer $\underline{\delta^* = 0.35\delta}$.

6.6 The Momentum Thickness

Another useful boundary-layer property is the momentum thickness. Figure 6.6 will help to understand this concept.

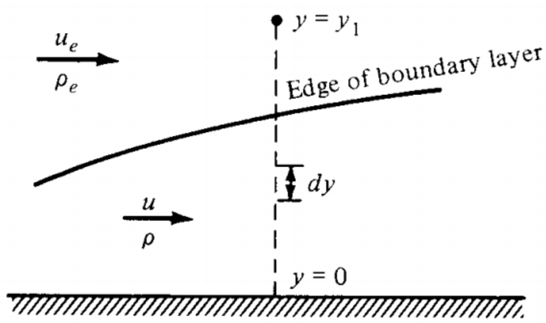

Figure 6.6: The Momentum Thickness [5]

Let us consider a mass flow through a segment dy which is given as

$$dm = \rho u dy \tag{6.69}$$

The momentum flow through this segment is then

$$dy = dm\ u = \rho u^2 dy \tag{6.70}$$

In a segment in the free stream, the momentum flow is

$$dy = dm\ U_\infty = \rho U_\infty u dy \tag{6.71}$$

And the decrement of momentum flow can be defined as

$$\rho u(U_\infty - u)dy \tag{6.72}$$

The integral from the wall to the streamline passing through $(0,y_1)$ will then give the total decrement.

$$\int_0^{y1} \rho u(U_\infty - u)dy \tag{6.73}$$

Let us now assume that the missing momentum flow in the free stream is $\rho_\infty U_\infty^2 \theta$. Then again, according to momentum conservation we can state

$$\rho_\infty U_\infty^2 \theta = \int_0^{y1} \rho u(U_\infty - u)dy \tag{6.74}$$

$$\boxed{\theta = \int_0^{y1} \frac{\rho u}{\rho_\infty U_\infty}\left(1 - \frac{u}{U_\infty}\right) dy} \tag{6.75}$$

We can again use the relation $\frac{u}{U_\infty} = f'(\eta)$.

$$\theta = \sqrt{\frac{\mu x}{U_\infty}} \int_0^{\eta 1} f'(\eta)(1 - f'(\eta))d\eta \tag{6.76}$$

Equation 6.76 can only be evaluated numerically and results in

$$\boxed{\theta(x) = \frac{0.664x}{\mathrm{Re}_x^{1/2}}} \tag{6.77}$$

$$\boxed{\frac{\theta}{c} = \frac{0.664\left(\frac{x}{c}\right)^{1/2}}{\mathrm{Re}_c^{1/2}}} \tag{6.78}$$

We find that the momentum thickness is proportional to the square root of x. We can also find, using previously obtained relations that for the flat-plate boundary layer $\underline{\theta = 0.13\delta}$ and $\underline{\theta = 0.39\delta^*}$.

7 The von Kármán and Pohlhausen Approximate Solution

Apart from the Blasius solution of the boundary-layer equation, it is also possible to use the von Kármán (and Pohlhausen) solution to determine the properties of the boundary layer from some approximated velocity profile of the flow above an infinitesimally thin flat plate. Let us return to the boundary-layer equations in Section 5.4.

$$\boxed{\frac{\partial u}{\partial x}+\frac{\partial v}{\partial y}=0 \qquad \text{Continuity}} \tag{7.1}$$

$$\boxed{u\frac{\partial u}{\partial x}+v\frac{\partial u}{\partial y}=-\frac{1}{\rho}\frac{dp_\infty}{dx}+\frac{\mu}{\rho}\left(\frac{\partial^2 u}{\partial y^2}\right) \qquad \text{x-momentum}} \tag{7.2}$$

$$\text{At the wall:} \qquad u(x,0)=0, \quad v(x,0)=0 \qquad \text{(no slip condition)} \tag{7.3}$$

$$\text{At the boundary layer edge:} \qquad u(x,\infty)=U_\infty \tag{7.4}$$

$$\text{And} \qquad \frac{\partial^k u}{\partial y^k}(x,\infty)=0 \tag{7.5}$$

Furthermore at the boundary layer edge:

$$\boxed{U_\infty\frac{dU_\infty}{dx}=-\frac{1}{\rho}\frac{dp_\infty}{dx} \qquad \text{(Euler's equation)}} \tag{7.6}$$

Using Equation 7.2 and 7.6, the x-momentum becomes

$$u\frac{\partial u}{\partial x}+v\frac{\partial u}{\partial y}=U_\infty\frac{dU_\infty}{dx}+\nu\left(\frac{\partial^2 u}{\partial y^2}\right) \qquad \left(\frac{\mu}{\rho}=\nu\right) \tag{7.7}$$

$$u\frac{\partial u}{\partial x}+v\frac{\partial u}{\partial y}-U_\infty\frac{dU_\infty}{dx}-\nu\left(\frac{\partial^2 u}{\partial y^2}\right)=0 \tag{7.8}$$

We can rewrite the left hand side using some mathematical manipulation.

$$(u-U_\infty)\left(\frac{\partial u}{\partial x}+\frac{\partial v}{\partial y}\right)=0 \qquad \text{(Continuity equation)} \tag{7.9}$$

$$u\frac{\partial u}{\partial x}+u\frac{\partial v}{\partial y}-U_\infty\frac{\partial u}{\partial x}-U_\infty\frac{\partial v}{\partial y}=0 \tag{7.10}$$

We can use this to rewrite expression 7.8.

$$u\frac{\partial u}{\partial x}+v\frac{\partial u}{\partial y}-U_\infty\frac{dU_\infty}{dx}-\nu\left(\frac{\partial^2 u}{\partial y^2}\right)+\left(u\frac{\partial u}{\partial x}+u\frac{\partial v}{\partial y}-U_\infty\frac{\partial u}{\partial x}-U_\infty\frac{\partial v}{\partial y}=0\right)=0 \tag{7.11}$$

Rewriting Equation 7.11 will eventually lead to

$$\nu\frac{\partial^2 u}{\partial y^2}=(U_\infty-u)\frac{dU_\infty}{dx}+u\frac{\partial(U_\infty-u)}{\partial x}+(U_\infty-u)\frac{\partial u}{\partial x} \tag{7.12}$$

$$\nu\frac{\partial^2 u}{\partial y^2}=(U_\infty-u)\frac{dU_\infty}{dx}+\frac{\partial}{\partial x}\left(u(U_\infty-u)\right) \tag{7.13}$$

Now integrate with respect to y and using the relation that $\left(\frac{\partial u}{\partial y}\right)_{y=0}=\frac{\tau_w}{\mu}$:

$$\nu\frac{\partial u}{\partial y}_{y=0}=\int_0^{y1}\left\{(U_\infty-u)\frac{dU_\infty}{dx}+\frac{\partial}{\partial x}\left(u(U_\infty-u)\right)\right\}dy \tag{7.14}$$

$$\nu\frac{\partial u}{\partial y}_{y=0}=\nu\frac{\tau}{\mu}=\frac{\tau}{\rho} \tag{7.15}$$

$$\frac{\tau}{\rho}=\frac{dU_\infty}{dx}\int_0^{y1}(U_\infty-u)dy+\frac{d}{dx}\int_0^{y1}u(U_\infty-u)dy \tag{7.16}$$

$$\frac{\tau}{\rho}=\frac{dU_\infty}{dx}U_\infty\int_0^{y1}(1-\frac{u}{U_\infty})dy+\frac{d}{dx}U_\infty^2\int_0^{y1}\frac{u}{U_\infty}(1-\frac{u}{U_\infty})dy \tag{7.17}$$

Let us now recall the equations for the displacement thickness and momentum integral for incompressible flow, Equation 6.75 and 6.63. We can substitute Equation 6.75 and 6.63 to obtain the von Kármán momentum integral for incompressible flow

$$\frac{\tau}{\rho} = \frac{dU_\infty}{dx} U_\infty \delta^* + \frac{d}{dx} U_\infty^2 \theta \tag{7.18}$$

In order to obtain an equation for the boundary-layer thickness $\delta(x)$we need to assume a velocity profile. A second, third and (Pohlhausen's) fourth-order polynomial function will be used to approximate the velocity profile.

7.1 Second Order Velocity Profile

A second-order, quadratic function is of the form

$$u(x, y) = a + by + cy^2 \tag{7.19}$$

Three boundary conditions are needed to determine the coefficients.

$$\begin{aligned} \text{At the wall :} \qquad & u(0) = 0 \\ \text{At the boundary layer edge :} \qquad & u(\delta) = U_\infty \quad \text{and} \quad \frac{\partial u(\delta)}{\partial y} = 0 \end{aligned}$$

Applying the boundary conditions we find the unknown parameters

$$a = 0 \qquad b = \frac{2U_\infty}{\delta(x)} \qquad c = -\frac{U_\infty}{\delta(x)} \tag{7.20}$$

$$\text{so that} \quad \frac{u(x, y)}{U_\infty} = 2\frac{y}{\delta}\left(1 - \frac{1}{2}\frac{y}{\delta}\right) \tag{7.21}$$

We have obtained a result similar to the Blasius equation except that here $\eta = \frac{y}{\delta(x)}$.

$$\frac{u(\eta)}{U_\infty} = 2\eta - \eta^2 \quad \text{for} \quad \eta \in [0, 1] \quad \text{and} \tag{7.22}$$

$$\frac{u(\eta)}{U_\infty} = 1 \quad \text{for} \quad \eta \geq 1. \tag{7.23}$$

Subsequently, we want to derive an expression for the boundary-layer thickness. Let us return to Equation 7.18.

$$\frac{\tau}{\rho} = \frac{dU_\infty}{dx} U_\infty \delta^* + \frac{d}{dx} U_\infty^2 \theta \tag{7.24}$$

Analysing the equation, we observe that the free stream velocity U_∞ is constant (i.e. for the Blasius solution) and the equation reduces to

$$\frac{\tau_w}{\rho} = \frac{d}{dx} U_\infty^2 \theta \tag{7.25}$$

If we derive the expressions for τ_w and θ (which has the boundary layer thickness included), we obtain an expression for the boundary-layer thickness $\delta(x)$.

$$\theta = \int_0^{y1} \frac{u}{U_\infty}\left(1 - \frac{u}{U_\infty}\right) dy \tag{7.26}$$

$$\frac{\theta}{\delta} = \int_0^{y,1\delta} \frac{u}{U_\infty}\left(1 - \frac{u}{U_\infty}\right) d\eta \tag{7.27}$$

Substituting Equation 7.22 in Equation 7.27 we obtain

$$\frac{\theta}{\delta} = \frac{2}{15} \tag{7.28}$$

The wall shear stress is defined as

$$\tau_w = \mu \left(\frac{\partial u}{\partial y}\right)_{y=0} \tag{7.29}$$

For this quadratic function τ_w becomes

$$\tau_w = \frac{2\mu U_\infty}{\delta(x)} \tag{7.30}$$

Combining Equation 7.30 and 7.28 in Equation 7.25

$$\frac{2\mu U_\infty}{\delta(x)} = \rho U_\infty^2 \frac{d\delta}{dx}\frac{2}{15} \tag{7.31}$$

We can now rearrange and integrate to derive the boundary layer thickness.

$$\int_0^\delta \delta'(x)\delta dx = \int_0^x \frac{15\mu}{\rho U_\infty} dx \tag{7.32}$$

$$\delta(x) = \frac{\sqrt{30}x}{\mathrm{Re}_x^{1/2}} \tag{7.33}$$

$$\boxed{\delta(x) = \frac{5.48x}{\mathrm{Re}_x^{1/2}}} \tag{7.34}$$

$$\boxed{\frac{\delta}{c} = \frac{5.48\left(\frac{x}{c}\right)^{1/2}}{\mathrm{Re}_c^{1/2}}} \tag{7.35}$$

Another parameter we want to derive is the local skin friction coefficient $c_f(x)$ which is defined as

$$c_f = \frac{\tau}{\frac{1}{2}\rho U_\infty^2} \tag{7.36}$$

And the total skin friction coefficients

$$C_f = \frac{1}{c}\int_0^c c_f dx \tag{7.37}$$

Substituting the obtained expressions of the boundary-layer thickness δ in the stress tensor τ and subsequently in the local skin friction coefficient we derive the expressions for the local and total skin friction coefficients.

$$\boxed{c_f(x) = \frac{0.73}{\mathrm{Re}_x^{1/2}} = \frac{0.73}{\mathrm{Re}_c^{1/2}}\left(\frac{x}{c}\right)^{-1/2}} \tag{7.38}$$

$$\boxed{C_f = \frac{1.46}{\mathrm{Re}_c^{1/2}}} \tag{7.39}$$

7.2 Third Order Velocity Profile

Let us now consider a third-order, cubic function

$$u(x,y) = a + by + cy^2 + dy^3 \tag{7.40}$$

The function can also be written in terms of η

$$\frac{u(x,y)}{U_\infty} = a + b\eta + c\eta^2 + d\eta^3 \qquad\qquad \eta = \frac{y}{\delta} \tag{7.41}$$

To determine the coefficients, we will need an additional boundary condition. Let us examine the x-momentum. On the wall (y=0), we previously derived

$$-\frac{1}{\rho}\frac{\partial p}{\partial x} + \nu \frac{\partial^2 u}{\partial y^2}_{y=0} = 0 \tag{7.42}$$

Substituting Equation 7.6 in 7.42 we obtain the additional boundary condition

$$\left(\frac{\partial^2 u}{\partial y^2}\right)_{y=0} = -\frac{U_\infty}{\nu}\frac{dU_\infty}{dx} \tag{7.43}$$

Let us define

$$\boxed{-\frac{U_\infty}{\nu}\frac{dU_\infty}{dx} = -\Lambda} \tag{7.44}$$

The boundary conditions are

$$f(0) = 0 \qquad f(1) = 1 \qquad f'(1) = 0 \qquad f''(0) = -\Lambda \tag{7.45}$$

Solving the set of equations, we obtain

$$a = 0 \qquad b = \frac{3}{2} + \frac{1}{4}\Lambda \qquad c = -\frac{1}{2}\Lambda \qquad d = -\frac{1}{2} + \frac{1}{4}\Lambda \tag{7.46}$$

$$\text{so that} \quad \frac{u(x,y)}{U_\infty} = \frac{3}{2}\eta - \frac{1}{2}\eta^3 + \Lambda\frac{1}{4}\eta(\eta-1)^2 \quad \text{for} \quad \eta \in [0,1] \quad \text{and} \tag{7.47}$$

$$\frac{u(\eta)}{U_\infty} = 1 \quad \text{for} \quad \eta \geq 1. \tag{7.48}$$

Using the same steps as for the second-order velocity profile, we obtain the expressions for the momentum integral, wall shear stress and boundary layer thickness. We again use the assumption that the free stream velocity is constant i.e. the Blasius solution ($\Lambda = 0$).

$$\frac{\theta}{\delta} = \frac{234}{1680} \tag{7.49}$$

$$\tau_w = \frac{3\mu U_\infty}{2\delta(x)} \tag{7.50}$$

$$\boxed{\delta(x) = \frac{4.64x}{\mathrm{Re}_x^{1/2}}} \tag{7.51}$$

$$\boxed{\frac{\delta}{c} = \frac{4.64\left(\frac{x}{c}\right)^{1/2}}{\mathrm{Re}_c^{1/2}}} \tag{7.52}$$

With the derived expressions of the boundary-layer thickness and wall shear stress, we can derive the skin friction coefficients

$$\boxed{c_f(x) = \frac{0.647}{\mathrm{Re}_x^{1/2}} = \frac{0.647}{\mathrm{Re}_c^{1/2}}\left(\frac{x}{c}\right)^{-1/2}} \tag{7.53}$$

$$\boxed{C_f = \frac{1.29}{\mathrm{Re}_c^{1/2}}} \tag{7.54}$$

7.3 Pohlhausen's Fourth Order Velocity Profile

We will finally consider a fourth-order, quartic velocity profile which was used by Pohlhausen.

$$\frac{u(x,y)}{U_\infty} = a + b\eta + c\eta^2 + d\eta^3 + e\eta^4 \tag{7.55}$$

The additional boundary condition comes from the boundary condition at the edge of the boundary layer where all the derivatives ($\frac{\partial^k u}{\partial y^k}$ =0 for k≥1) because the velocity becomes uniform. Therefore, all the boundary conditions are:

$$f(0) = 0 \qquad f(1) = 1 \qquad f'(1) = 0 \qquad f''(1) = 0 \qquad f''(0) = \Lambda \tag{7.56}$$

Solving the set of equations gives us the coefficients

$$a = 0 \qquad b = \frac{1}{6}\Lambda + 2 \qquad c = -\frac{1}{2}\Lambda \qquad d = \frac{1}{2}\Lambda - 2 \qquad e = -\frac{1}{6}\Lambda + 1 \tag{7.57}$$

$$\frac{u(x,y)}{U_\infty} = 2\eta - 2\eta^3 + \eta^4 + \Lambda\frac{1}{6}\eta(\eta-1)^3 \quad \text{for} \quad \eta \in [0,1] \quad \text{and} \tag{7.58}$$

$$\frac{u(\eta)}{U_\infty} = 1 \quad \text{for} \quad \eta \geq 1. \tag{7.59}$$

The equations for the momentum integral, wall shear stress and boundary-layer thickness (while assuming a constant free stream velocity, $\Lambda = 0$) then become

$$\frac{\theta}{\delta} = \frac{37}{315} \tag{7.60}$$

$$\tau_s = \frac{2\mu U_\infty}{\delta(x)} \tag{7.61}$$

$$\boxed{\delta(x) = \frac{5.84x}{\mathrm{Re}_x^{1/2}}} \tag{7.62}$$

$$\boxed{\frac{\delta}{c} = \frac{5.84\left(\frac{x}{c}\right)^{1/2}}{\mathrm{Re}_c^{1/2}}} \tag{7.63}$$

With the derived expressions of the boundary layer thickness and stress tensor we can derive the skin friction coefficients

$$\boxed{c_f(x) = \frac{0.685}{\mathrm{Re}_x^{1/2}} = \frac{0.685}{\mathrm{Re}_c^{1/2}}\left(\frac{x}{c}\right)^{-1/2}} \tag{7.64}$$

$$\boxed{C_f = \frac{1.37}{\mathrm{Re}_c^{1/2}}} \tag{7.65}$$

8 Comparison of the Blasius and von Kármán Approximations

The boundary-layer thickness and velocity profiles are compared below.

$$\text{Blasius}: \delta(x) = \frac{4.92x}{\mathrm{Re}_x^{1/2}} \qquad u(x,y) = U_\infty f'(\eta)$$

$$\text{Second-Order}: \delta(x) = \frac{5.48x}{\mathrm{Re}_x^{1/2}} \qquad \frac{u(x,y)}{U_\infty} = 2\eta - \eta^2$$

$$\text{Third-Order}: \delta(x) = \frac{4.64x}{\mathrm{Re}_x^{1/2}} \qquad \frac{u(x,y)}{U_\infty} = \frac{3}{2}\eta - \frac{1}{2}\eta^3 + \Lambda\frac{1}{4}\eta(\eta-1)^2$$

$$\text{Fourth-Order}: \delta(x) = \frac{5.84x}{\mathrm{Re}_x^{1/2}} \qquad \frac{u(x,y)}{U_\infty} = 2\eta - 2\eta^3 + \eta^4 + \Lambda\frac{1}{6}\eta(\eta-1)^3$$

In order to compare the Blasius solution to the von Kármán solutions we first need to find a relation between the two.

$$\text{Blasius}: \eta = y\sqrt{\frac{U_\infty \rho}{\mu x}} = \frac{y}{x}\mathrm{Re}_x^{1/2} \tag{8.1}$$

$$\text{von Kármán}: \eta = \frac{y}{\delta(x)} \tag{8.2}$$

When we substitute the boundary layer thickness, obtained from the Blasius solution, into Equation 8.2, we obtain the relation

$$\eta_{Blasius} = 4.92\eta \tag{8.3}$$

In Figure 8.1, η is plotted against $\frac{u}{U_\infty}$ and the four velocity profiles are compared.

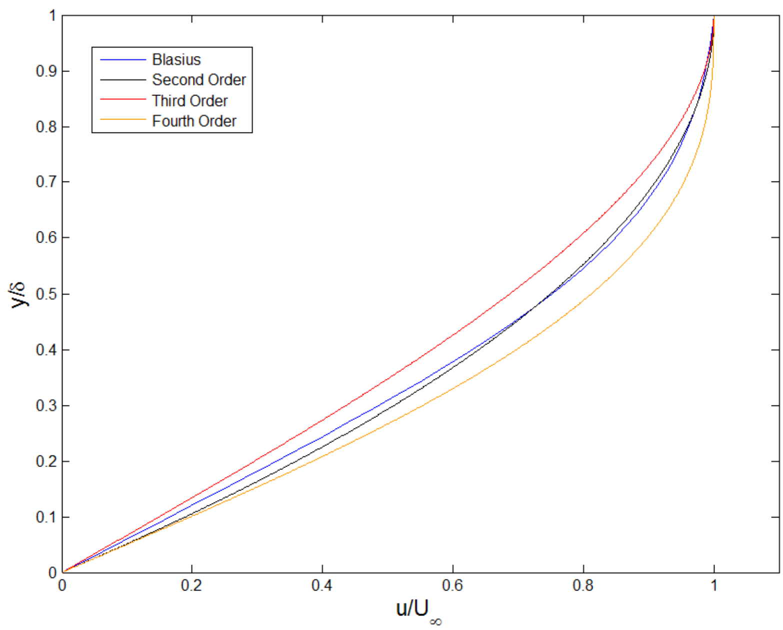

Figure 8.1: Comparison of the velocity profiles

The second-order velocity profile appears to be closest to the Blasius solution. The third and fourth-order models deviate substantially from the Blasius equation.

The results of the boundary layer thickness are shown in Figure 8.2.

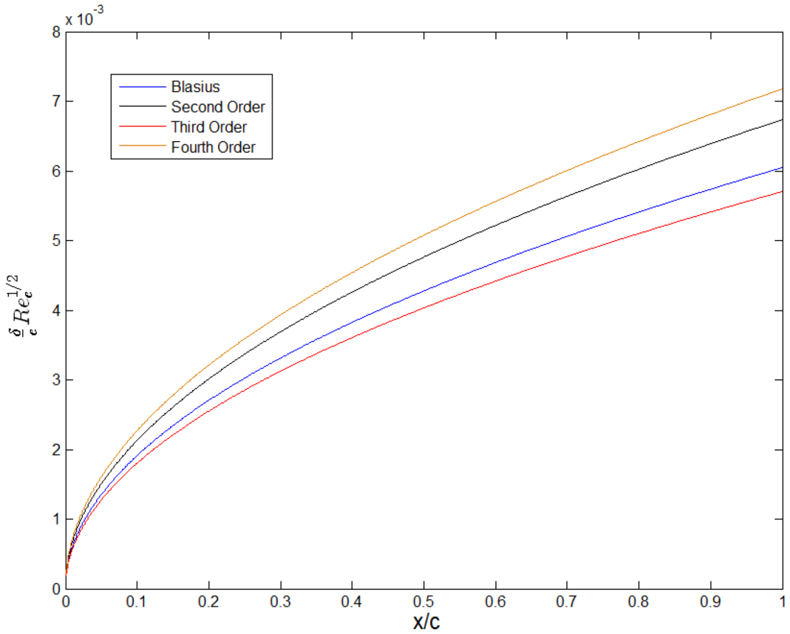

Figure 8.2: Comparison of the boundary-layer thickness

In Figure 8.2 we observe that the second-order approximation is relatively close to the Blasius solution. The boundary-layer thickness graph shows even more deviation between the Blasius equation and the fourth-order approximation. The third-order approximation seems more accurate here.

The skin friction coefficients for the Blasius and von Kármán are listed below and are plotted in Figure 8.3.

$$\text{Blasius}: c_f = \frac{0.664}{\mathrm{Re}_x^{1/2}} \qquad C_f = \frac{1.328}{\mathrm{Re}_c^{1/2}}$$
$$\text{Second Order}: c_f = \frac{0.73}{\mathrm{Re}_x^{1/2}} \qquad C_f = \frac{1.46}{\mathrm{Re}_c^{1/2}}$$
$$\text{Third Order}: c_f = \frac{0.647}{\mathrm{Re}_x^{1/2}} \qquad C_f = \frac{1.29}{\mathrm{Re}_c^{1/2}}$$
$$\text{Fourth Order}: c_f = \frac{0.685}{\mathrm{Re}_x^{1/2}} \qquad C_f = \frac{1.37}{\mathrm{Re}_c^{1/2}}$$

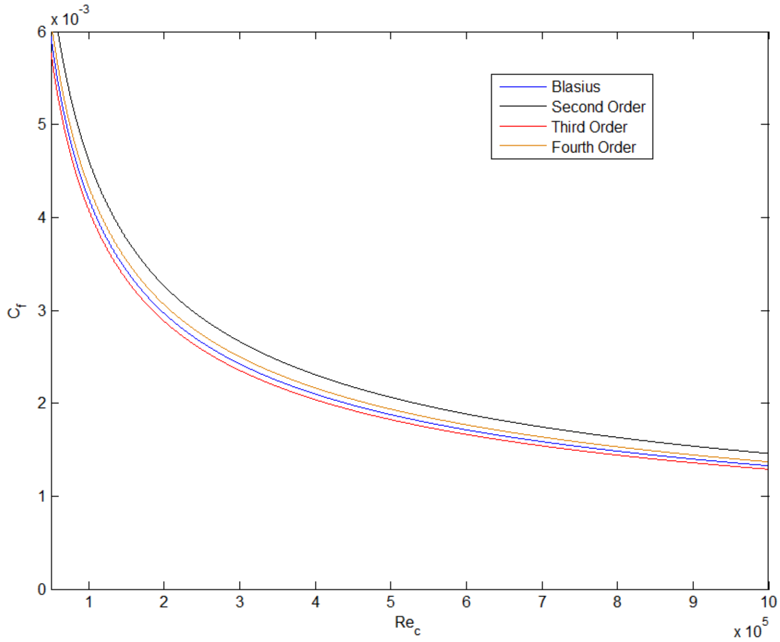

Figure 8.3: Comparison of the Skin Friction coefficients

The comparison of the skin friction coefficients shows that the third and fourth-order are closest to the Blasius solution. The second-order deviates the most in this plot.

Overall it is difficult to say which von Kármán approximation fits best with the Blasius equation. The different plots show different results. A comparison with experimental results should show which von Kármán approximation fits best.

9 The Velocity Boundary Layer for Turbulent Flow

Turbulence is still an unsolved problem in fluid dynamics. The formulas used to describe turbulence here are therefore based on data from experiments combined with theory.

9.1 The Boundary Layer Thickness

The velocity boundary layer thickness for incompressible turbulent flow over a flat plate is given as

$$\boxed{\delta(x) \cong \frac{0.37x}{\mathrm{Re}_x^{1/5}}} \tag{9.1}$$

$$\boxed{\frac{\delta}{c} \cong \frac{0.37}{\mathrm{Re}_c^{1/5}} \left(\frac{x}{c}\right)^{4/5}} \tag{9.2}$$

Instead of the velocity boundary layer thickness to be proportional to $x^{-1/2}$ for laminar flow, it is proportional to $x^{-4/5}$ for turbulent flow. Figure 9.1 shows the difference between laminar and turbulent flow for an air flow of 15m/s i.e. Re_c=$1 \cdot 10^6$.

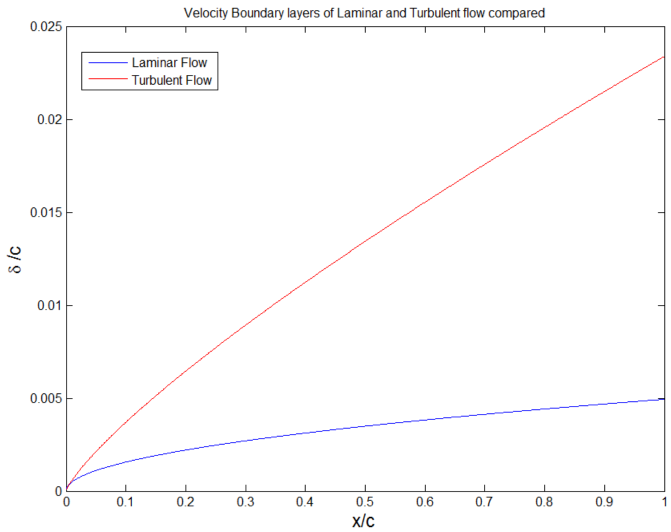

Figure 9.1: The comparison of the velocity boundary-layers for laminar and turbulent flow Re_c=$1 \cdot 10^6$

9.2 The Skin Friction Coefficients

The local and total skin friction drag coefficient for incompressible turbulent flow over an infinitesimally flat plate are given as

$$\boxed{c_f(x) \cong \frac{0.0592}{\mathrm{Re}_c^{1/5}} \left(\frac{x}{c}\right)^{-1/5}} \tag{9.3}$$

$$\boxed{C_f \cong \frac{0.074}{\mathrm{Re}_c^{1/5}}} \tag{9.4}$$

Note that for the laminar flow the skin friction coefficient was proportional to $\mathrm{Re}_c^{-1/2}$ and for turbulent flow it is proportional to $\mathrm{Re}_c^{-1/5}$.

9.3 The Power Law Velocity Profile

The velocity profile for turbulent flow, which is based on empirical data and was suggested by Prandtl, is the power law velocity profile

$$\frac{u}{U_\infty} = \left(\frac{y}{\delta}\right)^{1/n} \tag{9.5}$$

where the n-component is a function of the Reynolds number. For a flat plate n is somewhere between 5 and 7, depending on the properties of the plate.

10 Transitional Flow

The complete flow over a flat plate is illustrated in Figure 10.1.

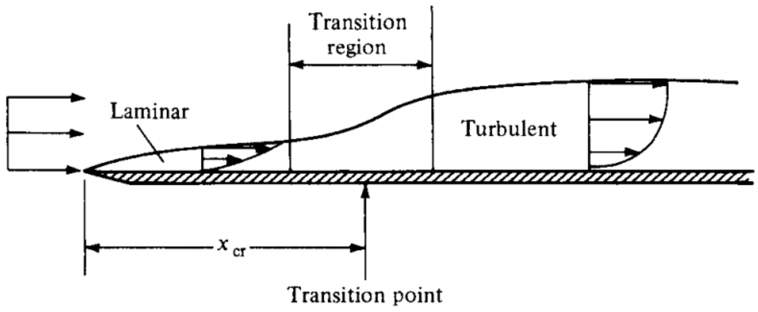

Figure 10.1: Laminar transition to turbulent flow [5]

10.1 Transition

From the leading edge the flow in the boundary-layer will be laminar. Friction will retard the flow and will cause the boundary layer thickness to increase. At a specific critical distance, transition will occur from laminar to turbulent flow. This transition will occur within a finite region of the plate. However, for simplicity we will assume the transition region as a single point, the transition point. The critical Reynolds number is defined as

$$\mathrm{Re}_{cr} = \frac{\rho_\infty U_\infty x_{cr}}{\mu_\infty} \tag{10.1}$$

In most cases the critical Reynolds number for air flow over a flat plate will be approximately 500,000, based on empirical data. The critical Reynolds number for the plate we will use will be determined experimentally. For now we will just assume it to be 500,000. At a free stream velocity of 10 m/s, transition will take place at

$$x_{cr} = \frac{\mathrm{Re}_{cr}\nu}{U_\infty} = 0.7556m \tag{10.2}$$

A graph which illustrates the boundary-layer thickness for a critical Reynolds number of 500,000 and free stream velocity of 10 m/s and 20 m/s with laminar and turbulent flow is shown below. The transition region is not taken into account. The Blasius solution is used for the laminar boundary layer thickness.

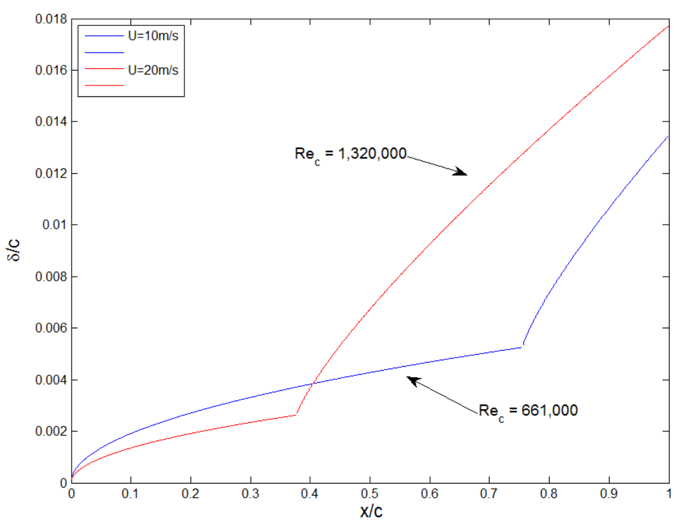

Figure 10.2: Laminar to Turbulent flow over flat plate

There are a number of factors that can have an influence on the boundary layer transition [3]:

1. The Streamwise Pressure Gradient
2. The Surface Roughness
3. The Turbulence Level in the Wind Tunnel
4. The Wall Temperature
5. Suction
6. Vibrations of the plate itself
7. Acoustic Disturbances

In current understandings, transition to turbulence is caused by the development of unstable Tollmien-Schlichting waves. Initially, disturbances in the boundary-layer will develop into unstable modes which will grow downstream inside the boundary layer. When these modes reach a certain amplification, the flow becomes turbulent. This amplification factor is used in the modelling of the flow over the plate in XFOIL and is further discussed in section 11.4. However, detailed theory on the Tollmien-Schlichting will not be further addressed in this report.

Figure 10.3 below shows the critical distance as a function of the free stream velocity plotted for different critical Reynolds numbers.

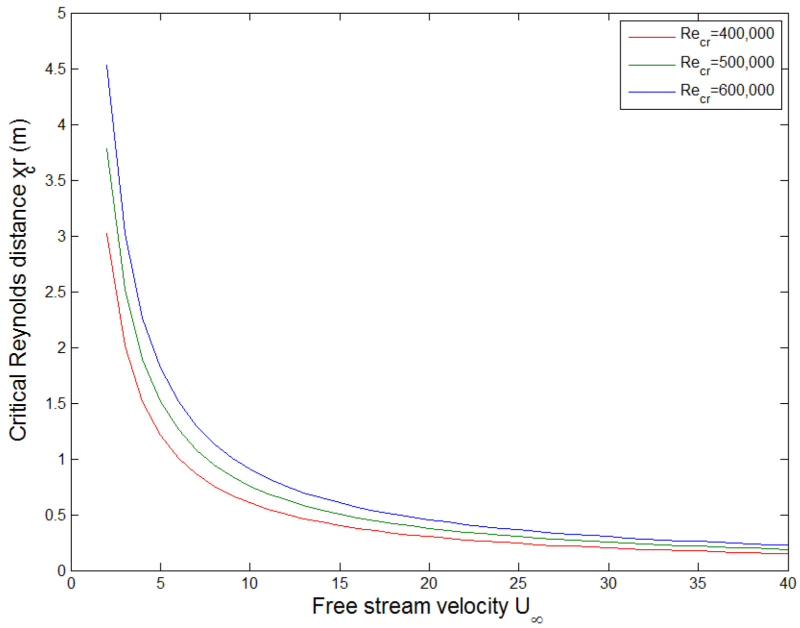

Figure 10.3: The Boundary Layer Thickness as a function of the free stream velocity

10.2 The Skin Friction Coefficient

We would also like to find the total skin friction coefficient for transitional flow. The local skin friction coefficients for laminar and turbulent flow were defined as

$$\text{Laminar} : c_f(x) = \frac{0.664}{\text{Re}_c^{1/2}} \left(\frac{x}{c}\right)^{-1/2} \qquad \text{(Blasius)}$$

$$\text{Turbulent} : c_f(x) \cong \frac{0.0592}{\text{Re}_c^{1/5}} \left(\frac{x}{c}\right)^{-1/5}$$

We now need to integrate piecewise to obtain the total skin friction coefficient for the entire plate.

Laminar and Turbulent flow:

$$C_f = \frac{1}{c}\int_0^{x_{cr}} \frac{0.664}{\mathrm{Re}_c^{1/2}}\left(\frac{x}{c}\right)^{-1/2} dx + \frac{1}{c}\int_{x_{cr}}^{c} \frac{0.059}{\mathrm{Re}_c^{1/5}}\left(\frac{x}{c}\right)^{-1/5} dx \tag{10.3}$$

$$C_f = \frac{1.33}{\mathrm{Re}_c^{1/2}}\left(\frac{x_{cr}}{c}\right)^{1/2} + \frac{0.074}{\mathrm{Re}_c^{1/5}}\left(1-\left(\frac{x_{cr}}{c}\right)^{4/5}\right) \tag{10.4}$$

$$\boxed{C_f = \frac{0.074}{\mathrm{Re}_c^{1/5}} + \frac{1}{\mathrm{Re}_c}\left(0.074\mathrm{Re}_{cr}^{4/5} - 1.33\mathrm{Re}_{cr}^{1/2}\right)} \tag{10.5}$$

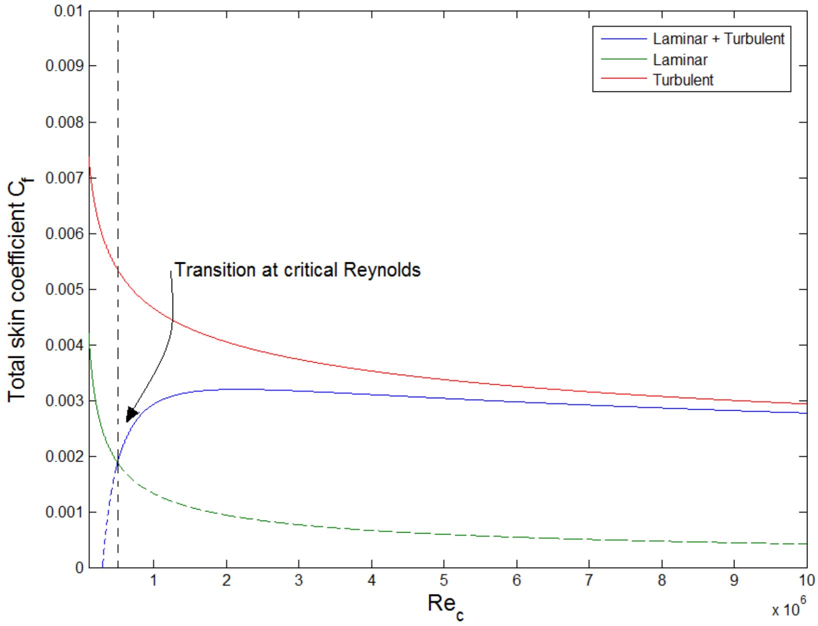

Figure 10.4: The total skin friction coefficient for Re_{cr}=500,000

10.3 The Drag Coefficient

In the experiments, the force by the air flow on the plate due to friction will be measured. To compare the results with the theory we need to obtain an expression for the drag coefficient. The drag coefficient for laminar flow is defined as

$$C_d \equiv \frac{2D}{\rho_\infty U_\infty^2 S} \tag{10.6}$$

Where ρ_∞ is the density far away in the stream, U_∞ is the free stream velocity, S is the reference area and D is the total drag force on the plate.

The drag force D over the entire plate, where w is the width of the plate is then

$$D = 2w\int_0^c \tau_w dx \tag{10.7}$$

With the definition of τ_w, the drag force for laminar flow becomes

$$D = 0.6640 * 2wc\left(\frac{\rho\mu U_\infty^3}{c}\right)^{1/2} \tag{10.8}$$

Substituting the obtained expression for D into the equation for the drag coefficient and rewriting will result in the total drag force coefficient of both sides of the plate

$$C_d = \frac{2.656}{\mathrm{Re}_c^{1/2}} \tag{10.9}$$

For Turbulent flow, the drag coefficient is given as

$$C_d = \frac{0.148}{\mathrm{Re}_c^{1/5}} \tag{10.10}$$

11 Flow over a Flat Plate Predicted by XFOIL

The plate that is used in the experiments is modelled using XFOIL (Version 6.99). Appendix A shows the dimensions of the plate. The leading edge is defined by a Hermite polynomial shape (set up by H.W.M. Hoeijmakers) in combination with a square root function and has a length of 5% of the entire plate. The trailing edge has a very sharp and fragile profile, defined by the last 70% of a NACA 4-series with a length of 20% of the plate. The plate has a thickness of 10mm, width of 890mm and length of 1000mm. The Matlab code which is used to generate the coordinates for XFOIL is shown in Appendix B.

The critical amplification factor in XFOIL is set to 5, which is most suitable for the silent Wind Tunnel of the UT as will be described in section 11.4.

11.1 The Leading Edge

The shape of the leading edge is described by a Hermite polynomial in combination with a square root function. The Hermite polynomial function is continuous in function value, slope, curvature and curvature derivative. The root function completes the nose and connects it with the middle section of the plate. The function of the plate in an (x,y) coordinate system is defined as

$$y(\xi) = \frac{t}{2}\left[b_1\xi^{1/2} + b_2\xi^{3/2} + f(0)P_1(\xi) + f'(0)Q_1(\xi) + f(1)P_2(\xi) + f'(1)Q_2(\xi)\right] \tag{11.1}$$

With

$$\xi = \frac{x - x_{nose}}{x_{plate} - x_{nose}} \qquad b_1 = \sqrt{8\frac{\Delta x}{t}\frac{(-R(0))}{t}}$$

$$b_2 = -16 + 5b_1$$

$$\begin{aligned} P_1(\xi) &= (1-\xi)^2(1+2\xi) & f(0) &= 0 \\ P_2(\xi) &= 1 - P_1(\xi) & f(1) &= 1 - b_1 - b_2 \\ Q_1(\xi) &= (1-\xi)^2\xi & f'(0) &= 3 - \frac{15}{8}b_1 - \frac{3}{8}b_2 \\ Q_2(\xi) &= -\xi^2(1-\xi) & f'(1) &= -\frac{1}{2}b_1 - \frac{3}{2}b_2 \end{aligned}$$

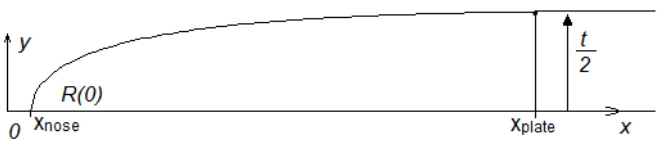

Figure 11.1: The Leading Edge

There are two free parameters, the length of the nose (Δx) and the radius of the leading edge ($R(0)$). These values are made dimensionless with the thickness t of the plate. The choice made for the present plate is

$$\frac{\Delta x}{t} = 5 \qquad \frac{R(0)}{t} = 0.2$$

The resulting shape of the leading edge is shown in Appendix A.

11.2 The Trailing Edge

The shape of the trailing edge is determined by the last 70% of a NACA 4-series and is 20% of the plate length. The NACA 4-series has a constant value and slope, but not a constant curvature. The function describing the coordinates is defined as:

$$\frac{y}{c} = \pm\frac{t}{2}\left[0.2969\sqrt{\frac{x}{c}} - 0.1260\left(\frac{x}{c}\right) - 0.3516\left(\frac{x}{c}\right)^2 + 0.2843\left(\frac{x}{c}\right)^3 - 0.01015\left(\frac{x}{c}\right)^4\right] \tag{11.2}$$

With $x = 0$ the location of the leading edge of the airfoil and $x = c$ its trailing edge. The resulting shape is shown in Appendix A.

11.3 Point Distribution

It was chosen to use a non-uniform point distribution, where the leading edge and trailing edge have about 4.5 times more points than the middle section. The maximum number of points you can use is 1000 (XFOIL does not allow more). The Matlab code in Appendix B shows how many points (i.e. panels) were eventually used for each section.

11.4 Turbulence Level of the Silent Wind Tunnel

It is given that the turbulence level (i.e. the environmental disturbance) of the Silent Wind Tunnel is determined as approximately 0.25% [9]. However, XFOIL uses the semi-empirical e^n method (based on linear stability theory) and it works with the amplification factor N (based on the Tollmien-Schlichting instability). The relation between the N-factor and turbulence level is [4]

$$N_T = -8.34 - 2.4\ln(\mathrm{Tu}) \tag{11.3}$$

The relation is graphically shown in Figure 11.2 and only holds for Tu>0.1%. It is based on Mack's relationship who proposed to (empirically) relate the N factor to the turbulence level.

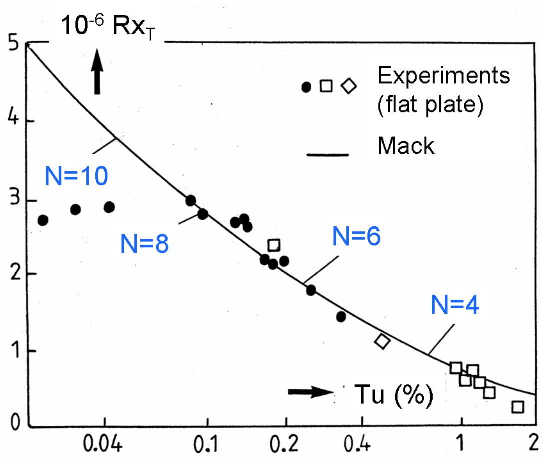

Figure 11.2: The e^n method related to the turbulence level according to Mack's relationship [6]

Using Equation 11.3 we find that for a turbulence level of 0.25%, the N factor is 5.02.

11.5 The Pressure Coefficient

First, we are interested in the dimensionless pressure coefficient [5] because it will give insight in the pressure gradient of the plate. The pressure gradient will indicate if the plate behaves as a infinitesimally flat plate. For a perfect flat plat $C_p = 0$ all along the surface of the plate. The pressure coefficient is defined as

$$\boxed{C_p \equiv \frac{p - p_\infty}{\frac{1}{2}\rho_\infty U_\infty^2}} \tag{11.4}$$

and it describes the dimensionless pressure throughout the flow. Where p is the static pressure at the point of interest, p_∞ is the free stream static pressure and ρ_∞ is the free stream density. The pressure coefficient describes the relative pressure throughout the flow. When the pressure coefficient is zero, the pressure is the same as in the free stream velocity. For $\mathrm{Re}_c = 5 \cdot 10^5$ the pressure coefficient along the plate is shown in Figure 11.3.

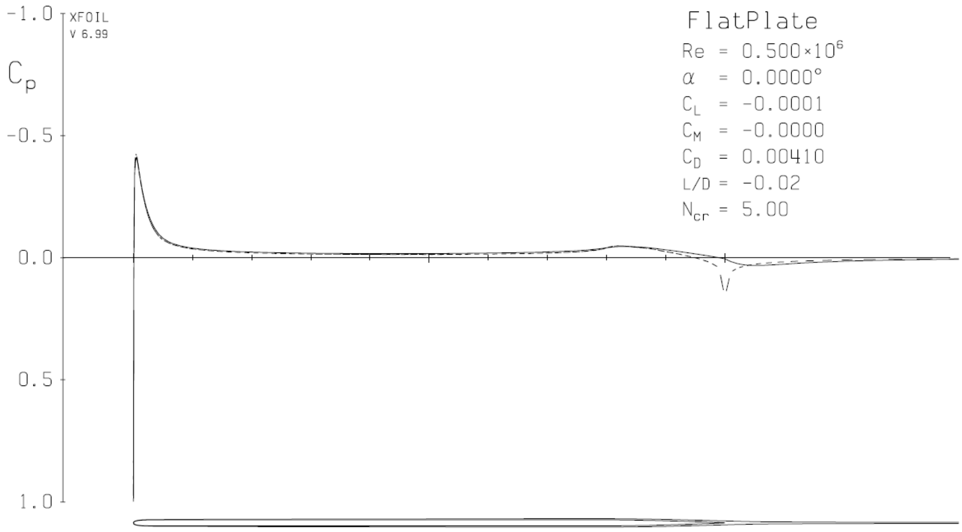

Figure 11.3: The pressure coefficient along the plate for a flow of $\text{Re}_c = 5 \cdot 10^5$

The graph shows us that the pressure coefficient along the plate is very close to zero which confirms that we can assume that the pressure along the plate is close to the free stream pressure and the velocity outside the boundary layer is close to the free stream velocity. The stagnation point (where C_p=1) can also be observed. Moreover, at the leading edge we observe that the pressure coefficient becomes negative indicating that the pressure becomes lower than the free stream pressure and the velocity exceeds the free stream value ($\frac{U}{U_\infty} \approx 1.2$). The results for a Reynolds number of $1 \cdot 10^6$ and $2 \cdot 10^6$ are shown in Figure 11.4 and 11.5 respectively

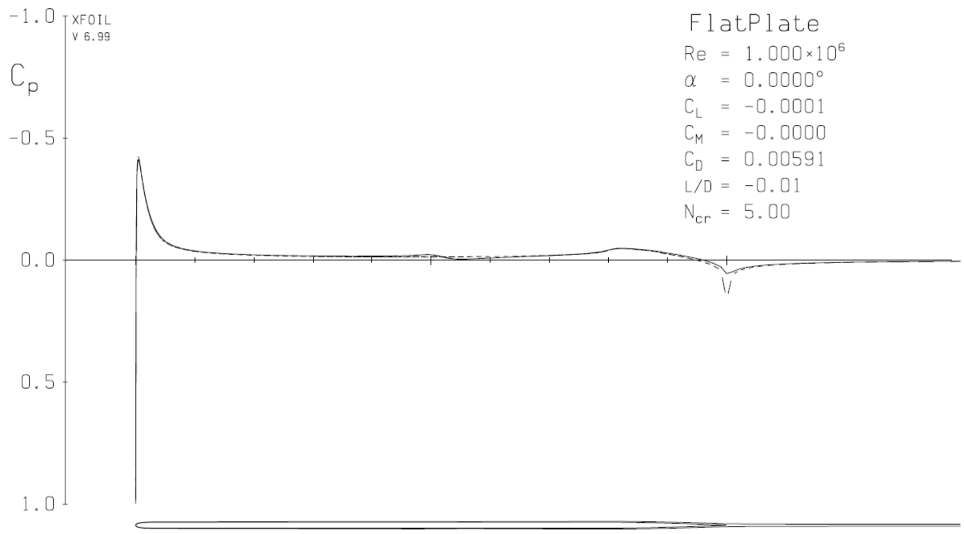

Figure 11.4: The pressure coefficient along the plate for a flow of $\text{Re}_c = 1 \cdot 10^6$

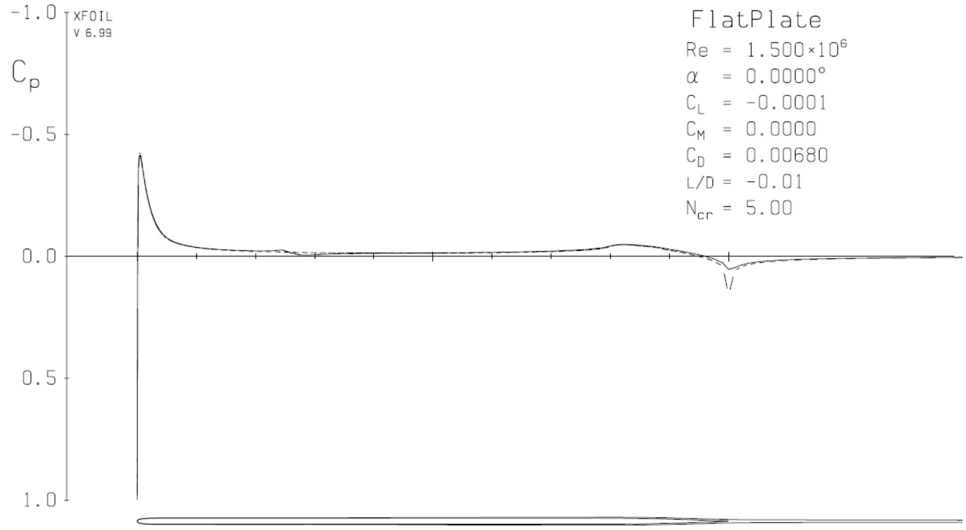

Figure 11.5: The pressure coefficient along the plate for a flow of $\mathrm{Re}_c = 1.5 \cdot 10^6$

The figures indicate that for higher Reynolds numbers, the flow can still be considered to be very similar to the flow along a flat plate of infinitesimally thickness placed flush in a uniform free stream. Therefore the Blasius solution should (with some accuracy) describe the flow over this plate.

11.6 The Skin Friction Coefficient

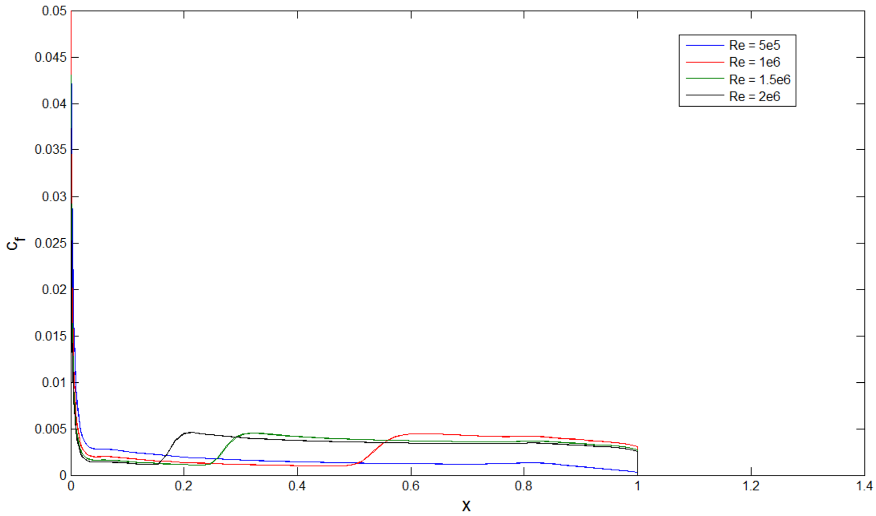

Figure 11.6: The local skin friction coefficient for various Reynolds numbers

The local skin friction coefficient is plotted in Figure 11.6 for various Reynolds numbers. The Reynolds number of $\mathrm{Re}_c = 5 \cdot 10^5$ shows the skin friction coefficient with full laminar flow. Higher Reynolds numbers show a transition from laminar to turbulent flow. The distance of the transition point from the leading edge decreases for increasing Reynolds numbers; Re_c=1e6, Re_c=1.5e6 and Re_c=2e6 result in $x_{tr}/c = 0.49$, 0.24 and 0.15 respectively.

11.6.1 XFOIL compared to the (Blasius) Theory

We would like to compare the XFOIL results with the (Blasius) theory to investigate if the plate behave as an infinitesimally flat plate. Figure 11.7 shows the local skin friction coefficient for a flow with $\mathrm{Re}_c = 5 \cdot 10^5$ (fully laminar) from XFOIL and the Blasius Theory .

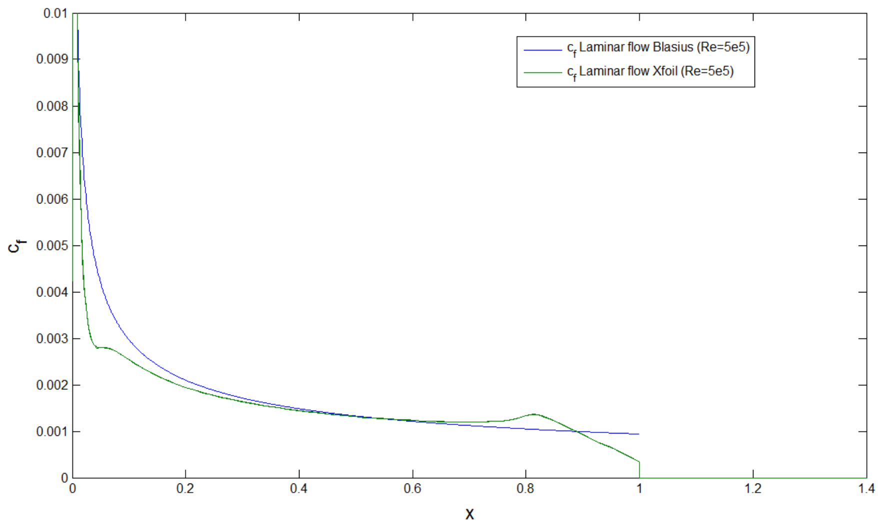

Figure 11.7: Comparison of the local skin friction coefficients for laminar flow of $\mathrm{Re}_c = 5 \cdot 10^5$

Apart from the deviation caused by the geometry of the plate used in XFOIL, the local skin friction coefficient for laminar flow, obtained from XFOIL is observed to be quite similar to the value of the skin friction coefficient according to Blasius' solution. The result for a (predominantly) turbulent flow with $\mathrm{Re}_c = 2 \cdot 10^6$ is shown in Figure 11.8.

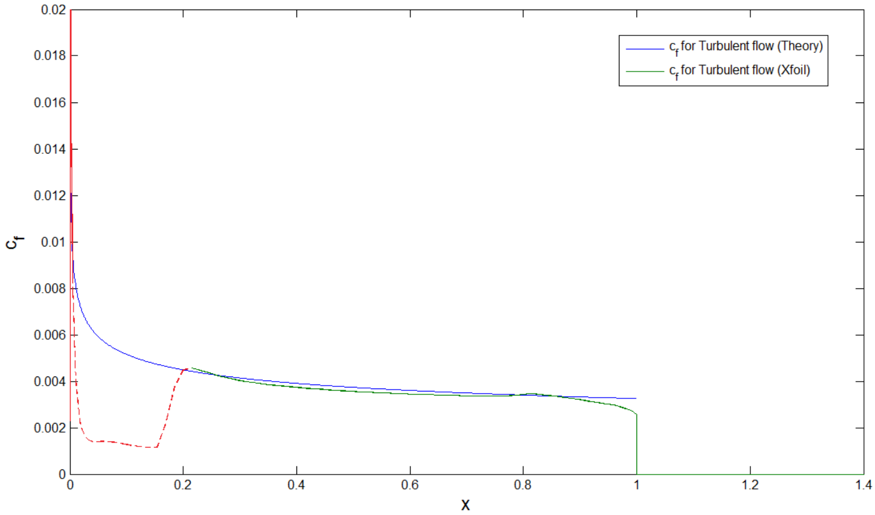

Figure 11.8: Comparison of the local skin friction coefficients for turbulent flow of $\mathrm{Re}_c = 2 \cdot 10^6$

Again, we observe great similarity between the local skin friction coefficient obtained from the (Blasius) theory and that predicted by XFOIL. This indicates that the designed plate should aerodynamically behave as an infinitesimally flat plate and the derived theory should describe the flow over the plate.

11.7 Boundary Layer Properties

The boundary layer properties are considered next, i.e. the boundary layer thickness, the displacement thickness and momentum thickness obtained from XFOIL. The results are shown below. The dashed line indicates the boundary-layer thickness δ/c.

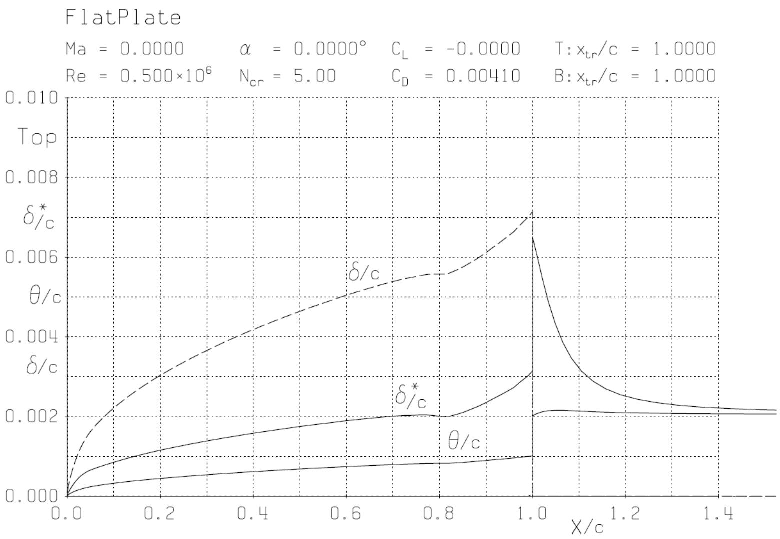

Figure 11.9: The displacement thickness, boundary layer thickness and momentum thickness for a flow with $\mathrm{Re}_c = 5 \cdot 10^5$.

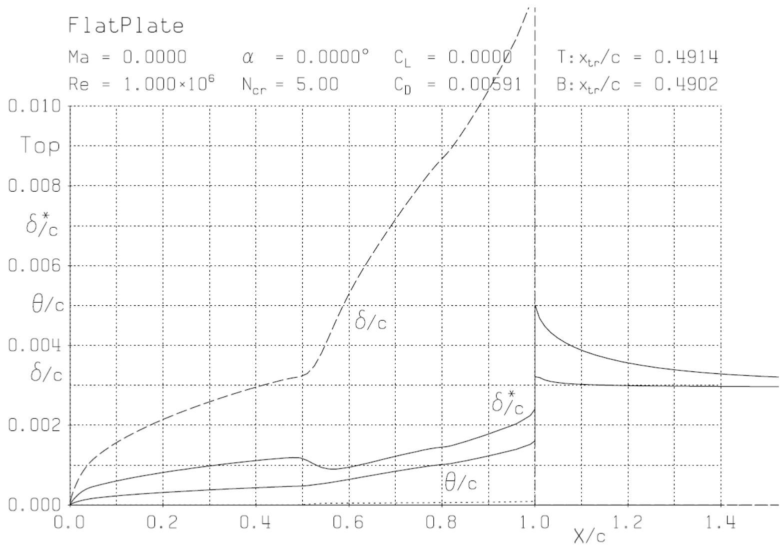

Figure 11.10: The displacement thickness, boundary-layer thickness and momentum thickness for a flow with $\mathrm{Re}_c = 1{\cdot}10^6$.

Figure 11.10 and 11.9 clearly show the relations between the boundary layer thickness, displacement thickness and momentum thickness as described in section 6.5 and 6.6. The properties for a flow with $\mathrm{Re}_c = 5 \cdot 10^5$ are mostly governed by laminar flow except for the forced transition caused by the change of geometry. It is hard to quantitatively compare these XFOIL results with the obtained theory (about the boundary-layer thickness etc.), but they seem quite similar.

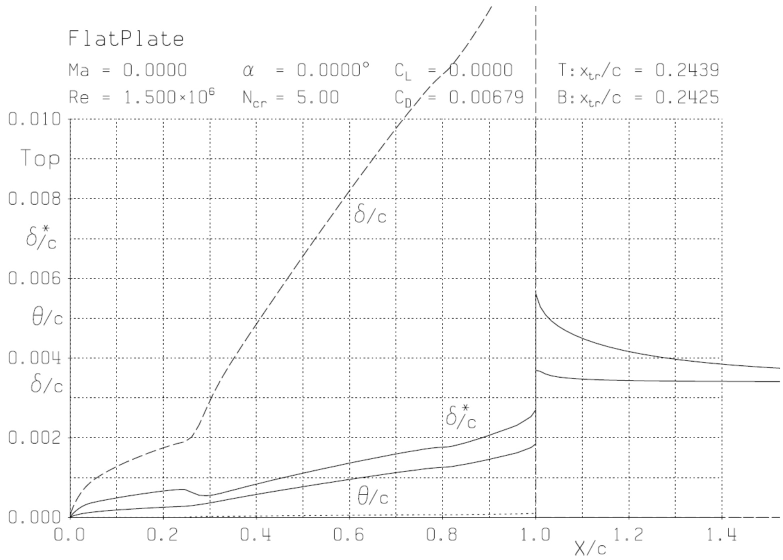

Figure 11.11: The displacement thickness, boundary-layer thickness and momentum thickness for a flow with $\mathrm{Re}_c = 1.5 \cdot 10^6$.

A final result is obtained for a flow with $\mathrm{Re}_c = 1.5 \cdot 10^6$. We observe that the difference between θ and δ^* becomes smaller in a turbulent flow. This can also be observed if we were to plot the kinematic shape factor H_k which gives the relation between θ and δ^*. However, because we are also able to observe this in these plots and the kinematic shape factor is not of interest in this research. Therefore, the kinematic shape factor graph is not shown.

12 Experimental Details

The measurements have been performed in the Silent Wind Tunnel of the University of Twente. The measurements on the velocity profile over the boundary layer of the flat plate have been conducted using a Pitot tube and a Hot Wire Anemometer. A measurement on the drag force is performed using load cells. The operational principles of the measurement devices will be explained below.

12.1 The Wind Tunnel

A schematic representation of the Silent Wind Tunnel is given in Figure 12.1. The test chamber is anechoic to reduce acoustic noise. The test section itself has a cross section of 0.7m x 0.9m and is 1.8m long. Moreover, the maximum velocity of the wind tunnel is 60 m/s. For velocities lower than 8 m/s, the flow in the test section becomes unstable. The turbulence level of the wind tunnel is around 0.25%. A heat exchanger is located downstream which cools the air that is heated because of friction in the circuit.

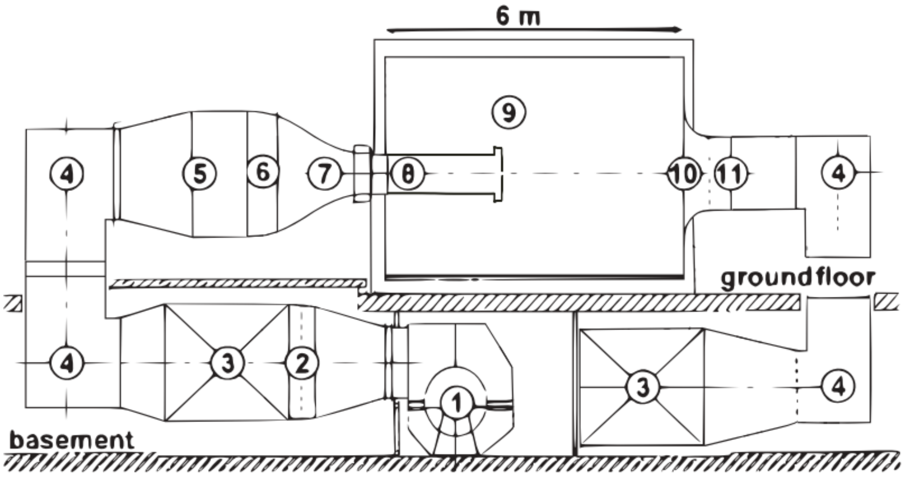

Figure 12.1: The Silent Wind Tunnel of University Twente. (1) Radial fan, 130 kW electric motor, (2) Heat exchanger, (3) Splitter-plate acoustic damper, (4) Corner vane, (5) Settling chamber, (6) Anti-turbulence screens, (7) Contraction 10 : 1, (8) Test section (0.9 m wide, 0.7 m high), (10) Flush intake, (11) Diffuser.

12.2 The Hot Wire Anemometer

The Hot Wire Anemometer, illustrated in Figure 12.2 , works on the principle of convective heat transfer. The wire is maintained at a constant temperature. As the air flow cools the wire, the applied voltage is increased to maintain a constant temperature. By measuring the voltage over the wire, the flow velocity is determined from a calibration reference. The wire is extremely thin (5μm in diameter) and therefore very sensitive to small fluctuations in the velocity. However, the wire is also very fragile and expensive. Caution must be taken when handling the Hot Wire during the experiments.

The HWA system consists of the Hot Wire probe (Dantec 55P11) which is connected to a Streamline 90N10 Frame with a A1863 coaxial cable of 4.0 meters. The streamline frame is connected to a computer with StreamWare Pro software v5.02. The measurements are performed with the StreamWare software.

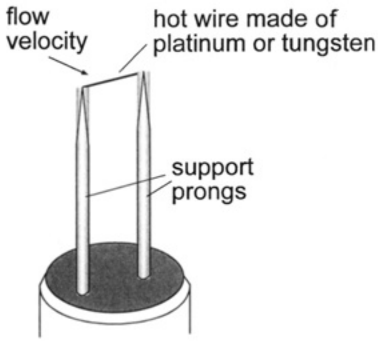

Figure 12.2: Hot Wire Anemometer [6]

12.3 Hot Wire Anemometer Calibration

Before every measurement, the HWA has to be calibrated. During the calibration, the Hot Wire is placed in an uniform flow with known velocity. The flow is generated by blowing through a nozzle with a pressure supply (see Appendix C2). The pressure in the nozzle is measured with a Betz manometer. With Bernoulli's equation the velocity is then determined. With the StreamWare software, the HWA is then calibrated. It is important that the calibration is performed in the wind tunnel in order for the results to be consistent. Moreover, the probe has to be in the same position (i.e. facing the flow in the same attitude) as it will be in the measurements.

12.4 The Pitot Tube

A Pitot tube is also used to measure the flow velocity. By measuring the static and stagnation pressure of the flow, the flow velocity can be obtained.

Bernoulli's equation for an incompressible flow states that along a streamline

$$p_1 + \frac{1}{2}\rho U_1^2 = p_2 + \frac{1}{2}\rho U_2^2$$

where point 1 is the stagnation point, point 2 an arbitrary static point and U the flow velocity. Because the velocity in the stagnation point is zero, the equation becomes

$$p_1 = p_2 + \frac{1}{2}\rho U_2^2$$

The flow velocity at point 2 can then be determine by measuring the pressure difference and using the density of the flow:

$$U_2 = \sqrt{\frac{2(p_1 - p_2)}{\rho}}$$

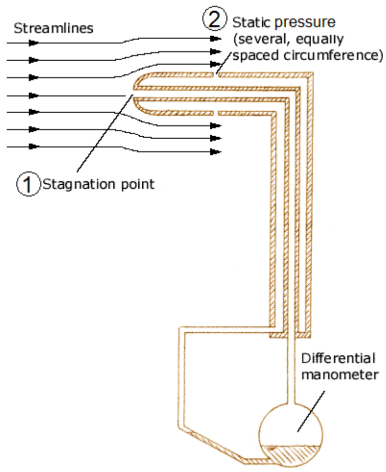

Figure 12.3: Pitot Tube Principle [7]

12.5 The Load Cell

The experimental set-up is shown in Figure 12.4. The plate is suspended by 4 rods in total. A rod through the middle of the plate pushes against both load cells. The second load cell is located on the other side of the test section. A load cell works on the principle of a strain gauge which under deformation will have a different electrical resistance. The load cell is calibrated by suspending a weight with known load to the plate through a pulley. Before the measurement, the voltage offset is zeroed. The measured voltage can then be used to calculate the exerted force.

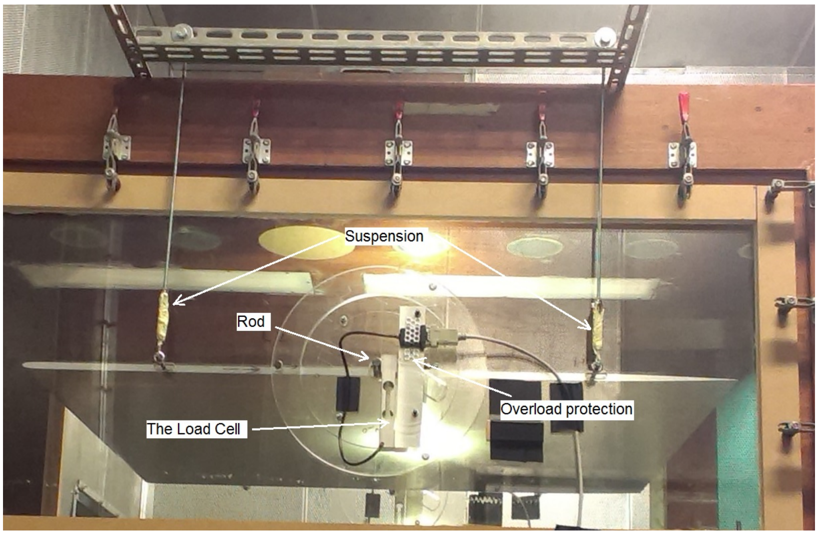

Figure 12.4: The set-up of the plate in the Wind Tunnel

13 Experimental Results

13.1 The Velocity Boundary-Layer Measurement with the Pitot tube

Initial measurements on the velocity profile have been performed with a Pitot tube which was custom made. The Pitot tube has a diameter of 3mm. Consequently, the velocity profile could not be measured closer than about 1.6mm from the surface of the plate.

The velocity in the wind tunnel is measured with a fixed Pitot tube in the wind tunnel which measures both static and stagnation pressure to determine the velocity in the wind tunnel. However, the Pitot tube which is used to determine the stagnation pressure in the boundary layer over the flat plat cannot measure the static pressure. Therefore, we will have a different offset in the measurement with respect to the velocity determination with the Pitot tube in the wind tunnel. This is the result of the different offset on each individual port of the measurement apparatus. However, because the results are made nondimensional, the pressure measured with Pitot 2 in the free stream, compared to the boundary-layer measurement should give valid results without an offset error. This is because we divide the free stream velocity with the boundary layer velocity, effectively dividing out the offset.

Moreover, it is important to note that the results have been corrected due to a different static pressure of the flow below the plate. It was measured that there is a streamwise pressure gradient below the plate. Therefore, the static pressure of the Pitot tube in the wind tunnel, used to determine the flow velocity, could not be used. The static pressure of the closest pressure orifice (orifice 3) in the wind tunnel was therefore used to determine the dynamic pressure and consequently the velocity profiles. The results of the streamwise distribution of the pressure in the test section of the wind tunnel can be found in section 13.4

The results of the Pitot tube measurements are shown in Figure 13.1-13.6 below. The velocity profile is measured in steps of 0.1mm and at a distance of x=0.62m from the leading edge. A comparison is made with the Blasius solution and Pohlhausen's 4th order approximation. Pohlhausen's 4th order approximation is plotted because the velocity profile tends to show the 4th order behaviour at higher velocities (i.e. higher Reynolds numbers). Because the boundary layer is thinner at higher Reynolds numbers, the region in the boundary layer in which measurements with the Pitot tube can be performed decreases with increasing velocity. Moreover, the boundary layer thickness from the measurements is determined with Matlab, using the criterion in Equation 6.56. To indicate a standard error (of 0.1 mm) in the determination, the red lines are plotted.

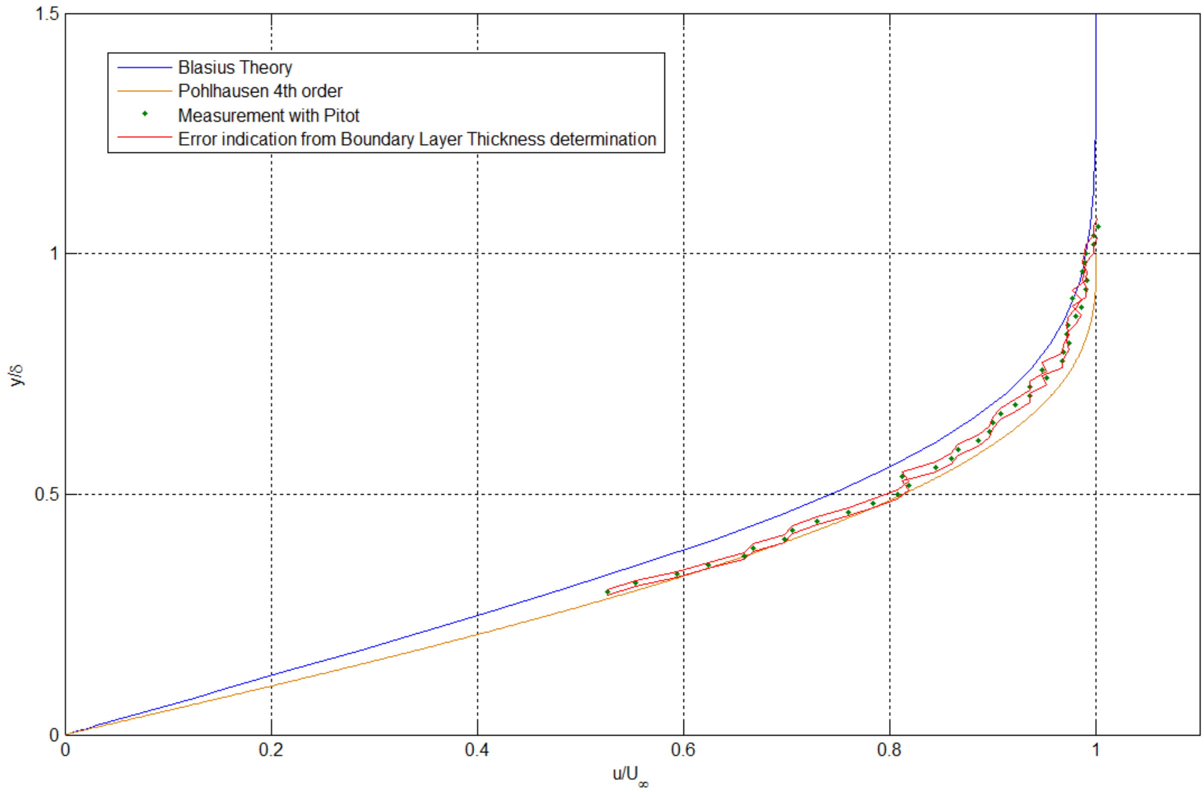

Figure 13.1: The velocity profile as measured with the Pitot tube with $\mathrm{Re}_x = 3.26 \cdot 10^5$ (U=8m/s).

Figure 13.1 also shows the instability of the Silent Wind Tunnel at low velocities.

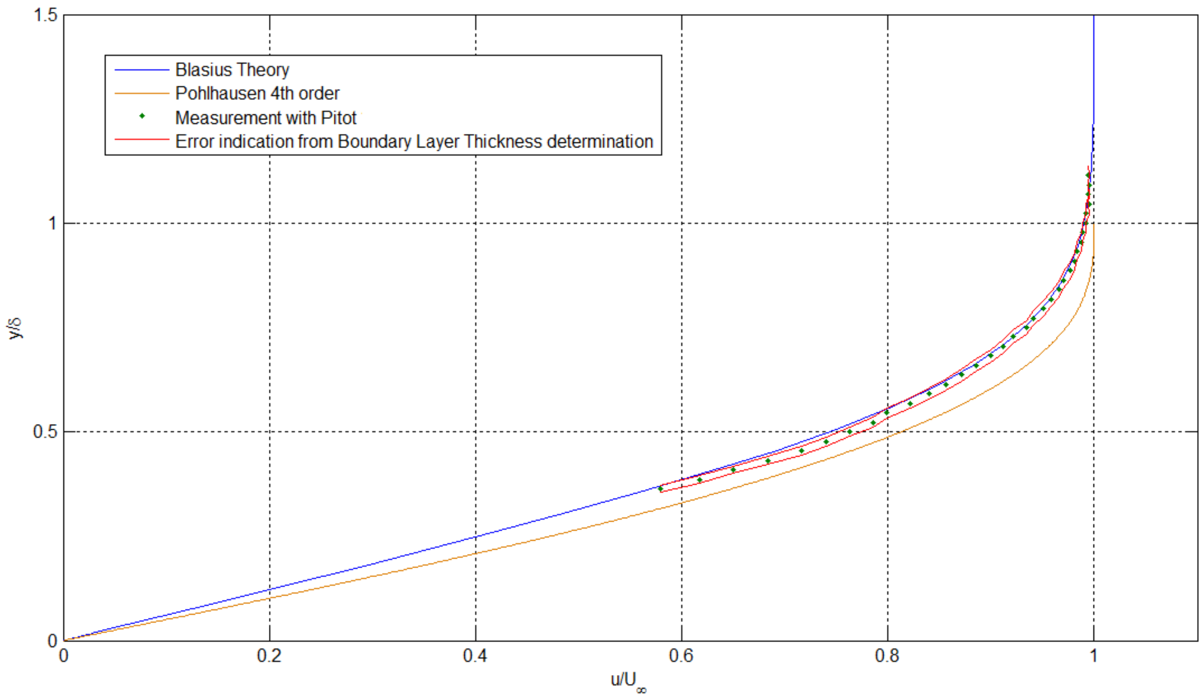

Figure 13.2: The velocity profile as measured with the Pitot tube with $\mathrm{Re}_x = 4.07 \cdot 10^5$ (U=10m/s).

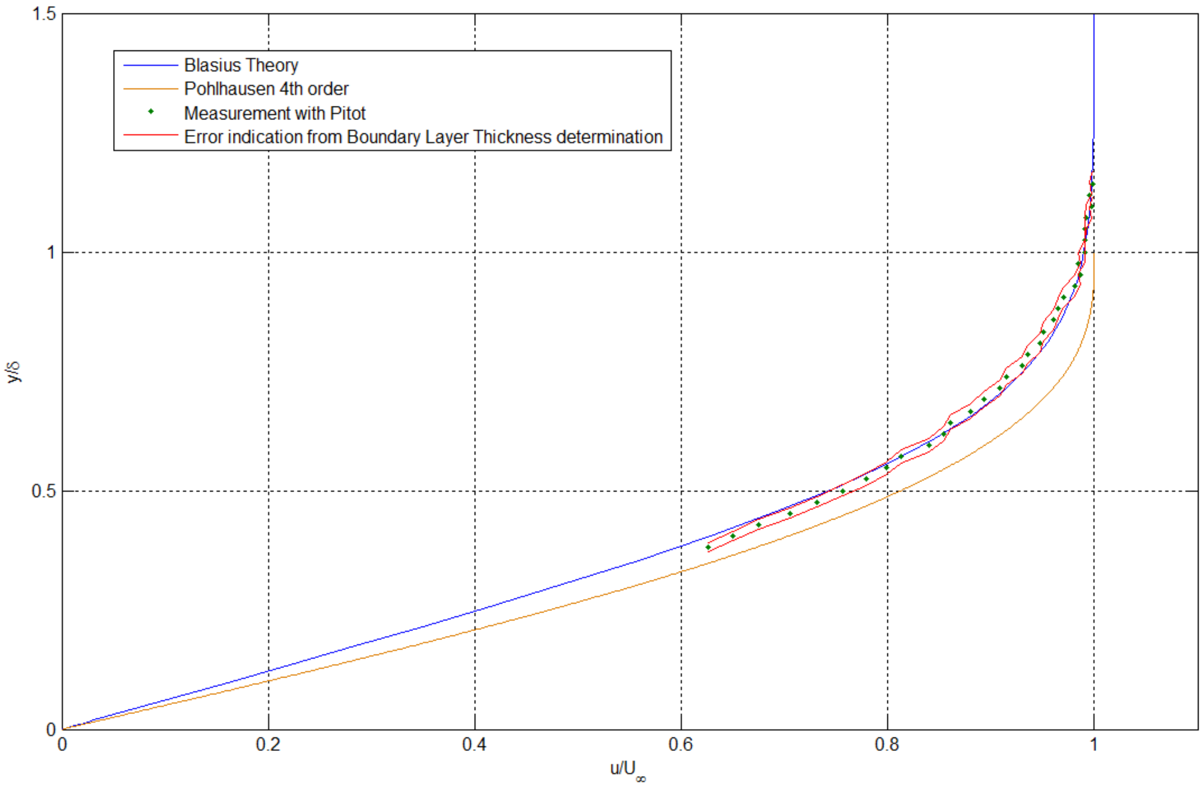

Figure 13.3: The velocity profile as measured with the Pitot tube with $\mathrm{Re}_x = 4.88 \cdot 10^5$ (U=12m/s).

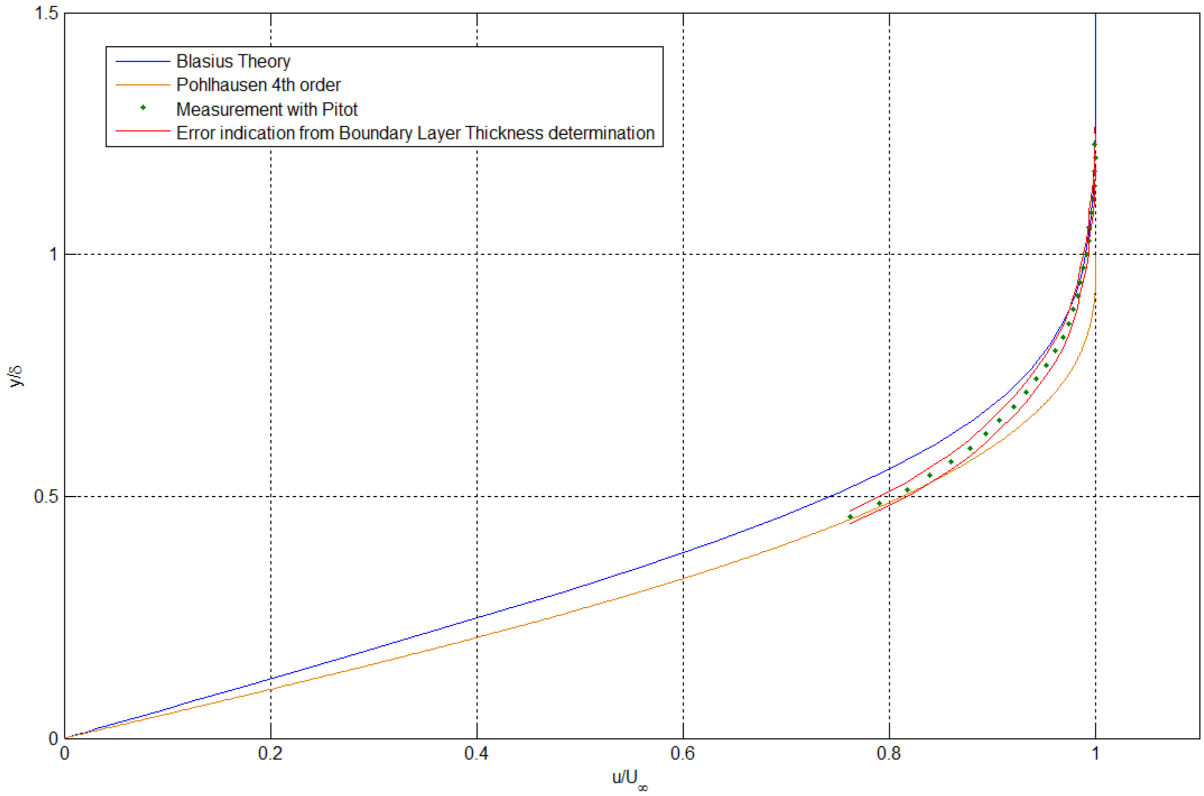

Figure 13.4: The velocity profile as measured with the Pitot tube with $\mathrm{Re}_x = 6.11 \cdot 10^5$ (U=15m/s).

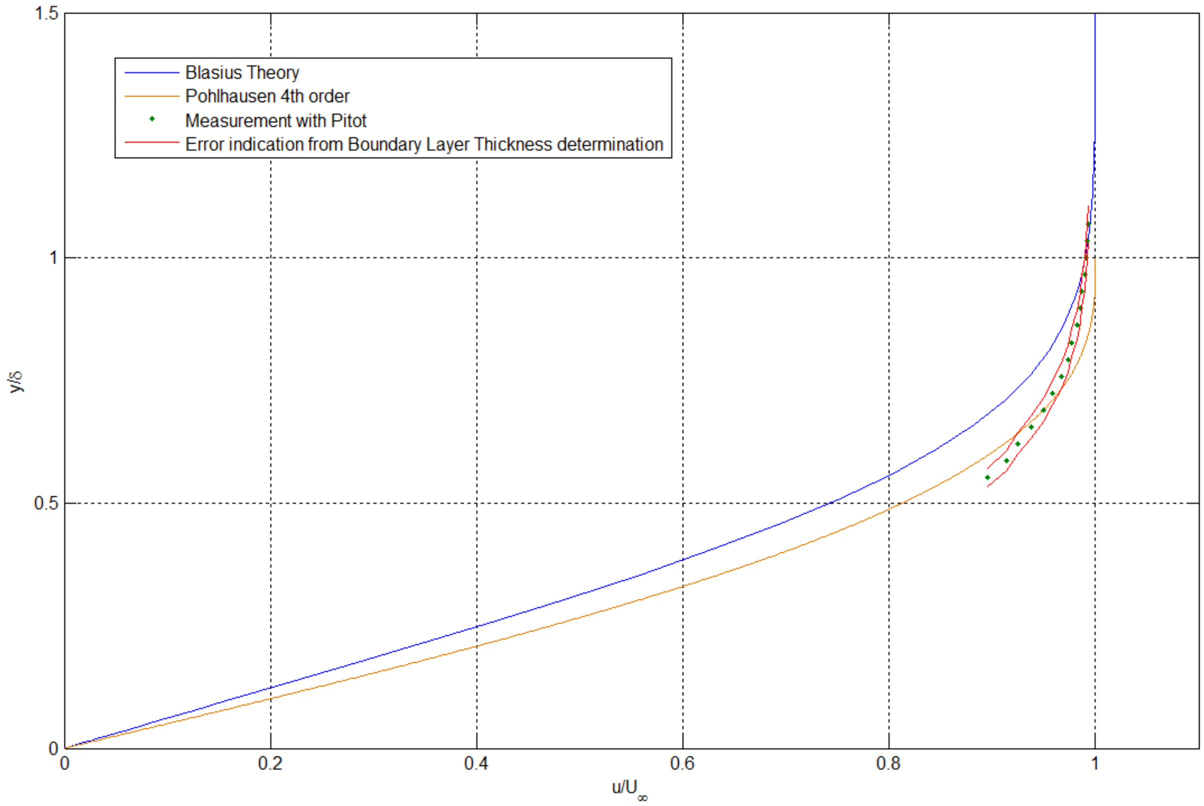

Figure 13.5: The velocity profile as measured with the Pitot tube with $\mathrm{Re}_x = 1.02 \cdot 10^6$ (U=25m/s).

We observe an unpredicted trend in the velocity profile. The shape of the velocity profile appears to curve with increasing Reynolds number. The deviation can be caused by a combination of an error in the boundary-layer thickness determination and some error in the determination of the free stream velocity. A slight variation of 0.1m/s in the measured free stream velocity will result in a less curved velocity profile. It could also be caused by disturbances in the flow. Therefore the measurement with a free stream velocity of 25 m/s ($\mathrm{Re}_x = 1.02 \cdot 10^6$) was repeated (at a different span of the plate) to verify the results. The resulting velocity profile of this second measurement in shown below.

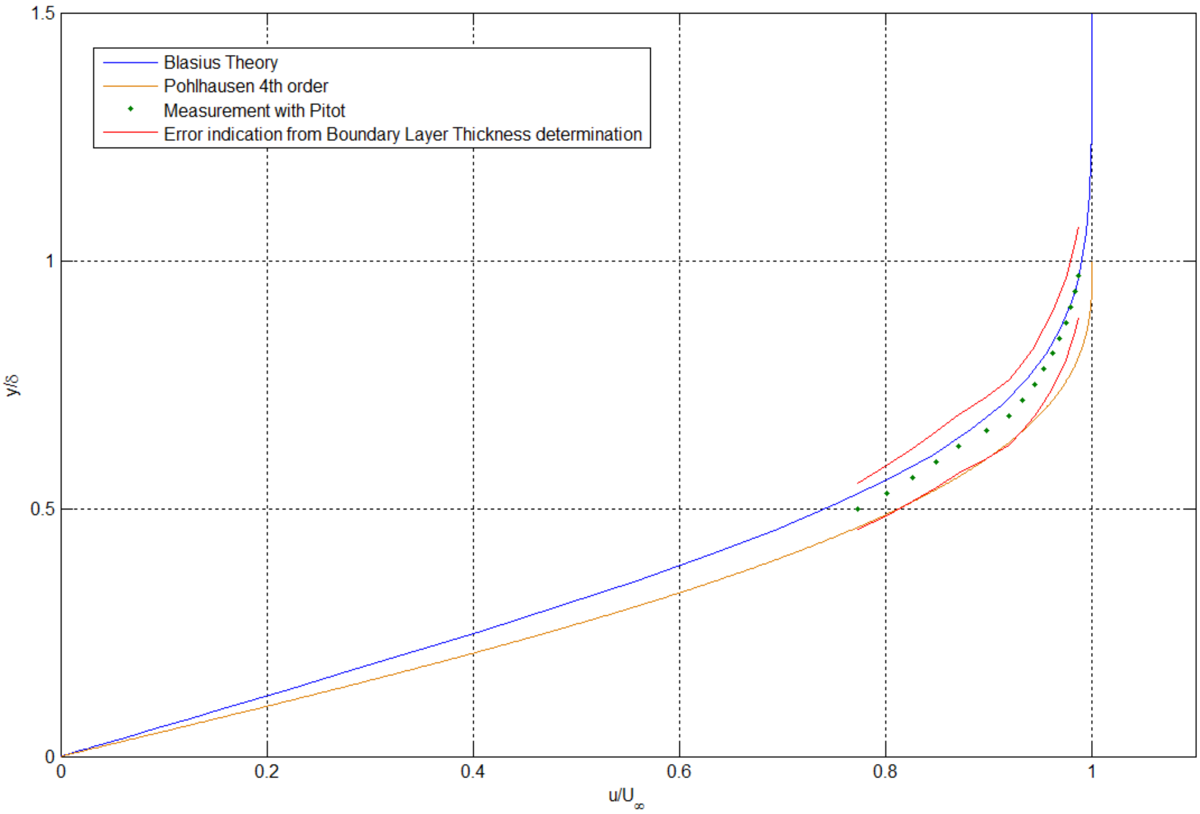

Figure 13.6: The second measurement on the velocity profile as measured with the Pitot tube with $\mathrm{Re}_x = 1.02 \cdot 10^6$ (U=25m/s).

The second velocity profile measurement seems much more in accordance with the Blasius Theory. However the difference between both measurements is striking. We found an indication that the velocity measured with the Pitot tube varies in the span of the plate which could have caused these results. Therefore the pressure along the span of the plate was measured to verify the assumption.

13.1.1 The Stagnation Pressure along the Span of the Plate

The Pitot tube was placed along the span of the plate to measure the stagnation pressure. For every measurement point, the distance between the plate and Pitot tube was set identical. The measurement starts at 5 cm from the center of the plate and ends at 15cm from the center of the plate. The pressure was measured at 2.0 mm and 2.5 mm from the surface of the plate. The result of the measurement is shown in Figure 13.7.

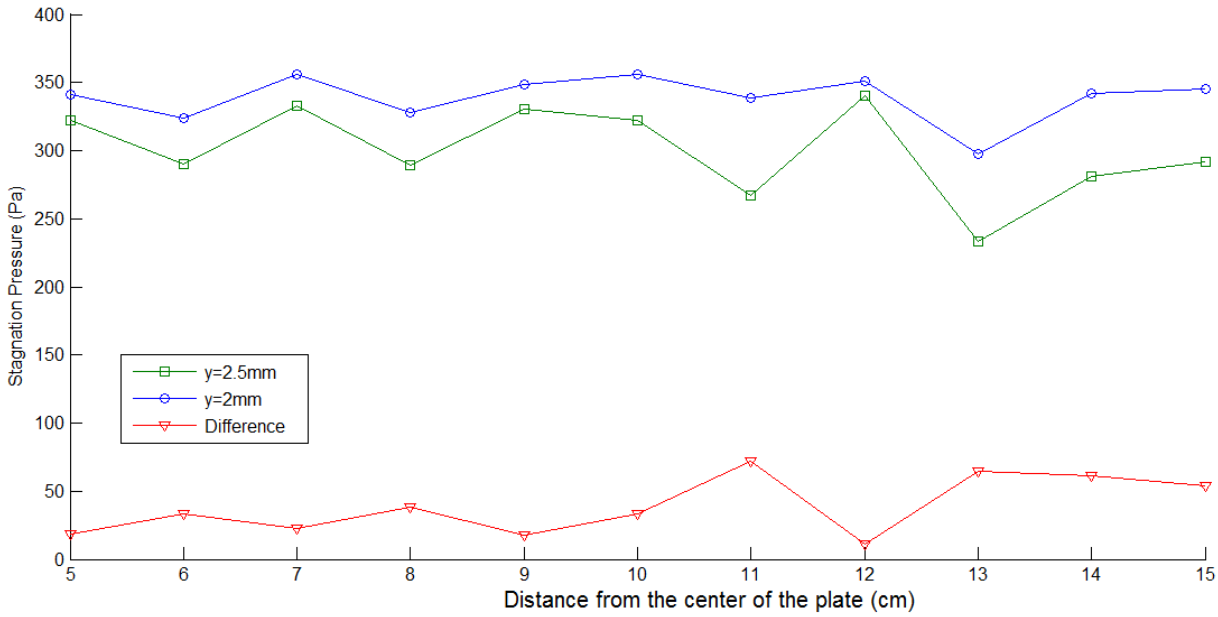

Figure 13.7: The stagnation pressure along the span of the plate

The pressure measurement shows that the velocity is not constant along the span of the plate at the measured velocity for 25 m/s ($\mathrm{Re}_x = 1.02 \cdot 10^6$) and therefore the flow is not uniform in this direction. These changes are presumably due to anomalies of the surface of the plate, possibly also indicating the development of so-called turbulent wedges. The difference between the stagnation pressures is also plotted. The difference shows that when one would determine the velocity profiles at the measurement points, the resulting velocity profiles are not equal as Figure 13.5 and 13.6 already showed.

13.1.2 The Boundary-Layer Thickness

The boundary-layer thicknesses that are determined from the Pitot measurements are shown below.

Re_x	$\frac{\delta}{x}\mathrm{Re}_x^{1/2}$ (Blasius=4.92)
$3.26 \cdot 10^5$	5.01
$4.07 \cdot 10^5$	4.56
$4.88 \cdot 10^5$	4.77
$6.11 \cdot 10^5$	4.45
$1.02 \cdot 10^6$	4.76 & 5.25

Table 1: The measured boundary layer thickness

13.1.3 Turbulent Flow Measurement

The velocity profile in a turbulent boundary layer has also been measured. The result is shown in Figure 13.8. Turbulence was induced with a turbulator strip placed just downstream of the leading edge. With a very sensitive microphone it has been determined that there was indeed turbulent flow. However, the flow over the plate was not fully turbulent. A small area downstream of the leading edge still showed laminar flow behaviour. The result of the turbulent flow measurement is compared with the power law velocity profile. The 1/5th power law appears to fit the measurement results best.

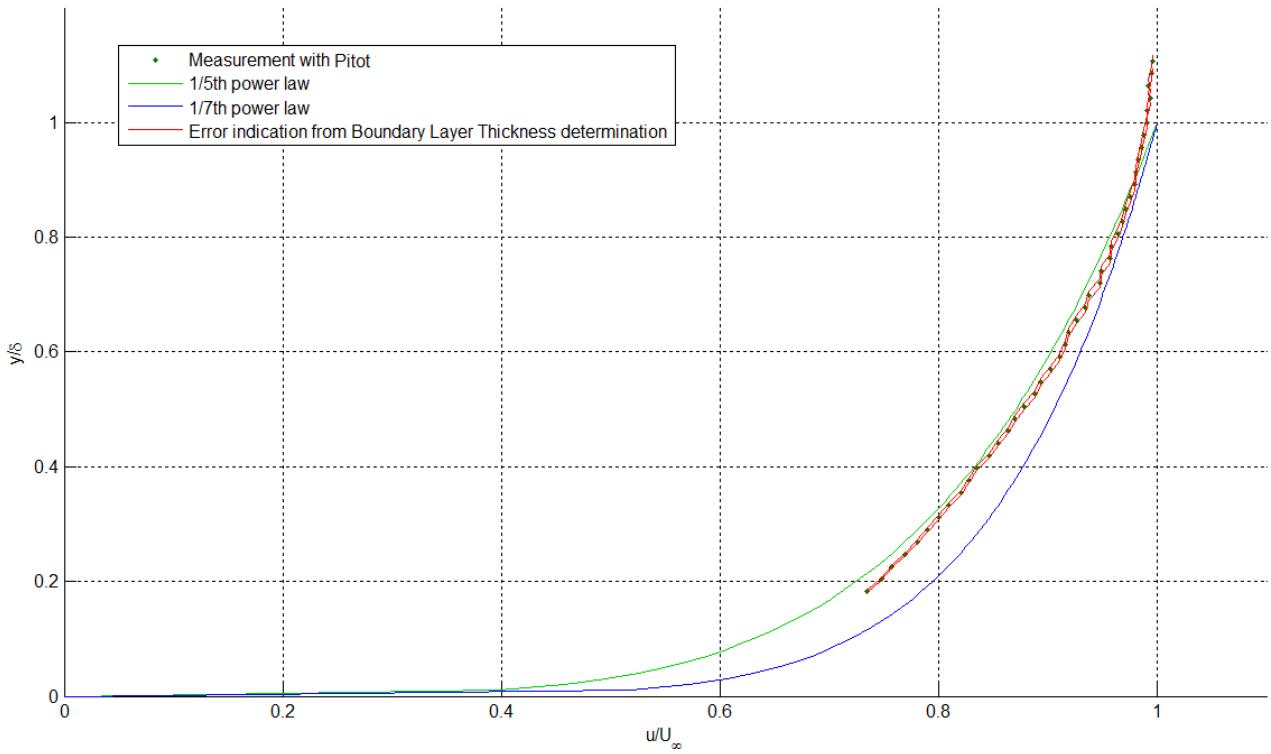

Figure 13.8: The velocity profile as measured with the Pitot in a tripped boundary layer with $\mathrm{Re}_x = 6.11 \cdot 10^5$ (U=15m/s). The boundary layer thickness is 9.3 mm.

13.2 The Velocity Boundary-Layer Measurement with the Hot Wire Anemometer

Figures 13.9 - 13.13 show the velocity profiles which have been measured with the HWA. The position of the HWA relative to the leading edge is the same as the position of the Pitot tube, a distance of x=0.62m from the leading edge. With the HWA it was very difficult to determine the distance from the plate since the HWA should not touch the plate. Therefore the HWA was placed increasingly closer to the plate until the measured voltage increased again, indicating that the wire was losing heat to the plate. From this starting position, the velocity was determined in steps of 0.1mm. Because of the difficulty in measuring the exact distance, the results have been fitted to the velocity profile according to Blasius. This does not change the shape of the graph but only shifts it in the y-direction.

The measurements at U=8m/s and U=10m/s are plotted starting at a distance of 0.1mm from the plate. The measurements at U=12m/s, U=15m/s and U=25m/s are plotted starting at a distance of 0.2mm from the plate. The measurements for U=12m/s and U=15m/s do not show the behaviour close to the plate and thus the starting distance was set at a longer distance from the plate.

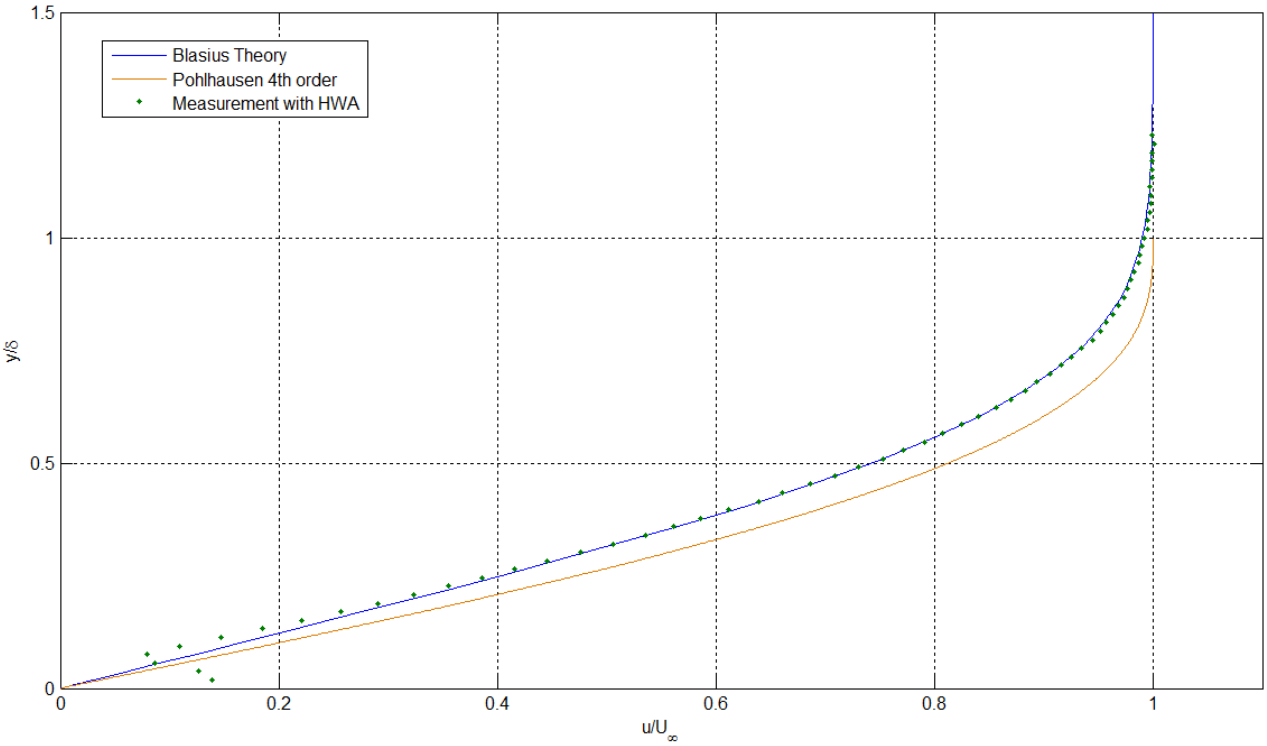

Figure 13.9: The velocity profile as measured with the Hot Wire with $Re_x = 3.26 \cdot 10^5$ (U=8m/s).

Figure 13.9 shows great similarity with the Blasius solution. The first few measurement points show the effects of heat transfer to the plate which can also be observed in the U=10m/s and U=25m/s measurement.

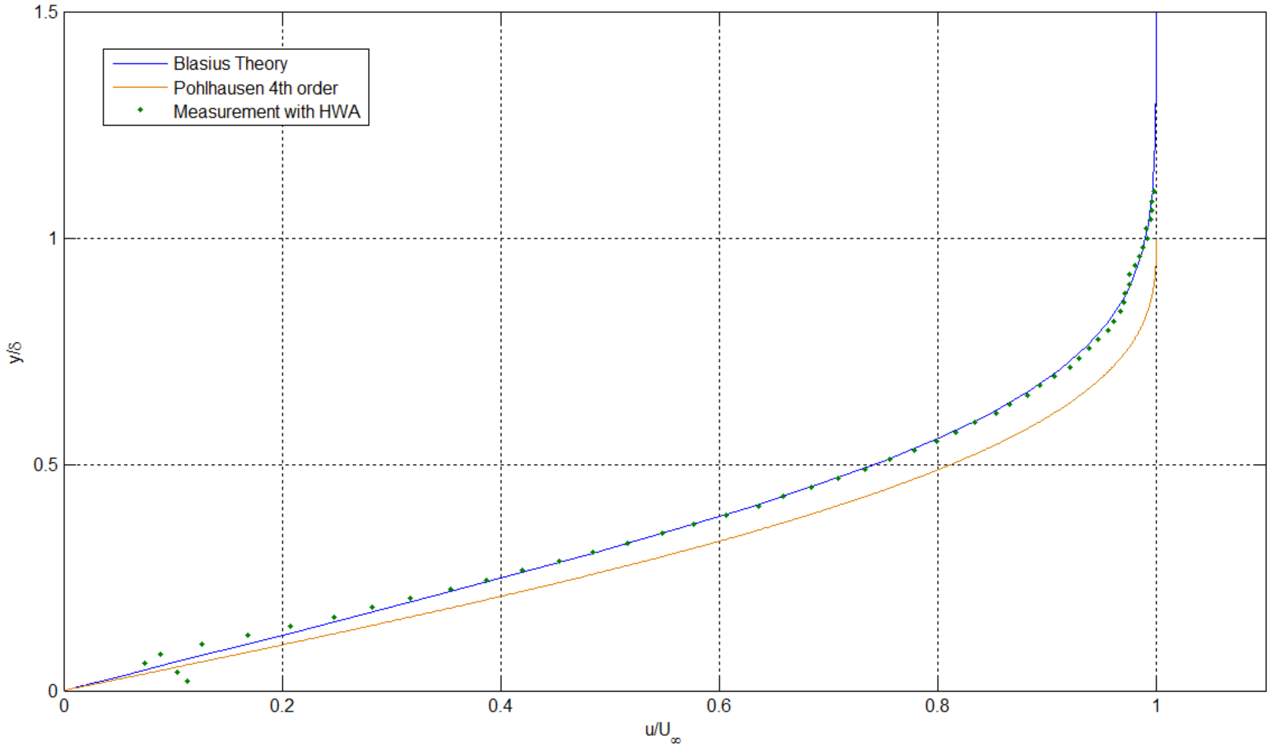

Figure 13.10: The velocity profile as measured with the Hot Wire with $\mathrm{Re}_x = 4.07 \cdot 10^5$ (U=10m/s).

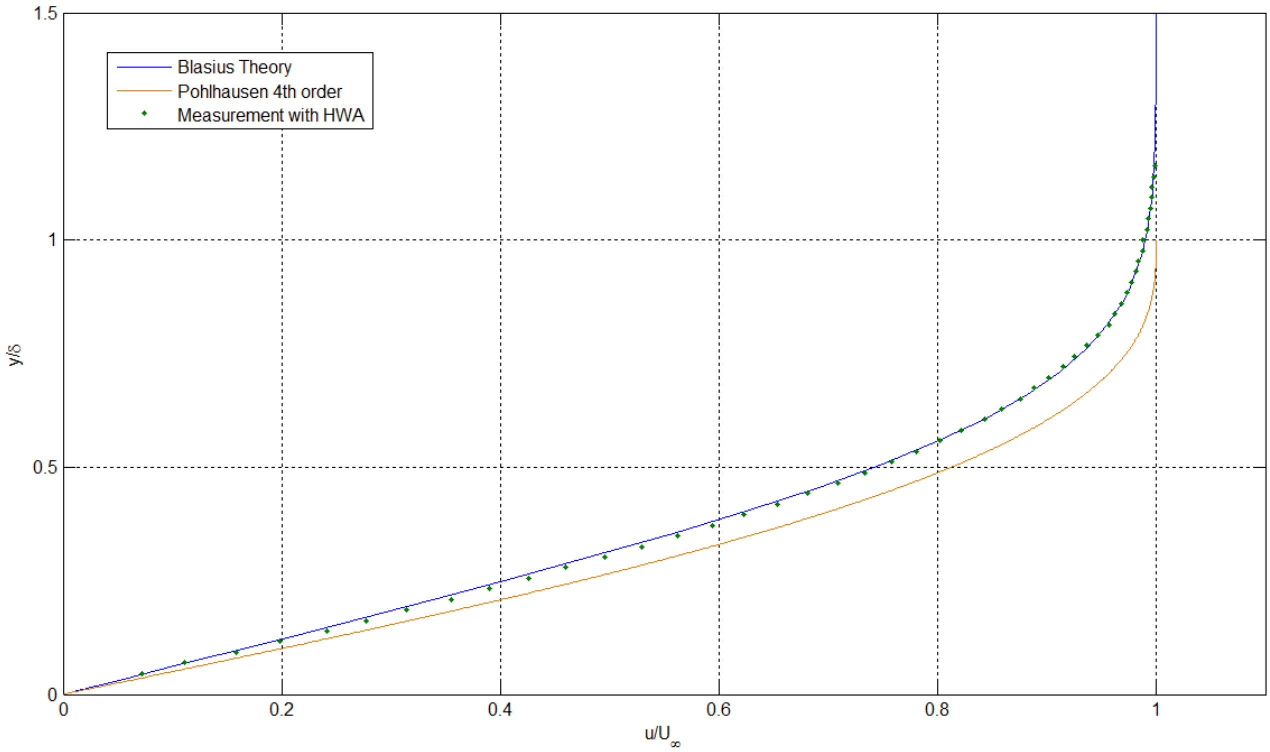

Figure 13.11: The velocity profile as measured with the Hot Wire with $\mathrm{Re}_x = 4.88 \cdot 10^5$ (U=12m/s).

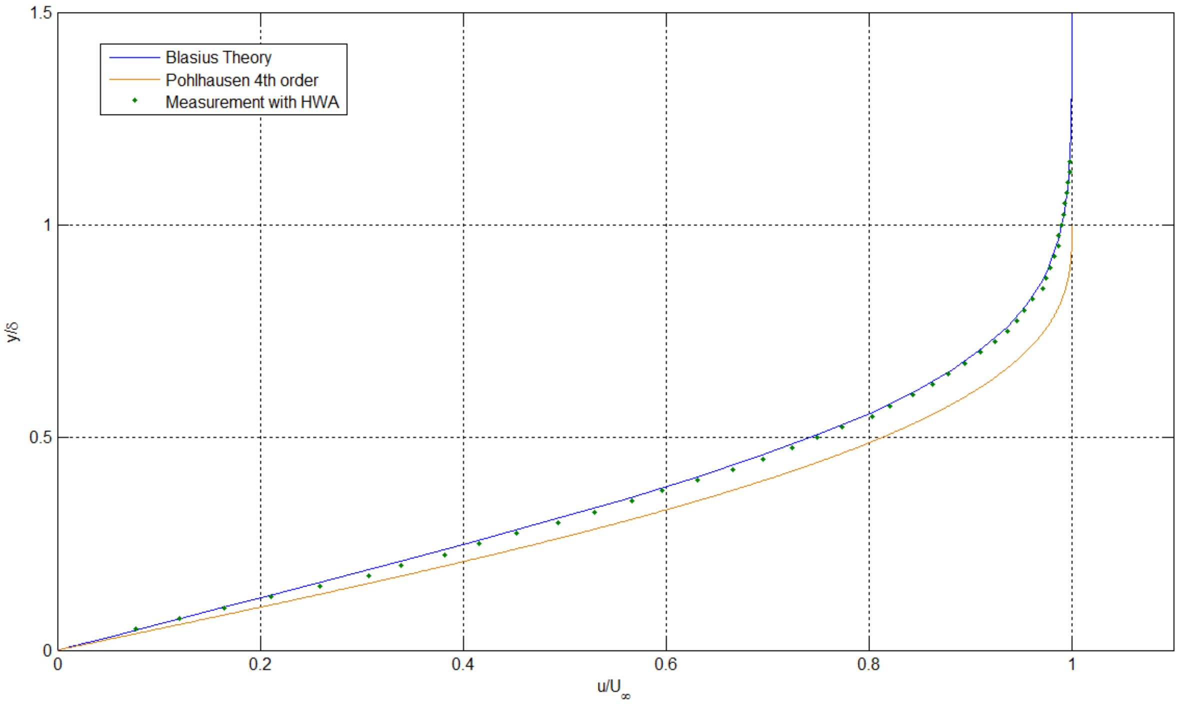

Figure 13.12: The velocity profile as measured with the Hot Wire with $\mathrm{Re}_x = 6.11 \cdot 10^5$ (U=15m/s).

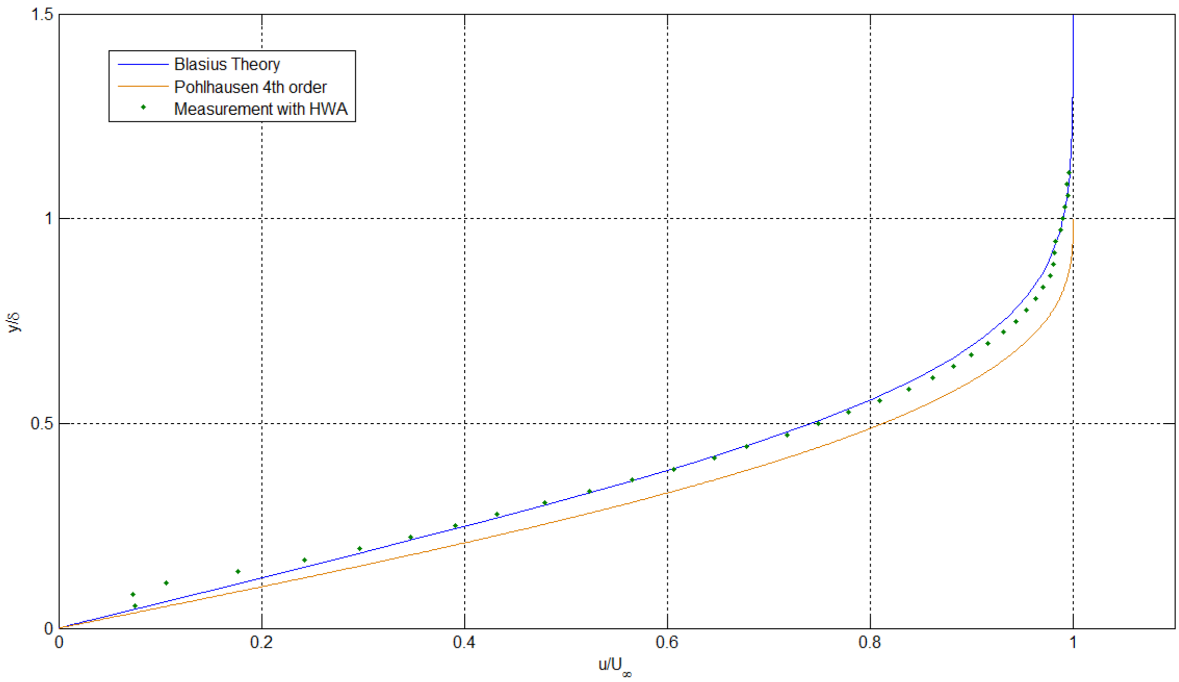

Figure 13.13: The velocity profile as measured with the Hot Wire with $\mathrm{Re}_x = 1.02 \cdot 10^6$ (U=25m/s).

The measurement for $\mathrm{Re}_x = 1.02 \cdot 10^6$ (U=25m/s) starts at a distance of 0.2mm from the plate to fit the velocity profile according to Blasius. Figure 14.5 shows the velocity profile with a starting distance set to 0.1mm from the plate, also compared with the Pitot Tube results. The Hot Wire velocity profile for U=25m/s also appears to have an increased curvature, somewhat similar to the Pitot tube velocity profile.

13.2.1 The Boundary Layer Thickness

The determined boundary layer thicknesses from the Hot Wire measurement are shown in the table below. In general, the Hot Wire measurements are closer to the Blasius Theory than the Pitot tube measurements.

Re_x	$\frac{\delta}{x}Re_x^{1/2}$, Pitot	$\frac{\delta}{x}Re_x^{1/2}$, Hot Wire
$3.26 \cdot 10^5$	5.01	4.92
$4.07 \cdot 10^5$	4.56	5.08
$4.88 \cdot 10^5$	4.77	4.89
$6.11 \cdot 10^5$	4.45	5.08
$1.02 \cdot 10^6$	4.76 & 5.25	5.9

Table 2: The measured boundary layer thickness from both measurements (Blasius Theory = 4.92)

13.3 The Drag Force

The results of the drag force measurements are shown below. Information about the load cell, which was used to determine the drag force, can be found in Appendix C.4. The results show transition at a quite high Reynolds number, which is not as expected. According to the theory and XFOIL simulations, the critical Reynolds number at which transition should occur is at approximately 500,000 whereas in the present experiment transition occurs at a Reynolds number of about 3,000,0000. A possible cause is the streamwise pressure gradient for which the results are represented in section 13.4. The measured drag coefficient for laminar flow is observed to be slightly higher than the value from theory, which is most likely caused by the interaction of the side walls of the wind tunnel with the boundary layer on the plate.

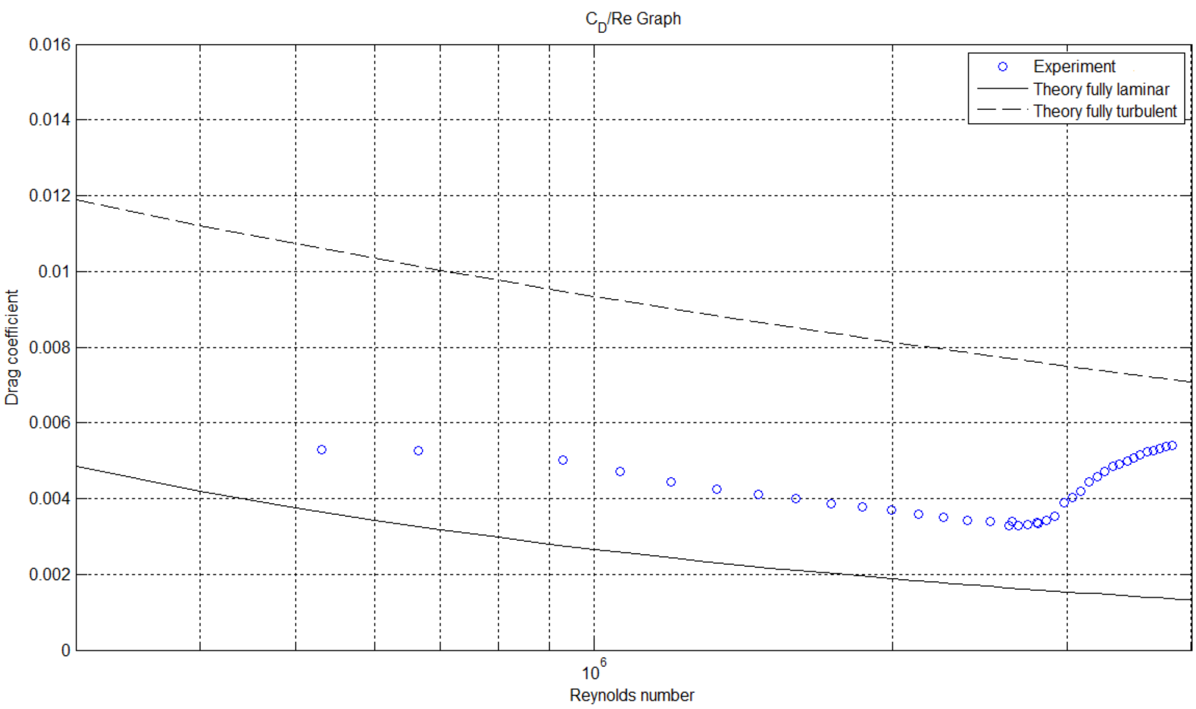

Figure 13.14: The drag coefficient measured using the load cells

Figure 13.14 shows two sets of measurements. One set in the lower Reynolds number range and a second set in the higher Reynolds number range, in which transition occurred. From these measurements we conclude that the load cell is not very sensitive in the lower Reynolds number range, where it gives a lower output voltage. It was also observed that the load cell is very sensitive to small variations in the temperature. A temperature change of 1 degree Celsius causes a change of approximately 0.02 in output voltage. Depending on the Reynolds number, there can be a small error in the drag coefficient of approximately 0.0005. The relative differences will however be small and reasonably valid in this research.

Furthermore, transition strips are placed on the plate to induce a turbulent flow inside the boundary layer. A measurement is done with a turbulator strip on one side, and another with a turbulator strip on both sides. The turbulator strips are placed just downstream of the leading edge of the plate. The location of the turbulator strip and results are shown below.

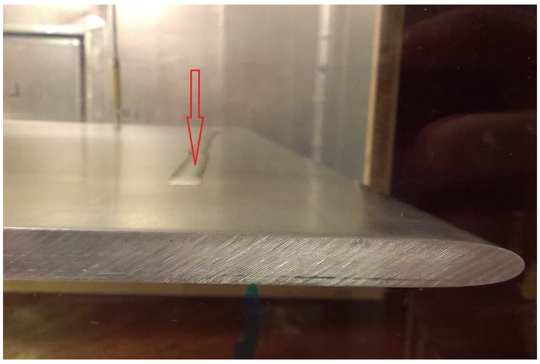

Figure 13.15: The placement of the turbulator strip

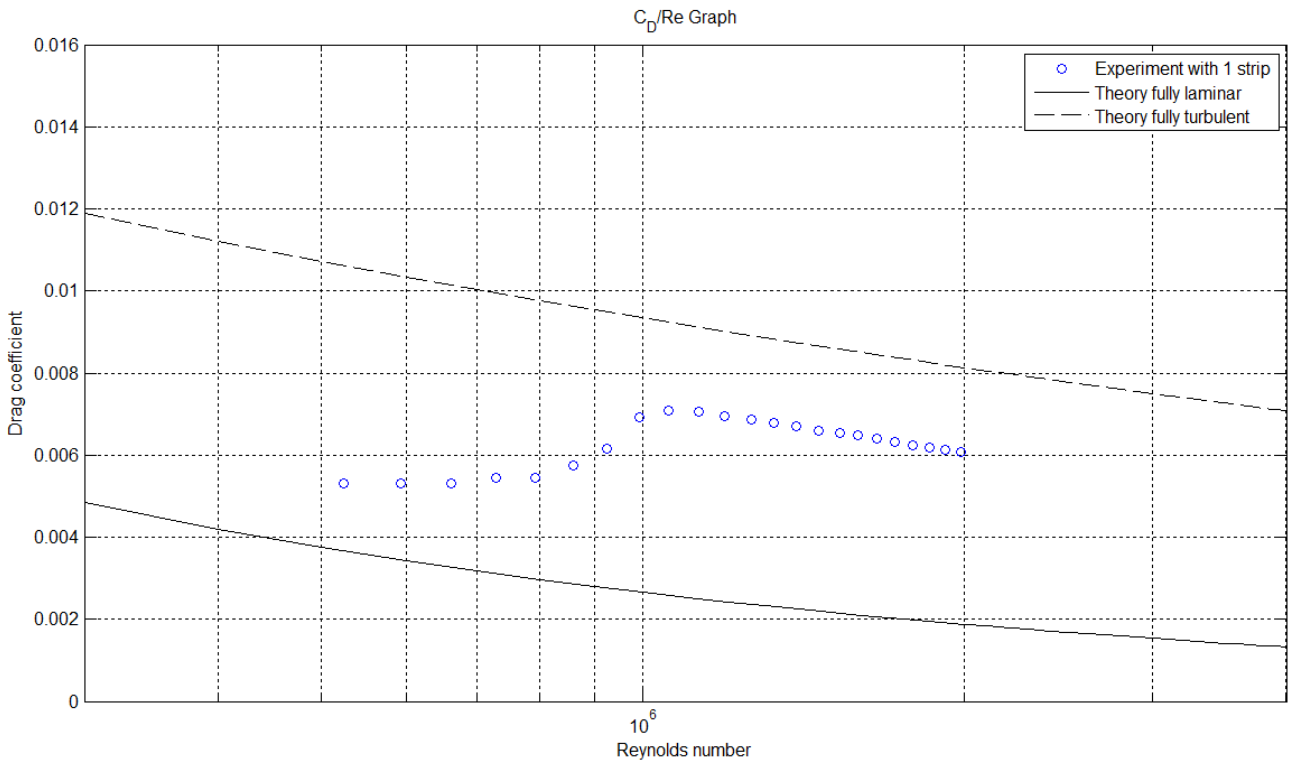

Figure 13.16: The drag coefficient measured with a turbulator strip on one side of the plate

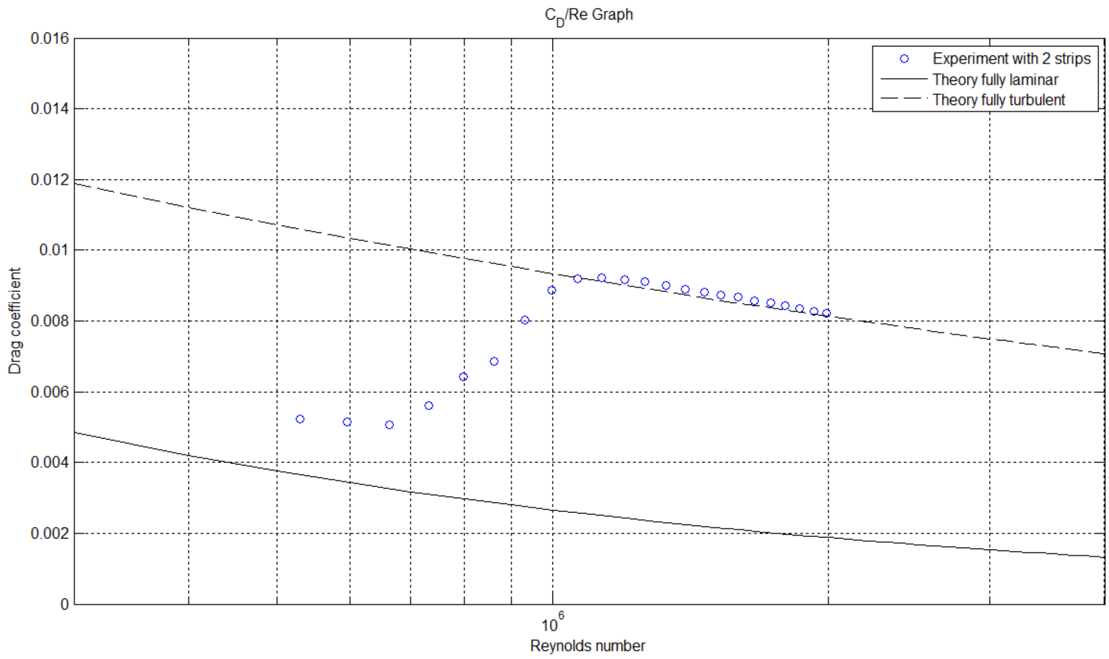

Figure 13.17: The drag coefficient measured with a turbulator strip attached to both sides of the plate

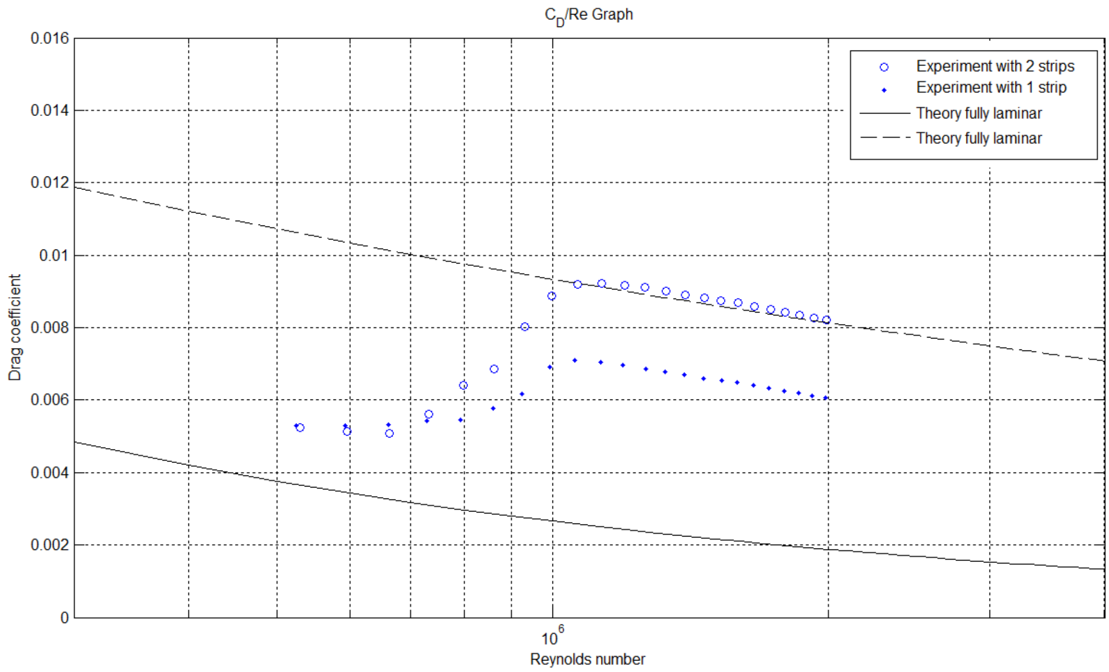

Figure 13.18: Comparison of the drag coefficient for the case of a turbulator strip on one side of the plate and the drag coefficient for a turbulator strip on both sides of the plate

Transition from laminar to turbulent flow now occurs at a lower Reynolds number which is as expected since we induced turbulence. At lower Reynolds numbers it appears that the turbulence is still damped in the boundary-layer and a turbulent boundary layer develops at approximately $\mathrm{Re}_c = 700{,}000$. For higher Reynolds numbers, the measured drag coefficient for turbulent flow, however, is observed to be very close to the theoretical value.

13.4 The Streamwise Pressure Gradient in the Silent Wind Tunnel

The results of the drag force measurements gave rise to a number of possibilities that could have caused the delayed transition. The most likely reasons are the turbulence level of the wind tunnel, acoustic disturbances or a change in streamwise pressure gradient. There has already been extensive research in the turbulence level of the wind tunnel from which was concluded that the turbulence level is around 0.25% [9]. In order for the turbulence level to have an influence on the delay of transition, the turbulence level would have to be very low (0.03%), which is highly unlikely. Because measuring acoustic disturbances was not possible, the possibility of a favourable streamwise pressure gradient was investigated. Initially, numerical simulations were performed with XFOIL in order to investigate the effects of a favourable pressure gradient.

13.4.1 XFOIL Simulations

To simulate a favourable pressure gradient in XFOIL, the plate was placed at a small positive angle of attack. Figure 13.19 and 13.20 show an angle of attack of 0.5° and 1.0°, respectively, which result in a small favourable pressure gradient along the lower surface of the plate. Table 3 shows the transition point for various angles of attack.

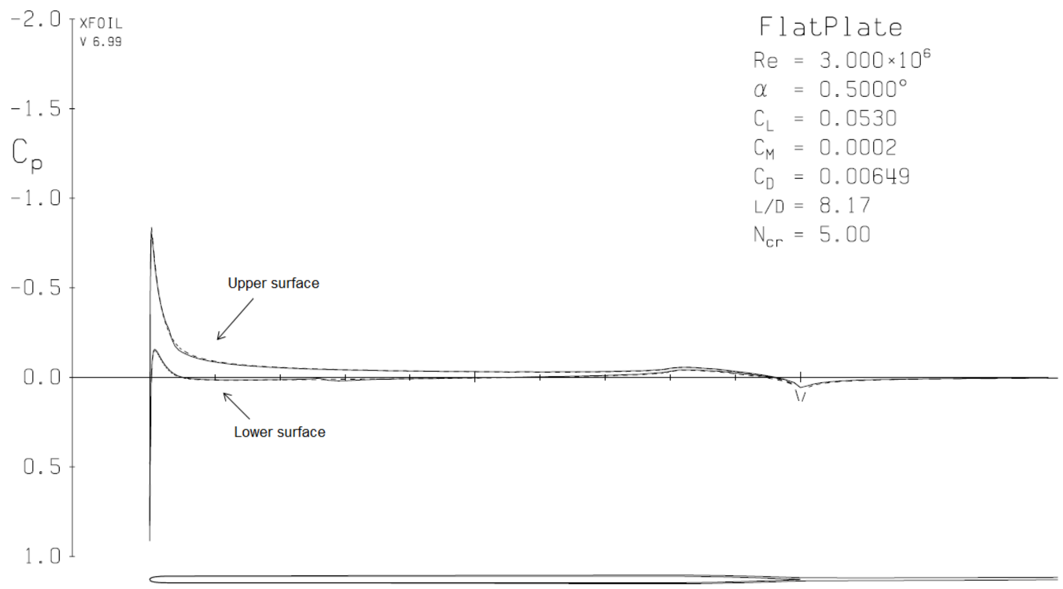

Figure 13.19: The pressure coefficient obtained from XFOIL for the plate at an angle of attack of 0.50°

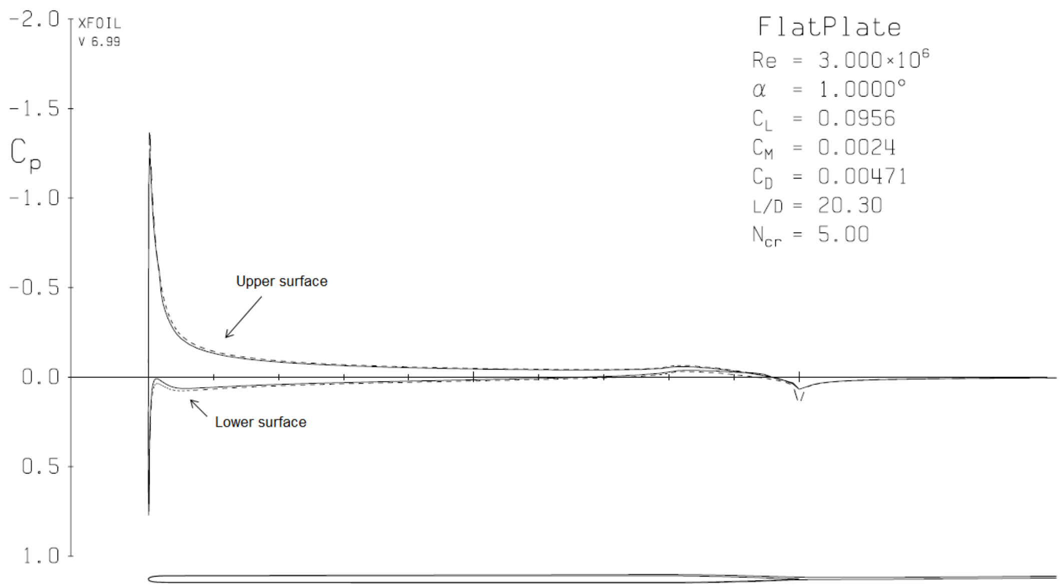

Figure 13.20: The pressure coefficient obtained from XFOIL for the plate at an angle of attack of 1.00°

α	transition point (x/c)
0.5	0.2593
0.75	0.4612
0.85	0.6145
1.0	0.9348

Table 3: The transition point on the lower surface of the plate for various angles of attack

The table shows that transition is indeed delayed for a relatively small pressure gradient. The pressure coefficient at an angle of attack of 1° is 0.07 at most. These numerical simulations have shown that a relative small pressure gradient can delay transition.

13.4.2 Experimental Results

The streamwise pressure gradient in the wind tunnel is measured with 5 pressure orifices. Appendix C.3 shows the location of the pressure orifices in the Silent Wind Tunnel of the University of Twente. The results of the measurement are shown below. Figure 13.21 shows the streamwise distribution of the pressure without the plate installed and Figure 13.22 shows the distribution with the plate installed. The dashed line in Figure 13.22 indicates the position of the plate.

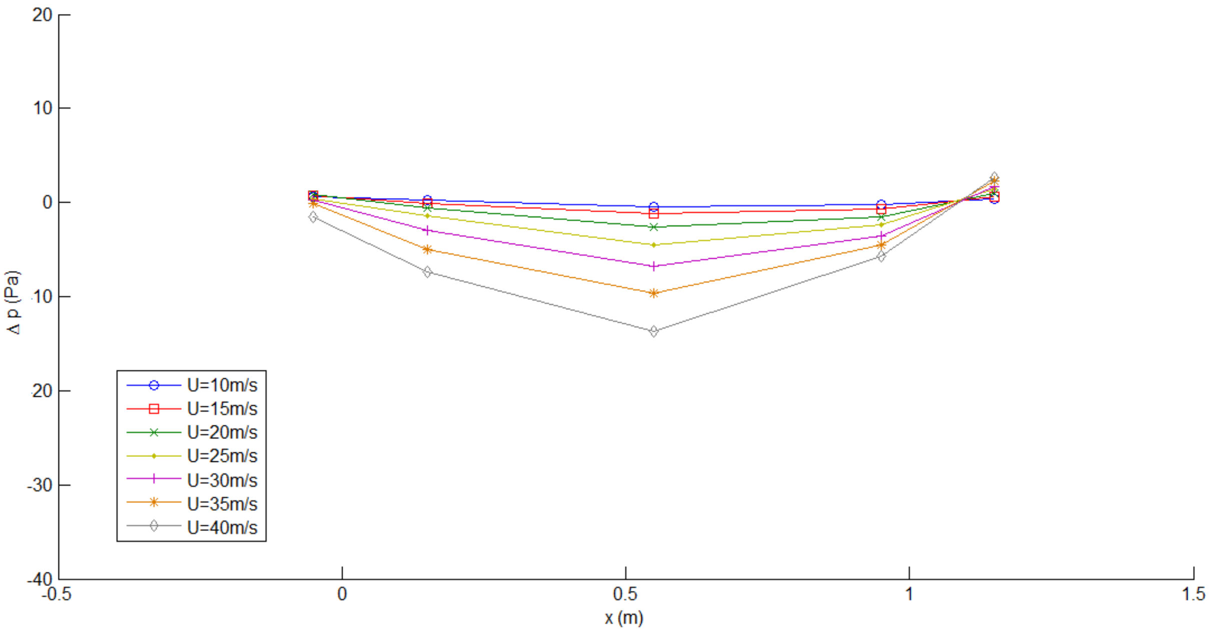

Figure 13.21: The streamwise distribution of the pressure in the Silent Wind Tunnel without the plate installed

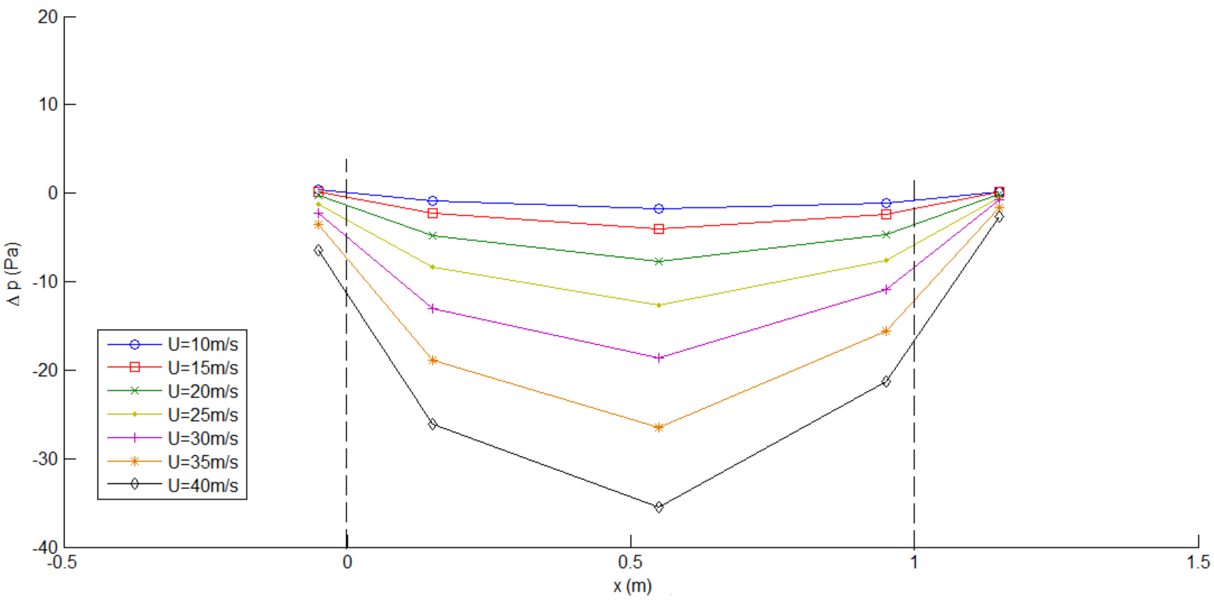

Figure 13.22: The streamwise distribution of the pressure in the Silent Wind Tunnel with the plate installed

The measurement shows that the test section of the Silent Wind Tunnel has a pressure gradient which is enhanced when the plate is installed. It is therefore possible that the pressure gradient is responsible for the delayed transition. Follow-up research should further investigate the effects of the streamwise pressure gradient on transition.

14 Comparison

In this chapter the velocity profiles obtained with the Pitot Tube and Hot Wire are compared. The results are compared for each free stream velocity. Figure 14.6 also shows the comparison of all the Hot Wire measurements and Figure 14.7 shows the comparison of all the Pitot tube measurements.

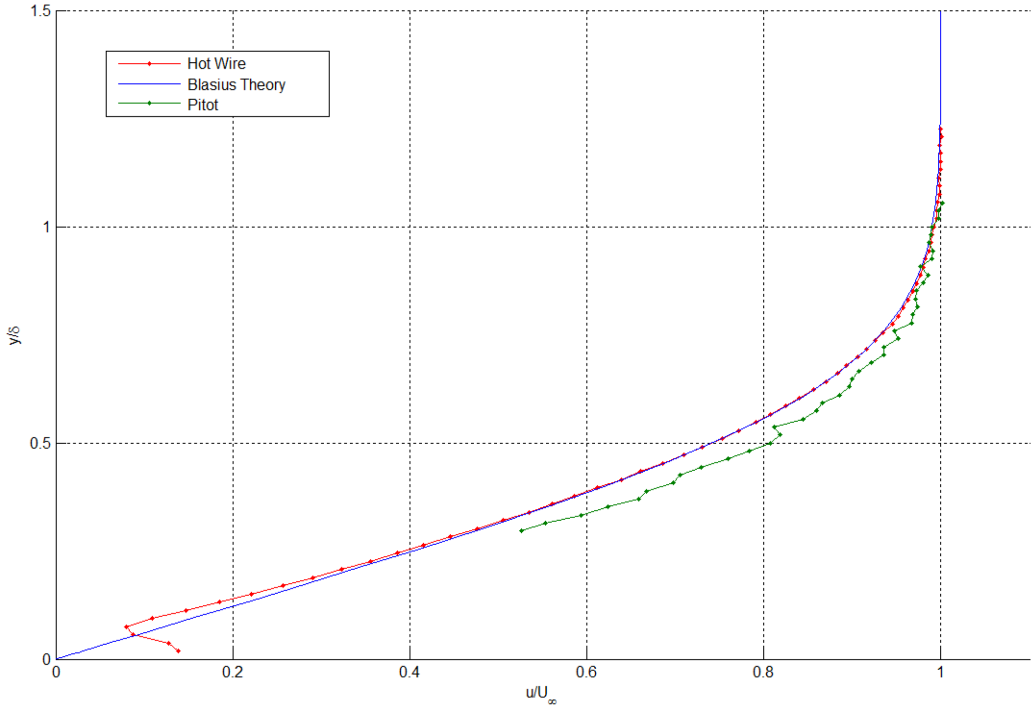

Figure 14.1: Comparison of the results of the HWA, Pitot and Blasius velocity profiles for $\mathrm{Re}_x = 3.26 \cdot 10^5$ (U=8m/s)

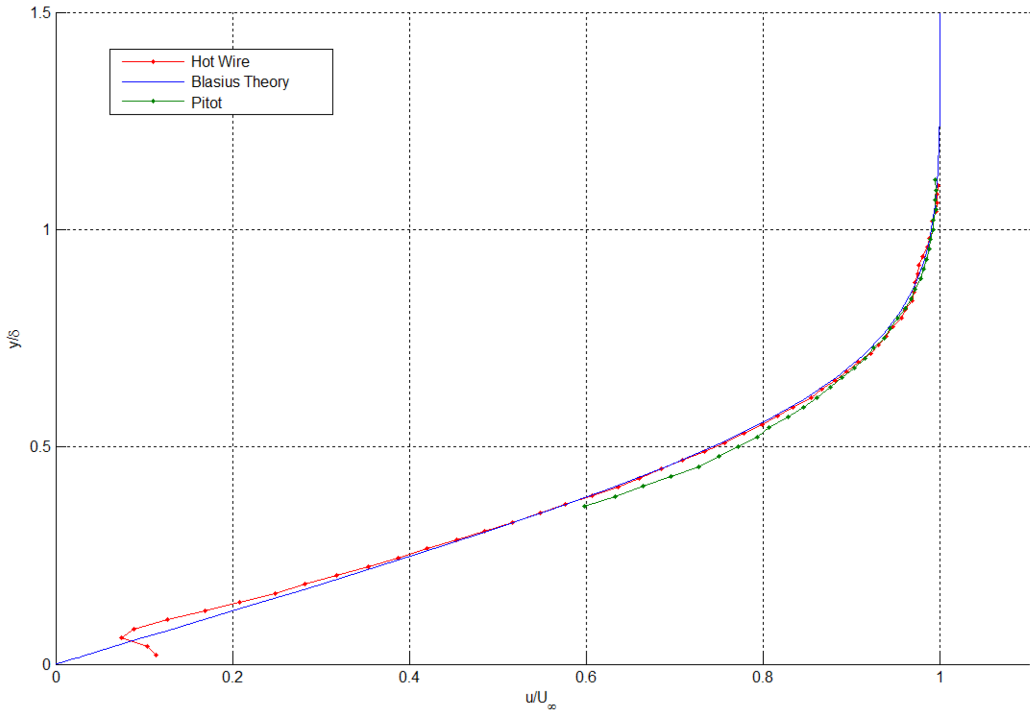

Figure 14.2: Comparison of the results of the HWA, Pitot and Blasius velocity profiles for $\mathrm{Re}_x = 4.07 \cdot 10^5$ (U=10m/s)

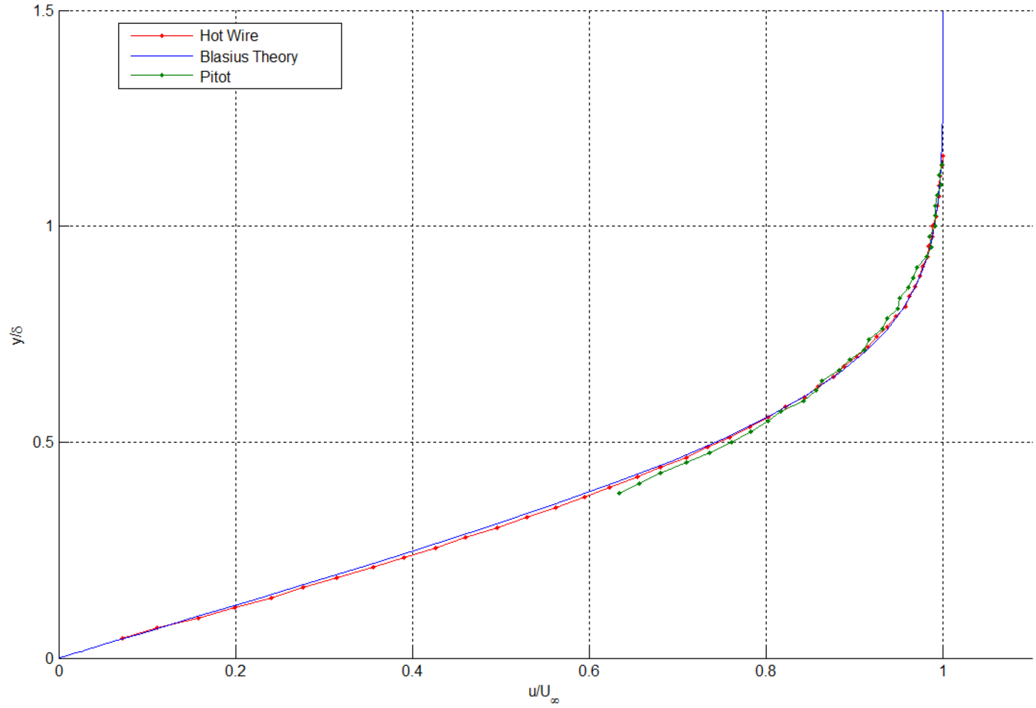

Figure 14.3: Comparison of the results of the HWA, Pitot and Blasius velocity profiles for $\mathrm{Re}_x = 4.88 \cdot 10^5$ (U=12m/s)

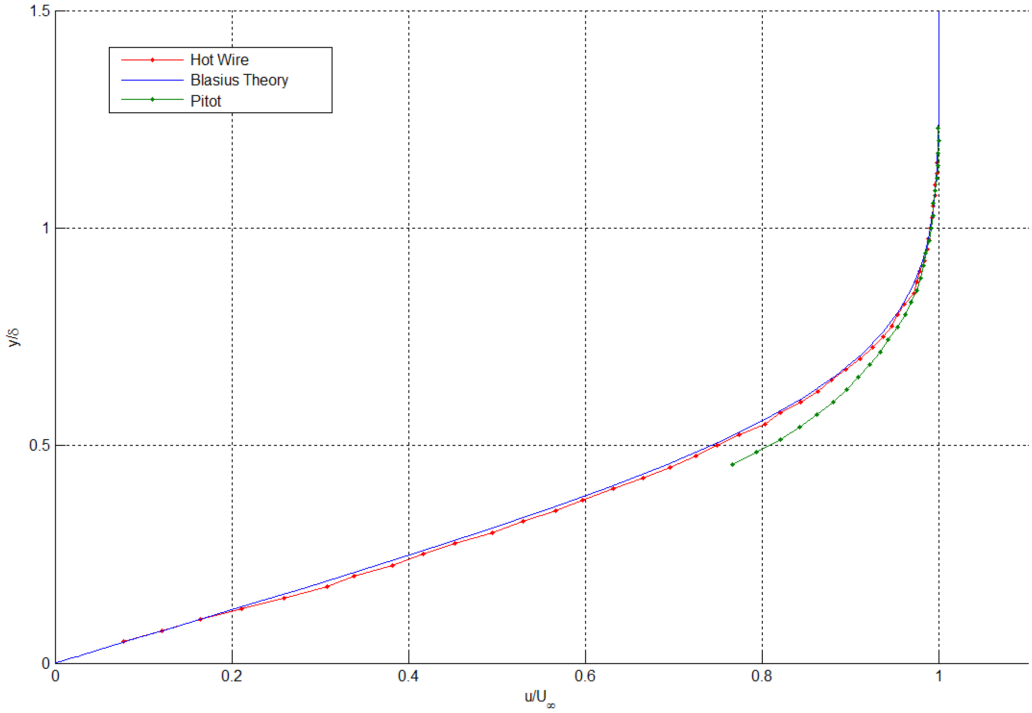

Figure 14.4: Comparison of the results of the HWA, Pitot and Blasius velocity profiles for $\mathrm{Re}_x = 6.11 \cdot 10^5$ (U=15m/s)

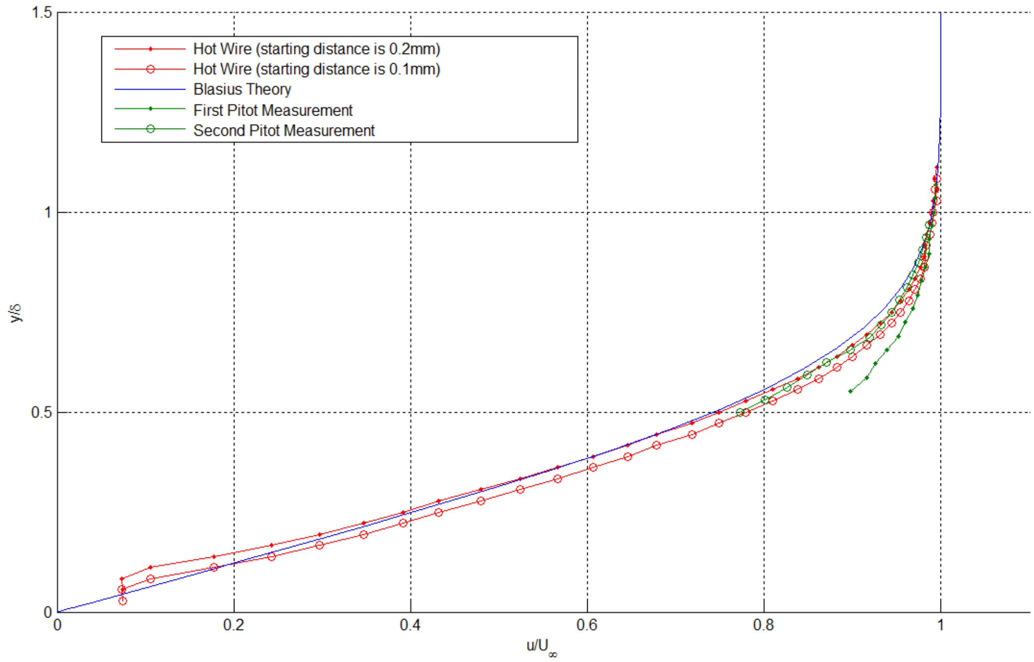

Figure 14.5: Comparison of the results of the HWA, Pitot and Blasius velocity profiles for $\mathrm{Re}_x = 1.02 \cdot 10^6$ (U=25m/s)

Figure 14.5 shows an additional Hot Wire velocity profile. This is the velocity profile for which the starting distance from the plate is set to 0.1mm instead of 0.2mm. This small adjustment, however, results in a velocity profile that overlaps with the profile of the second Pitot tube measurement. It can therefore be concluded that the same behaviour in the velocity profile is measured with both the Hot Wire and Pitot tube. This is, however, not conclusive.

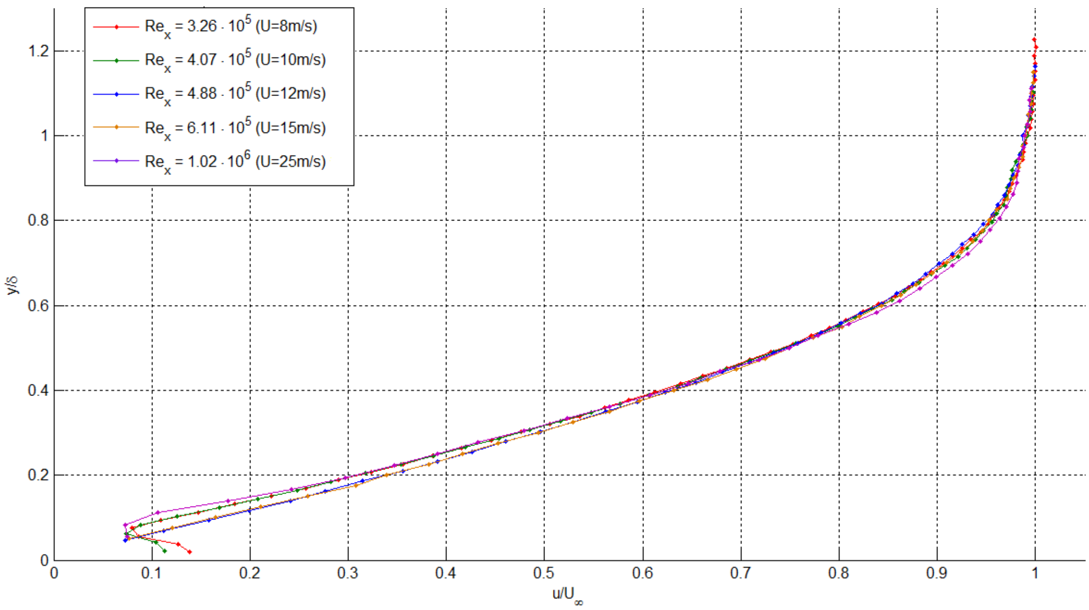

Figure 14.6: Comparison of the results of all the HWA measurements

Figure 14.6 shows that the velocity profiles from the Hot Wire measurements are observed to be very similar when plotted in terms of the similarity variables, i.e. u/U_∞ = function of $y/\delta(x)$, which is a very good result.

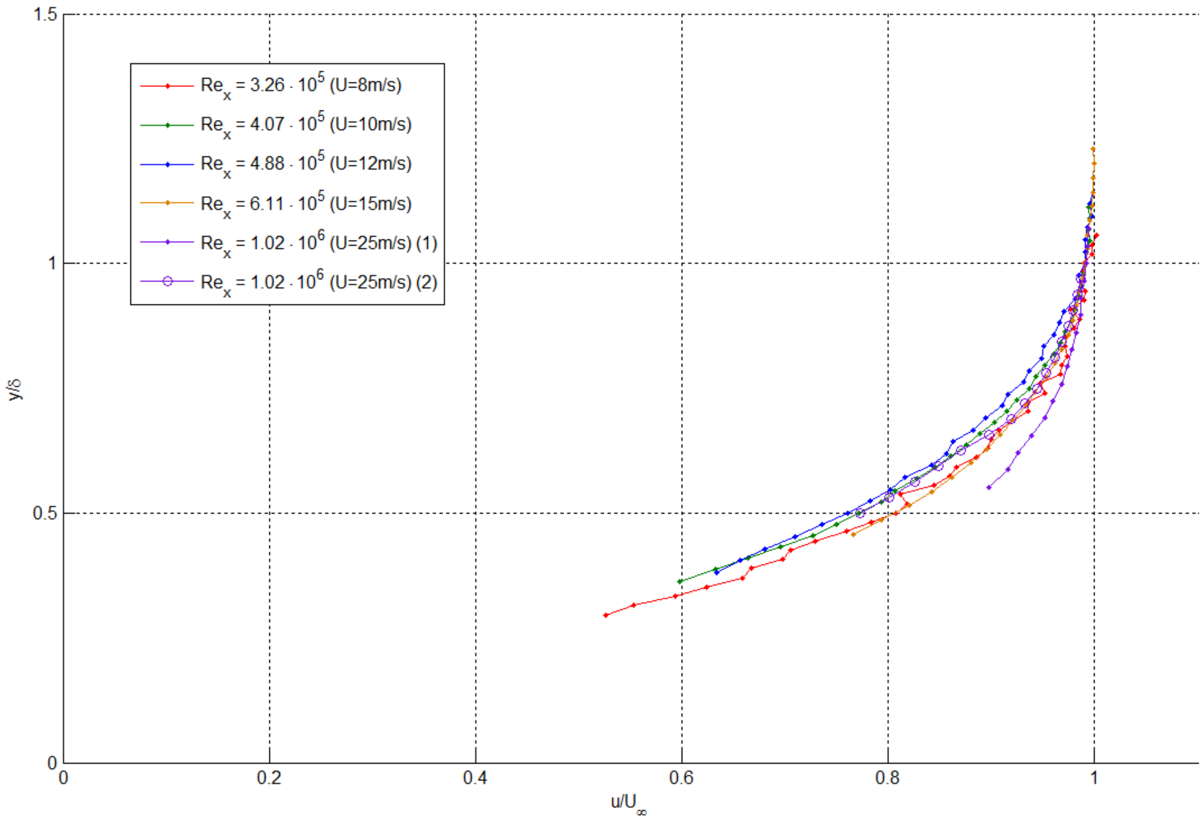

Figure 14.7: Comparison of all the Pitot tube measurements

The comparison of all Pitot tube measurements do not collapse as nicely from the HWA results for the U=8m/s, U=15m/s and U=25m/s measurements. A follow-up research should investigate if the variation in the velocity profile relates to anomalies of the surface of the plate as was described in section 13.1.1.

15 Discussion

15.1 The Pitot Tube Measurement

If one wants to be more accurate in a measurement with the Pitot tube, some details should be taken into consideration. The pressure difference between the static pressure and stagnation pressure is determined with two different Pitot tubes which are not on the same streamline and Bernoulli's equation does not hold. Moreover, the static pressure below the plate was found to be not identical to the static pressure measured with the Pitot tube in the wind tunnel. Therefore a more accurate method would be to place the Pitot tubes on the same streamline as much as possible or a Pitot tube should be designed which can measure the stagnation and static pressure in the boundary layer.

15.2 The Hot Wire Measurement

In the Hot Wire measurements, the temperature was not logged. However, a temperature change in the flow will have an effect on the voltage which is applied on the HWA. Unfortunately, in this research there was not another opportunity to repeat the measurements and log the temperature. In a follow-up study this should be taken into consideration. Equation 15.1 shows the relation to compensate for the change in ambient temperature from a reference temperature $T_{a,r}$ to the actual temperature T_a which will change the reference voltage $E_{w,r}$ to E_w. The equation has been obtained from Bruun [8]

$$E_w = E_{w,r} \left(\frac{T_w - T_a}{T_w - T_{a,r}} \right)^{1/2} \tag{15.1}$$

The determination of the distance between the HWA and the plate has also proven to be quite a challenge. We did not have the appropriate tools to determine the distance of the HWA from the plate. The heat transfer from the Hot Wire to the plate also had an influence, specifically close to the plate which can be observed in some of the measurements. However, by referencing the data to the Blasius Theory these effects were minimized.

15.3 The Load Cell Measurement

The drag force measurement gave a very clear picture of the transition from laminar to turbulent flow. However, the temperature of the flow in the wind tunnel affects the measurement of the load cell and thus the accuracy of the measurement. However, these effects were absolute and did not have an influence on the transition delay. Nonetheless a less temperature sensitive load cell should be used in future measurements.

16 Conclusions and Recommendations

16.1 Conclusion

Numerical simulations with XFOIL showed that the designed plate behaves aerodynamically as an infinitesimally thin flat plate. With a Hot Wire Anemometer and a Pitot tube we were able to measure the laminar and turbulent velocity profile of the boundary layer on the flat plate. The results showed great similarity with the derived theory. The result of the drag force measurement, specifically the value of the drag coefficient matched well with the derived theory. However, the measurements can be performed more accurately if more appropriate methods are used.

The possibility of the presence of disturbances (i.e. turbulent wedges) in the boundary layer at a velocity of U=25m/s ($\mathrm{Re}_x = 1.02 \cdot 10^6$) were observed with the Pitot tube. Furthermore, the result of the drag force measurement showed a delayed transition of the flow over the plate in de Silent Wind Tunnel at $\mathrm{Re}_c \approx 3 \cdot 10^6$. It was found that the pressure gradient in the test section of the Silent Wind Tunnel is a possible cause of the transition delay.

16.2 Recommendations

Based on the performed research, a number of recommendations are made for follow-up research.

The measurement with the Pitot tube showed some divergent results compared to the Blasius Theory and Hot Wire measurement. The discussed difference in stagnation pressure along the span of the plate indicated anomalies in the boundary layer flow. Further research should investigate the development of disturbances (i.e. turbulent wedges) over the plate in the wind tunnel and the effect of the disturbances on the measurement.

It should be considered to find a more accurate method to measure the velocity profile with the Pitot tube. The used method to calculate the velocity with the stagnation and static pressure was adequate in this research. Though, a more accurate method to measure the static pressure closer to the Pitot tube should be reviewed.

During the Hot Wire measurement, it was difficult to determine the exact distance between the Hot Wire and the surface of the plate. Accurate methods to determine the exact distance between the Hot Wire and the surface of the plate should be reviewed. A possibility would be to use a laser. Another follow-up study can be considered where one would derive a model for the heat loss of the Hot Wire when it gets closer to the surface of the plate.

To investigate the effects of the streamwise pressure gradient on transition, a follow-up research should be conducted in which the plate is installed at a specific angle of attack to change the streamwise pressure gradient. Numerical simulations with XFOIL showed that an angle of attack of 1 ° should be sufficient to change the streamwise pressure gradient. The effects of the streamwise pressure gradient on transition can then be analyzed. It can also be considered to investigate the origin of the streamwise pressure gradient in the test section of the Silent Wind Tunnel.

The accuracy of the drag force measurement can be increased if a less temperature sensitive load cell is used, especially for the lower Reynolds number range. It should therefore be considered to use another load cell for measurements at low Reynolds numbers.

17 References

1. Dr. R. Hagmeijer, Dictaat 'Inleiding Stromingsleer', Februari 2013, University of Twente.
2. H.W.M. Hoeijmakers, lecture slide 8, Stromingsleer en Warmteoverdracht, University of Twente, 2014.
3. Tuncer Cebeci and Jean Cousteix, 'Modeling and Computation of Boundary-Layer Flow.', Second Edition.
4. D. Arnal, G. Casalis and R. Houdeville, 'Practical Transition Prediction Methods: Subsonic and Transonic Flows', ONERA/DMAE, Toulouse.
5. John D. Anderson Jr., 'Fundamentals of Aerodynamics', 4^{th} edition, McGraw-Hill International Edition.
6. Jack Chen, 'Journal of Microelectromechanical Systems' , Vol. 12, No. 6, December 2003.
7. 'Pitot Static Tubes Theory', 23-05-2014, http://www.efunda.com/designstandards/sensors/pitot_ tubes/pitot_ tubes_ theory.cfm
8. H.H. Bruun, 'Hot-Wire Anemometry: Principles and Signal Analysis', June 8 1995.
9. Ir. Emiel Koopmans and Jelle Will, 'Turbulence Intensity Measurements of the 130kW Silent Wind Tunnel', December 2013

Appendix

A The Dimensions of the Plate

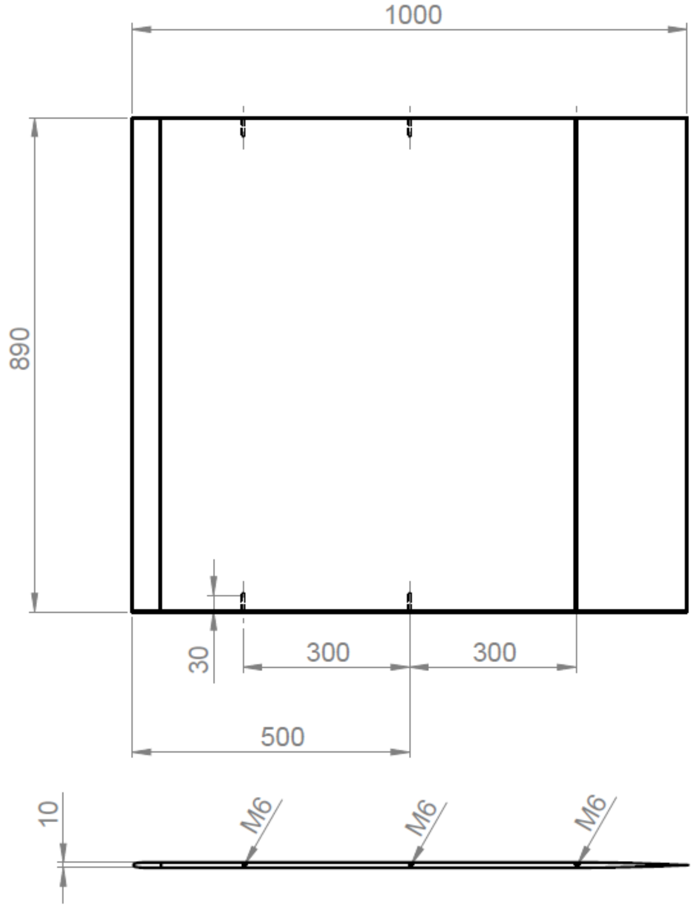

The Leading Edge (Hermite Polynomial):

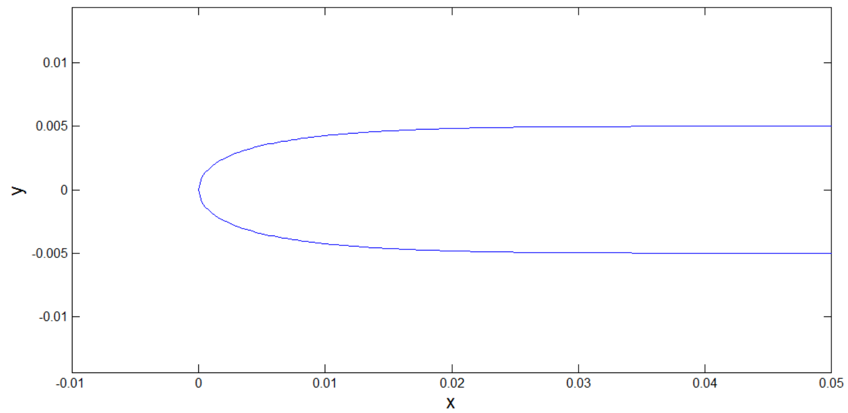

The Trailing Edge (last 70% of NACA 4-series):

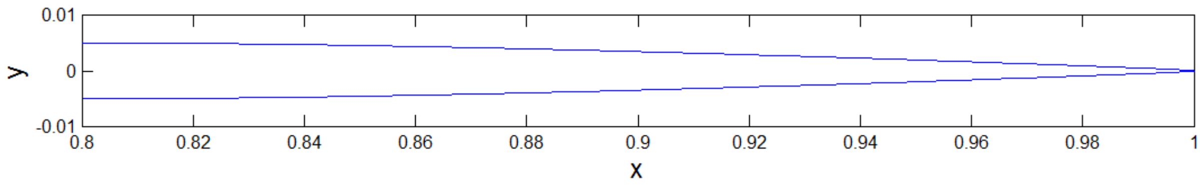
0.01
0
-0.01
y
0.8
0.82
0.84
0.86
0.88
0.9
0.92
0.94
0.96
0.98
1
x

B Matlab Code

```
clear all
close all
clc

%% General Parameters

% Flat plate parameters
LE = 'Harry'
TE = 'NACA0010';
le_perc = 0.05;
te_perc = 0.20;
thickness = 0.01;


% Define grid size
nr_panels_le = 223;
nr_panels_te = 223;
nr_panels_mid = 50;
nr_panels_tot = nr_panels_le + nr_panels_te + nr_panels_mid;
% number of points is two times as large.

%% Symbolic curve
syms x;

folder = '01_Nose_Harry';
airfoil_name = ['LE(' LE '-' num2str(le_perc) '-R0.2)_TE(' TE '-' ...
num2str(te_perc) ')_T(' num2str(thickness) ')'];

%% Leading edge
DeltaX = le_perc/thickness;
    R0 = 0.2;

    b1 = sqrt(8*DeltaX*R0);
    b2 = -16.0 + 5*b1;
    f1 = 1 - b1 - b2;
    df0 = 3.0 - 15.0*b1*0.125 - 3.0*b2*0.125;
    df1 = -0.5*b1 -1.5*b2;

    x_LE_temp = x./le_perc;

    P1 = (1+2.0.*x_LE_temp).*(1.0-x_LE_temp).*(1.0-x_LE_temp);
    P2 = 1.0 - P1;
    Q1 = x_LE_temp.*(1.0-x_LE_temp).*(1.0-x_LE_temp);
    Q2 = -x_LE_temp.*x_LE_temp.*(1.0-x_LE_temp);
    y_LE_temp = 0.5.*(sqrt(x_LE_temp).*(b1 + b2.*x_LE_temp) + df0*Q1 + ...
    f1*P2 + df1*Q2);

    curve_LE = y_LE_temp.*thickness;

% Middle
curve_Middle = thickness/2;

% Trailing edge
NACA0010 = 0.1/0.2*(0.2969.*sqrt(x)-0.126.*x-0.3516.*x.^2+0.2843.*x.^3- ...
    0.1015.*x.^4);
    diff_NACA0010 = diff(NACA0010);
    maximum = solve(diff_NACA0010==0);
    real_maximum = maximum(1);
    y_value_maximum = subs(NACA0010,x,real_maximum);

    x_TE_temp = (x-(1-te_perc/(1-real_maximum)))./(te_perc/(1-real_maximum));
    y_TE_temp = 0.05/y_value_maximum*subs(NACA0010,x,x_TE_temp);

    curve_TE = y_TE_temp.*10*thickness;

%% Plotting Flat Plate Shape
figure(1)
axis equal
hold on;

%% Leading edge
x_values_LE = 0:le_perc/nr_panels_le:le_perc;
y_values_LE = subs(curve_LE,x,x_values_LE);
plot(x_values_LE,y_values_LE);
plot(x_values_LE,-y_values_LE);

% Middle
x_values_Middle = le_perc:(1-te_perc-le_perc)/nr_panels_mid:(1-te_perc);
y_values_Middle(1:length(x_values_Middle)) = subs(curve_Middle,x,x_values_Middle);

figure(1)
plot(x_values_Middle,y_values_Middle);
```

```
plot(x_values_Middle,-y_values_Middle);

% Trailing edge
x_values_TE = (1-te_perc):te_perc/nr_panels_te:1;
y_values_TE = subs(curve_TE,x,x_values_TE);
figure(1)
plot(x_values_TE,y_values_TE);
plot(x_values_TE,-y_values_TE);

%% Create one file with all coordinates
x_coord_upper = zeros(nr_panels_tot,1);
x1 = x_values_LE';
x2 = x_values_Middle';
x3 = x_values_TE';
x_coord_upper(1:(length(x1)))=x1(1:(length(x1)));
x_coord_upper((length(x1)):(length(x1)+length(x2)-1))=x2(1:length(x2));
x_coord_upper((length(x1)+length(x2)-2):(length(x1)+length(x2)+length(x3)-3))= ...
x3(1:length(x3));

y_coord_upper = zeros((length(x1)+length(x2)+length(x3)-3),1);

for i = 1:length(x_coord_upper)
    if x_coord_upper(i)<le_perc
        y_coord_upper(i) = subs(curve_LE,x,x_coord_upper(i));
    elseif x_coord_upper(i)>(1-te_perc)
        y_coord_upper(i) = subs(curve_TE,x,x_coord_upper(i));
    else
        y_coord_upper(i) = subs(curve_Middle,x,x_coord_upper(i));
    end
end

x_coord = [flipdim(x_coord_upper,1); 0; x_coord_upper];
y_coord = [-flipdim(y_coord_upper,1); 0; y_coord_upper];

Xfoil_Airfoil_File = [x_coord,y_coord];
%% Check if the maximum number of points in Xfoil is not exceeded
length(Xfoil_Airfoil_File)
if length(Xfoil_Airfoil_File)<1000
save('FlatPlate.txt', 'Xfoil_Airfoil_File', '-ASCII','-append')
else
    close all
    errordlg('Maximum number of points exceeded. Please Reduce','Writing Error');
end
```

C Measurement Apparatus

C.1 The Pitot Tube

Figure C.1 shows the custom made Pitot tube. The tube has a diameter of 3mm. The tip of the Pitot tube is located at a distance of approximately 620mm from the leading edge. The Pitot tube is not located exactly in the middle of the span of the plate, though this is not expected to have an effect on the results of the measurement.

Figure C.1: The Pitot tube that was used in the measurements

C.2 Hot Wire Anemometer

Figure C.2 shows the calibration of the Hot Wire in the Silent Wind Tunnel. The HWA has the same position in the tunnel as the Pitot tube. A 1-Dimensional 55P11 Probe from Dantec was used.

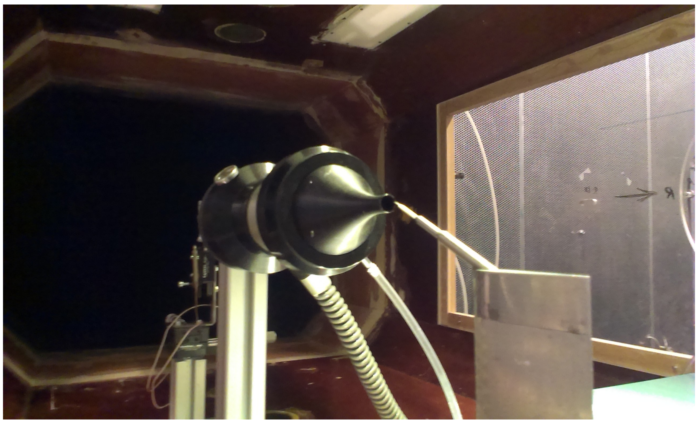

Figure C.2: The Hot Wire Anemometer during calibration

C.3 The Streamwise Pressure Gradient Measurement

Figure C.3 shows the position of the pressure orifices in the test section of the Silent Wind Tunnel. Pressure orifice 3 is shown as a lamp in the picture. However, it can be replaced by a pressure gate.

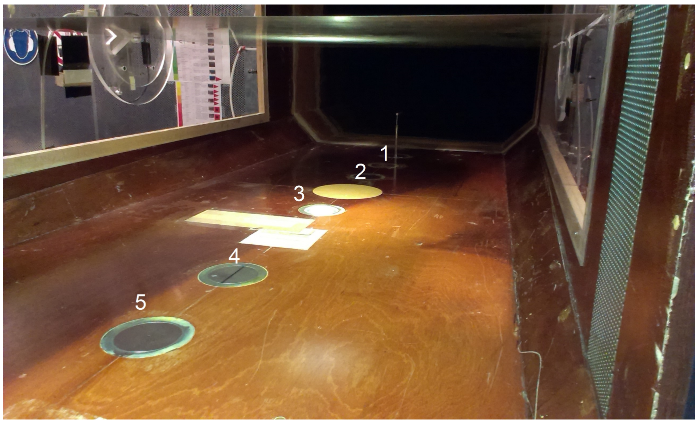

Figure C.3: The pressure gates from which the pressure distribution has been measured in the Silent Wind Tunnel

C.4 The Load Cell

Figure C.4 shows the load cell which measures the drag force. Another load cell is located at the other side of the test section.

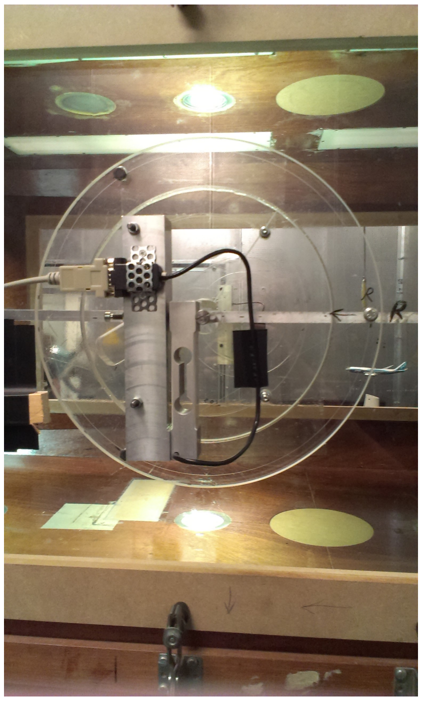

Figure C.4: The Load Cell